Quantitation of the effects of cellular glucocorticoid receptor concentration on dimerization.

Brendon Riekert

Thesis presented in partial fulfilment of the requirements for the degree

Master of Science in Biochemistry

in the Faculty of Science at Stellenbosch University

Supervisor: Prof. A. Louw

Co-supervisor: Prof. J. M. Rohwer

March 2021

Stellenbosch University https://scholar.sun.ac.za

Declaration

By submitting this thesis electronically, I declare that the entirety of the work contained therein is my own, original work, that I am the sole author thereof (save to the extent explicitly otherwise stated), that reproduction and publication thereof by Stellenbosch University will not infringe any third party rights and that I have not previously in its entirety or in part submitted it for obtaining any qualification.

Brendon Riekert

Date: March, 2021

Copyright © 2021 Stellenbosch University

All rights reserved

Stellenbosch University https://scholar.sun.ac.za

Summary

The glucocorticoids (GCs) are a group of steroids affecting virtually every cell in the body. The ability of the GCs to modulate the effects of the immune system is of particular interest therapeutically. Due to this characteristic, it is not surprising that the GCs have become the front line treatment in addressing a diverse array of inflammatory diseases ranging from sepsis to asthma.

The GCs are known to function by means of their cognate receptor, the glucocorticoid receptor (GR), which resides in the cytoplasm as a monomer, complexed to various chaperone proteins. Once activated by ligand binding, the GR is able to act via two classical pathways. In the first, the activated GR remains in its monomeric form and acts in a trans-repressive manner to attenuate pro-inflammatory signalling and is associated with the positive therapeutic effects of the GCs. Alternatively, the activated GR is able to form a homodimer and activate metabolic pathways through transactivation. This form of activation is associated with the negative side effects of the GCs.

The concentration of the GR in the body varies substantially, not only between different tissue types, but also within the same tissue in different disease states. Studies on GR concentration by Robertson *et al.* [1] has given rise to the ligand-independent dimerization model. This model suggests that higher concentrations of the GR lead to ligand independent dimerization that improves the sensitivity of tissues to GC stimulation through conformational changes that increase affinity of the GR for the ligand. Subsequent research by Barry [2] produced an *in silico* model of the GR dimerization cycle highlighting the importance of fluctuations in k_{off} as opposed to the k_{on} in affecting the affinity of the receptor for ligands at increasing GR concentrations, stressing the importance of ligand residence time in ligand receptor interactions.

The experiments of Robertson *et al.* [1] were completed using the human GR. However, another pharmacologically sound model is that of the mouse GR, which at present offers the

Stellenbosch University https://scholar.sun.ac.za

advantage of the recently developed monomeric GR construct, the GRmon and offers superior dimerization resistance when compared to the classical GRdim construct. Furthermore, the new fluorescence correlation spectroscopy technique for the observation of oligomers, the number and brightness assay (N&B), offers a unique opportunity to observe concentration dependent GR oligomerization by a confocal microscope [3].

The current project illustrates a comprehensive means of translating the previously defined physiologically relevant GR concentrations to the confocal microscope using median fluorescence intensity measurement. Furthermore, a method is proposed to use the N&B technique to observe ligand independent dimerization in the mouse model.

Finally, a pilot investigation was conducted using the N&B method to capture 30 minutes of the oligomerization behaviour of the mouse GR following stimulation with the GR agonist dexamethasone, and some challenges which could be overcome in future research are highlighted. To our knowledge, this is the first time the N&B technique has been attempted on the African continent.

Stellenbosch University https://scholar.sun.ac.za

Opsomming

Die glukokortikoïede (GK) is ‘n groep steroïede wat ‘n effek op feitlik elke sel in die liggaam uitoefen. In terme van terapeutiese gebruik is die GK van groot belang weens hul effek op die immuunstelsel. Weens hierdie eienskape is dit geensins verrassend dat die GK in die voorste linie staan as ‘n medikasie vir ‘n wye verskeidenheid siektes van sepsis tot asma nie.

Die GK oefen hul effekte deur middel van hul verwante reseptor, die glukokortoïed reseptor (GR) uit, wat as ‘n deel van ‘n metgesel proteïenkompleks in die sitoplasma van die sel voorkom. Sodra geaktiveer deur ligand kan GR volgens een van twee moontlike klasieke roetes optree. Volgens die eerste roete, die trans-onderdrukkende roete, word pro-inflammatoriese seine onderdruk deur middel van monomeriese GR proteïne. Hierdie roete word met die positiewe effekte van GK’s geassosieer. Die tweede moontlike roete, die trans-aktiverende roete, is afhanklik van ‘n dimeriese vorm van die GR, en lei tot transkripsie van metaboliese gene. Die trans roete word met die newe-effekte van die GK geassosieer.

Die konsentrasie van die GR in die liggaam wissel nie net afhangende van die weefsel tipe in die liggaam nie, maar ook tussen gesonde en siek weefsel. Onlangse navorsing oor GR konsentrasie deur Robertson *et al*. [1] het gelei tot die formulering van die ligand-onafhanklike roete van dimerisering. Hierdie roete behels dat hoër konsentrasies van die GR lei tot ligand-onafhanklike dimerisering wat so die sensitiwiteit vir GK‘s verhoog deur struktuurveranderinge in die GR teweeg te bring wat die affiniteit van die GR vir GK‘s verhoog. Daaropvolgende navorsing deur [2] het gelei tot die daarstelling van ‘n *in silico* model van die GR dimerisasie siklus. In hierdie model word die onderliggende belangrikheid van veranderings in die k_{off} in pleks van die k_{on} geimpliseer as a ‘n faktor wat die affiniteit van die GR vir die ligand by toenemende konsentrasies GR te beïnvloed. Hierdie studie het dus die belangrikheid van molekulêre verblyftyd beklemtoon. Die eksperimente van Robertson *et al.* is met die menslikke GR model gedoen. Die muis GR model is egter ook ‘n geldige farmakologiese model wat tans die voordeel bied van die nuwe monomeriese GR konstruk, GRMon, wat dimerisasie beter

Stellenbosch University https://scholar.sun.ac.za

teenstaan as die klassiek GR dim konstruk. Verder bied die nuwe fluoressensie-korrelasie spektroskopie metode, die aantal en helderheid toets (N&B), ‘n unieke geleentheid waarmee konsentrasie afhanklike GR oligomerisasie m.b.v. die konfokale mikroskoop waargeneem kan word [3].

Hierdie projek sluit ‘n samevatting in wat die navorser in staat stel om vorige gedefinieerde fisiologiese relevante GR konsentrasies oor te dra na die konfokale mikroskoop sisteem d.m.v. mediaan lig intensiteit metings verky vanaf fluoresensie gesorteerde GR sel populasies. Verder word ‘n metode voorgestel om N&B te gebruik om ligand-onafhanklike GR dimerisasie in die muis model te bepaal.

Laastens is ‘n loods eksperiment uitgevoer wat die N&B metode gebruik om die oligomerisasie van muis GR oor 30 minute na stimulasie met die GR agonis, deksametasoon, te volg, en uitdagings vir toekomstige navorsing word bespreek. Hierdie is sover ons kon vasstel die eerste poging op die Afrika-vasteland om N&B toe te pas.

Stellenbosch University https://scholar.sun.ac.za

Acknowledgments

I would like to, in no particular order, offer my sincerest gratitude to the following persons, eukaryotes and institutions.

Prof. Ann Louw: For a challenging project, your continued guidance and utmost patience as an educator, especially when I decided to run off on an adventure when I wasn't entirely done with my project. Thank you greatly for having the dauntlessness to allow me into your laboratory and for keeping me on this project.

Professor Johann Rohwer: Thank you greatly for your guidance and wisdom.

Dr. Nicolette Verhoog: the person who taught me almost everything I know, for always being available for discussion and being a firm sounding board for my ideas. If it wasn't for you sometimes pointing out the fluorescent lining around a thesis-shaped cloud, I am certain I would not have been nearly as motivated to finish.

The laboratory for fluorescence dynamics (UCI): For your expertise and assistance during the 11th LFD Fluorescence imaging and dynamics workshop. Without your invaluable input and practical knowledge, set up of the number and brightness technique would not have been possible. Thank you for hosting me and entertaining many trivial questions.

My parents Timothy and Laceya Riekert, as cliché thank you's are generally the most sincere, thank you for the opportunities you have afforded me, keeping me fed, protected and being there to pick up the pieces when things don't go as planned.

Nara prefectural Seisho combined junior and senior high school, my colleagues and students.

Stellenbosch University https://scholar.sun.ac.za

Through your hard work and dedication, I found unexpected inspiration for my science-related endeavours a world away from my original home. 本当にありがとうございました.

My cell babies: For your great sacrifice and glowing goodness, thank you for keeping me sane through many long nights and producing somewhat usable data.

Janneke Rubow: For being my personal editor in chief and for quietly encouraging me from the side lines through every step of the way. Thank you for your love and support.

Sietske Rubow: For your honest, helpful feedback, support and believing in my project.

The central analytical facility of Stellenbosch, with special mention to Rozanne Adams and Lize Engelbrecht, for your professional demeanour, exquisite expertise and for invaluable training.

Stellenbosch University and the NRF, for financial support, I am truly grateful for the opportunities your gracious grant has afforded me.

Other students and friends, for helping me communicate my thoughts to other human beings, using human language in a way hopefully some of you could understand.

Stellenbosch University https://scholar.sun.ac.za

Contents

Stellenbosch University https://scholar.sun.ac.za

Stellenbosch University https://scholar.sun.ac.za

Stellenbosch University https://scholar.sun.ac.za

List of Figures

Stellenbosch University https://scholar.sun.ac.za

Stellenbosch University https://scholar.sun.ac.za

List of Tables

Stellenbosch University https://scholar.sun.ac.za

List of important abbreviations

ACTH	Adrenocorticotrophic hormone
AIDS	Acquired Immuno Deficiency Syndrome
BSA	Bovine Serum Albumin
CBG	Corticosteroid binding globulin
COS-1	Monkey Kidney Fibroblast-like Cells
CRH	Corticotrophin Releasing hormone
DBD	DNA binding domain
eGFP	Enhanced Green Fluorescent protein.
Dex	Dexamethasone
FCS	Fluorescence correlation spectroscopy
DMEM	Dulbecco's Modified Eagle Medium
DMSO	Dimethyl sulfoxide
FACS	Fluorescence Activated Cell Sorting
FBS	Fetal Bovine Serum
FITC	Fluorescein isothiocyanate
FRET	Fluorescent resonance energy transfer
GC	Glucocorticoid
GR	Glucocorticoid receptor
GRE	Glucocorticoid response element
t(1/2)	Half-life
HPA	Hypothalamic Pituitary Adrenal axis
Hsp	Heat shock protein
IL	Interleukin
LBD	Ligand Binding Domain
MAPK	Mitogen-activated protein kinase
nGRE	negative glucocorticoid response element

Stellenbosch University https://scholar.sun.ac.za

NR	Nuclear Receptor
N&B	Number and brightness
NTD	N-terminal domain
PBS	Phosphate Buffered Saline
RE	Response elements
TNF	Tumor necrosis factor

Stellenbosch University https://scholar.sun.ac.za

Chapter 1

Project motivation and outline

Introduction

Since the Nobel prize winning isolation and description of compound E (later renamed cortisone) by Kendel, Hench and Reichstein in 1950 [4] the glucocorticoids (GCs), in their endogenous or synthetic agonist forms, have risen to prominence as a successful treatment of chronic inflammatory diseases. However, despite the effectiveness of the GCs, many side effects are associated with chronic GC treatment and understanding the mechanism of GC action is therefore of utmost pharmacological interest.

The classical pathway of GC mediated gene activation represents an oversimplified and easy to understand mechanism of action for the GCs through the GR. It should be noted that the GCs also mediate responses via the mineralocorticoid receptor (MR) and that GR binding sites and response elements can vary considerably from the consensus and that a plethora of mechanisms for gene activation and suppression via the GR exist.

In this example the cognate receptor of the GCs, the glucocorticoid receptor (GR) exists in the cytoplasm as a monomer, complexed with a multitude of chaperone proteins awaiting activation by its ligand [5]. Following activation, conformational changes allow the GR to engage in one of two classical activation pathways. The first to be discussed, is known as trans-activation. In this instance, the GR forms a homodimer complex which is able to interact with its glucocorticoid response elements (GRE) on the DNA and enact the transcription of a variety of pro-metabolic genes. In accordance with the classical model of GR activation, dimerization is associated with the negative side effects of the GCs such as hyperglycemia, and muscle wastage associated with gluconeogenic pathways which the GCs are known to

Stellenbosch University https://scholar.sun.ac.za

regulate. Alternatively, the GR may remain in a monomeric form, and engage in what is known as trans-repression. In accordance with the classical pathway of GR activation, this pathway is considered to result in the positive anti-inflammatory effects of the GCs, with the GR disrupting the transcription of pro-inflammatory genes through competition and interaction with pro-inflammatory transcription factors.

However, a lesser understood aspect of the GR in particular, has been the effect of GR concentration on cellular responses to GC stimulation. A large spectrum of GR concentrations exists in the human body. This is evident between different tissues with values as low as 4.1 fmol GR/mg protein in peripheral blood mononuclear cells [6] of as high as 893 fmol GR/mg protein in keratinocytes [7]. Additionally, there also exists a wide variation in the concentration of GR in healthy vs. diseased tissues, with skin GR concentrations rising approximately 5 fold in Kaposi's sarcoma biopsies when compared to those of normal skin tissue [7].

Previous work by Robertson *et al.* [1] in the human GR model suggested what has now become known as the ligand-independent dimerization cycle of the GR. Importantly, this research clearly demonstrated the novel idea that the GR is able to dimerize in the absence of ligand. Furthermore, the effect of increasing GR concentration on the overall affinity of the GR for its ligand was also demonstrated. Subsequent *in silico* work by Barry [2] elucidated the effects of increasing GR concentration on the kinetic parameters underlying the dissociation constant (K_d). Specifically, they demonstrated that the dissociation rate (k_{off}) of the ligand from the GR is modulated by GR concentration and directly affects observed GC potency [2]. For these experiments, the k_{off} and k_{on} values were determined at equilibrium under laboratory conditions. However, as equilibrium is rarely achieved in *in vivo* systems [8], understanding of how the k_{off} and k_{on} changes during ligand/ receptor interactions is of critical interest in developing feasible pharmacological solutions.

Stellenbosch University https://scholar.sun.ac.za

Advancements in technology, in particular in the field of fluorescence correlation spectroscopy (FCS), have allowed the use of the confocal microscope for the observation of protein oligomerization, a cheap and simple system compared to other methods for the observation of oligomerization data and therefore a system highly suitable for use on the African continent where access to specialized equipment is often limited.

The current research project therefore aims to lay the foundation for future work describing receptor oligomerization kinetics in the concentration dependent mouse GR model, a highly relevant pharmacological model. This will be done by first translating previously defined physiologically relevant GR concentrations [1] established by Barry [2] for the FACS to the confocal system. Following this, the novel FCS technique, the number and brightness assay (N&B) [3], will be applied to investigate receptor dimerization under different conditions.

To accomplish this, the following aims were achieved in an incremental fashion. Firstly, the experiment required a pool of COS-1 Cells transfected with physiologically relevant concentrations of the eGFP tagged GR variants mGRwt, mGRdim and mGRmon. To do this we investigated the effects of the GR variant, initial transfection DNA concentration and time following transfection on the parameters of overall transfection efficiency as well as the distribution of GR expressing COS-1 cells, in terms of GR concentration within the transfected populations using FACS. These experiments yielded an optimum collection time point following transfection, yielding a distribution of physiologically relevant GR containing COS-1 cells for further experimentation.

Secondly, the research project aimed to acquire kinetic data and specifically, residence time information about GR oligomerization at physiologically relevant GR concentrations using the number and brightness assay. To achieve this, FACS-sorted fluorescent-tagged GR-containing COS-1 of physiologically relevant concentrations were transposed to the confocal microscope. Next, cells of physiologically-relevant concentrations were selected from mixed

Stellenbosch University https://scholar.sun.ac.za

populations using fluorescent signal strength as a measure of concentration and the number and brightness assay was used to ascertain the ratio of monomeric to dimeric GR protein complexes. Finally, the ligand dexamethasone was applied and time-dependent receptor dimerization was observed by means of N&B.

Chapter 2 provides background knowledge on the GCs and GR. A brief literature overview of the relevance of the glucocorticoids, their structure and their interactions with their cognate receptor, the glucocorticoid receptor (GR), is included. The importance of GR concentration in the effectiveness of GC upon the target cells of interest will be described.

In Chapter 3, the methods and results of *in vitro* experiments performed to characterize the behaviour of transfected GR constructs using fluorescence activated cell sorting (FACS) are presented. Using different fluorescently tagged mouse GR constructs with increasing dimerization abilities at different initial transfection concentrations, as well as by altering the time period of incubation following transfection, the expression distribution of GR within transfected cell populations was compared. The chapter concludes with a description of the optimum time and concentration required to produce a transfected population containing the physiologically relevant GR concentration spectrum of COS-1 cells.

In chapter 4 the methods and *in vitro* experiments for single cell GR containing cell experiments on the confocal microscope are discussed. In this section, methods used for translating FACS sorted cells to mean brightness values on the confocal microscope are introduced, after which the ability to sort cells from a mixed population of GR transfected cells is shown. The use of the N&B technique to observe ligand independent dimerization is demonstrated. Finally, the application of the N&B technique to a 30 min time course following ligand stimulation and the current limitations of this technique are discussed.

Stellenbosch University https://scholar.sun.ac.za

Chapter 5 contains an overview of the results of the preceding chapters and places these in the context of the broader body of scientific literature. The chapter concludes with the limitations of this study and provides potential future research endeavours.

Stellenbosch University https://scholar.sun.ac.za

Chapter 2

Glucocorticoids and the glucocorticoid receptor

2.1: The glucocorticoids

Steroids are a family of biologically active, organic polycyclic compounds of which hundreds are found in plants, animals and fungi. In eukaryotes, the steroids serve two primary functions. The steroids are employed to modify the viscosity of the lipid bi-layer of cell membranes or membrane fluidity. The other primary role of steroids is signal transduction.

All steroids share a common 17 carbon atom polycyclic core structure which is known as a gonane. The structure is composed of three cyclohexane rings flanked by one cyclopentane ring. Functional differences between the different steroids are provided by alterations to the functional groups which are attached to this 4 ring structure [9]. An example of the prototypical animal steroid cholesterol is shown in **figure 2.1.**

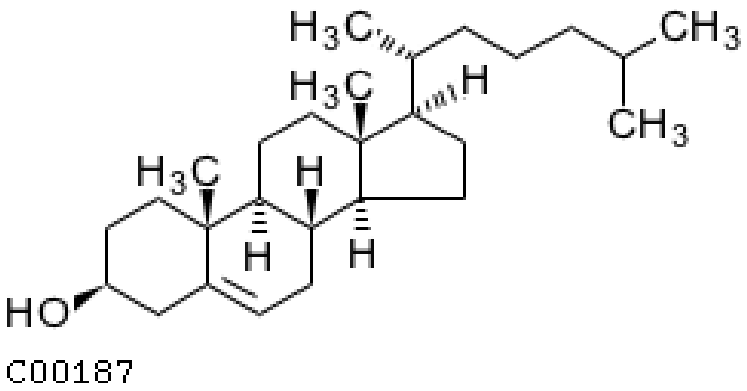

Figure 2.1: The structure of cholesterol, precursor molecule for various steroidal hormones. From genome[a].

[a] https://www.genome.jp/dbget-bin/www_bget?C00187

Stellenbosch University https://scholar.sun.ac.za

There are 5 classes of steroid hormones which are found in animals and these are specified by their physiological effects. These are the androgens, estrogens and progestogens, which influence sexual differentiation and reproduction; the mineralocorticoids, which control the excretion of electrolytes by the kidneys and influence blood volume; and finally the glucocorticoids (GC), which influence many aspects of metabolism and immune function [10,11].

Etymologically, the word glucocorticoid refers to the key characteristics of the molecules. First, **gluco**, derived from the word glucose, alludes to the effects of the GCs on glucose metabolism. Next, **corti** refers to the nexus of synthesis of the hormone, the adrenal cortex. Finally, and perhaps counterintuitively, **oid** refers to the steroidal nature of the hormones.

Glucocorticoids are often employed in the treatment of rheumatological and inflammatory conditions due to the hormone's ability to suppress the immune response. Since the Nobel prize winning extraction of cortisone by Harold Mason and Edward Kendall [8], the hormone, as well as its various commercial synthetic agonists, have seen widespread use, often being employed in novel ways to treat new illnesses. Recently for example, dexamethasone, a synthetic agonist of cortisol, has been employed to minimize diffuse lung damage due to the novel Corona virus, SARS-CoV-2 [11].

2.2 Control, synthesis and transport of the GCs

2.2.1 Control of the GC synthesis and release

Release and synthesis of the glucocorticoids is regulated by the hypothalamic-pituitary-adrenal axis (HPA-axis) via a simple cascade. Activation of the axis can be initiated by various stimuli. These may include circadian rhythms, injury, psychological stress, blood levels of cortisol or physical activity. Initial stimulus of hypophysiotropic neurons in the hypothalamus lead to the release of corticotropin-releasing hormone (CRH) [2,13]. The initial release of CRH

Stellenbosch University https://scholar.sun.ac.za

into the hypophysial portal vessels and subsequent binding to CRH receptors on the anterior pituitary leads to the release of adrenocorticotropic hormone (ACTH) into the bloodstream. ACTH binds primarily to receptors of the adrenocortical cells, and stimulates in particular, the cells of the zona fasciculata to synthesize and secrete glucocorticoids into the bloodstream [13] (**Fig. 2.2**).

The release of the GCs and subsequent influx of the molecule in the bloodstream in turn lead to a classical negative feedback mechanism which acts on the anterior pituitary gland, as well as the hypothalamus to stem further secretion of activation hormones [14].

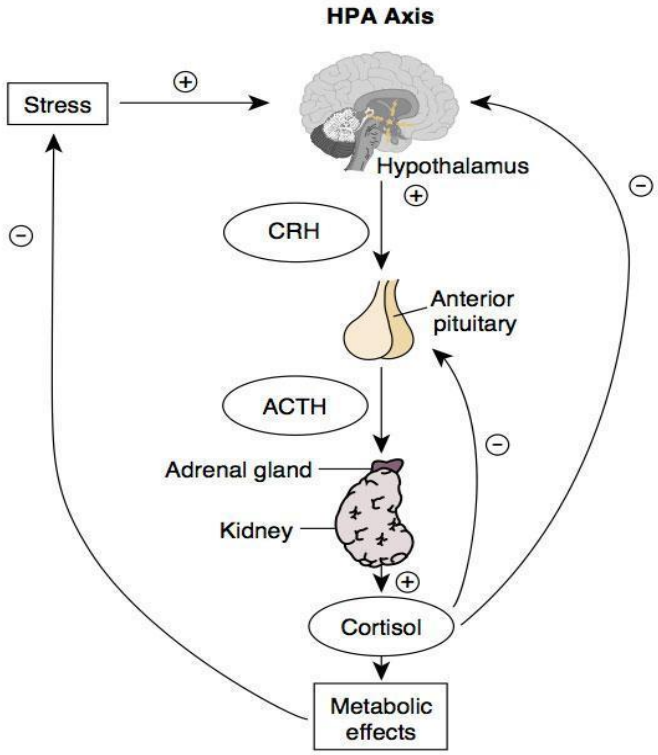

Figure 2.2: Schematic overview of the hypothalamic, pituitary adrenal axis including its negative feedback systems. A physical or psychological stress leads to the activation and secretion of corticotropin releasing hormone (CRH) by the hypothalamus. CRH in turn stimulates the release of adrenocorticotropic hormone (ACTH). Finally, ACTH stimulates the zona fasciculata of the adrenal glands to release the endogenous glucocorticoid, cortisol, to enact various metabolic effects to address the stress factor. Importantly, note the negative feedback loop which cortisol enacts on the hypothalamus and anterior pituitary.
Reproduced from embryology[a].

[a]https://embryology.med.unsw.edu.au/embryology/index.php%3Ftitle%3DFile:HPA_axis.jpg&rct

Stellenbosch University https://scholar.sun.ac.za

2.2.2 Biosynthesis of GCs

For animal species such as rats and mice the primary glucocorticoid is corticosterone, whereas cortisol is the main GC in humans [15]. Synthesis of the glucocorticoids, including cortisol, occurs in the adrenal glands, pyramidal structures situated above the kidneys [16]. In particular, synthesis is attributed to the zona fasciculata, the middle of three strata of the adrenal cortex. As with all steroids, biosynthesis of cortisol begins with cholesterol. Cholesterol enters the adrenal cortex via two routes. Approximately 80% of the daily requirement for steroid synthesis is acquired from diet, with cholesterol entering the cells directly via low density lipoproteins on the adrenal cells. Whether or not high density lipoproteins are taken up by receptors is not yet clear but may be possible. The remaining 20% of the required cholesterol needed is synthesized within the cell from acetate via a CoA reductase enzyme pathway within the cell [17].

Cholesterol is either utilized directly or stored as cholesterol esters within the cell for later use via a reverse hydrolysis reaction. Free cholesterol is chaperoned to the membrane of the mitochondria via a sterol transfer protein. Transfer of the hydrophobic molecule from the outer to inner mitochondrial membrane is mediated by the steroidogenic acute regulatory (StAR) proteins [16]. From here, the heme-containing side chain cleaving CYP11A1, catalyses the reaction from cholesterol to pregnenolone via three monooxygenase reactions after which pregnenolone is shuttled to the smooth endoplasmic reticulum [16]. Pregnenolone is then further converted to progesterone and 17α-hydroxyprogesterone. The latter is achieved by means of cytochrome p450 catalysis. A full list of reactions for the main steroidal hormones is provided in **Figure 2.3**.

Progesterone and 17α-hydroxyprogesterone are then further converted to II-deoxycortisol before being shuttled back to the mitochondria and finally catalysed to cortisol via a CYP11B1 hydroxylation reaction [12].

Stellenbosch University https://scholar.sun.ac.za

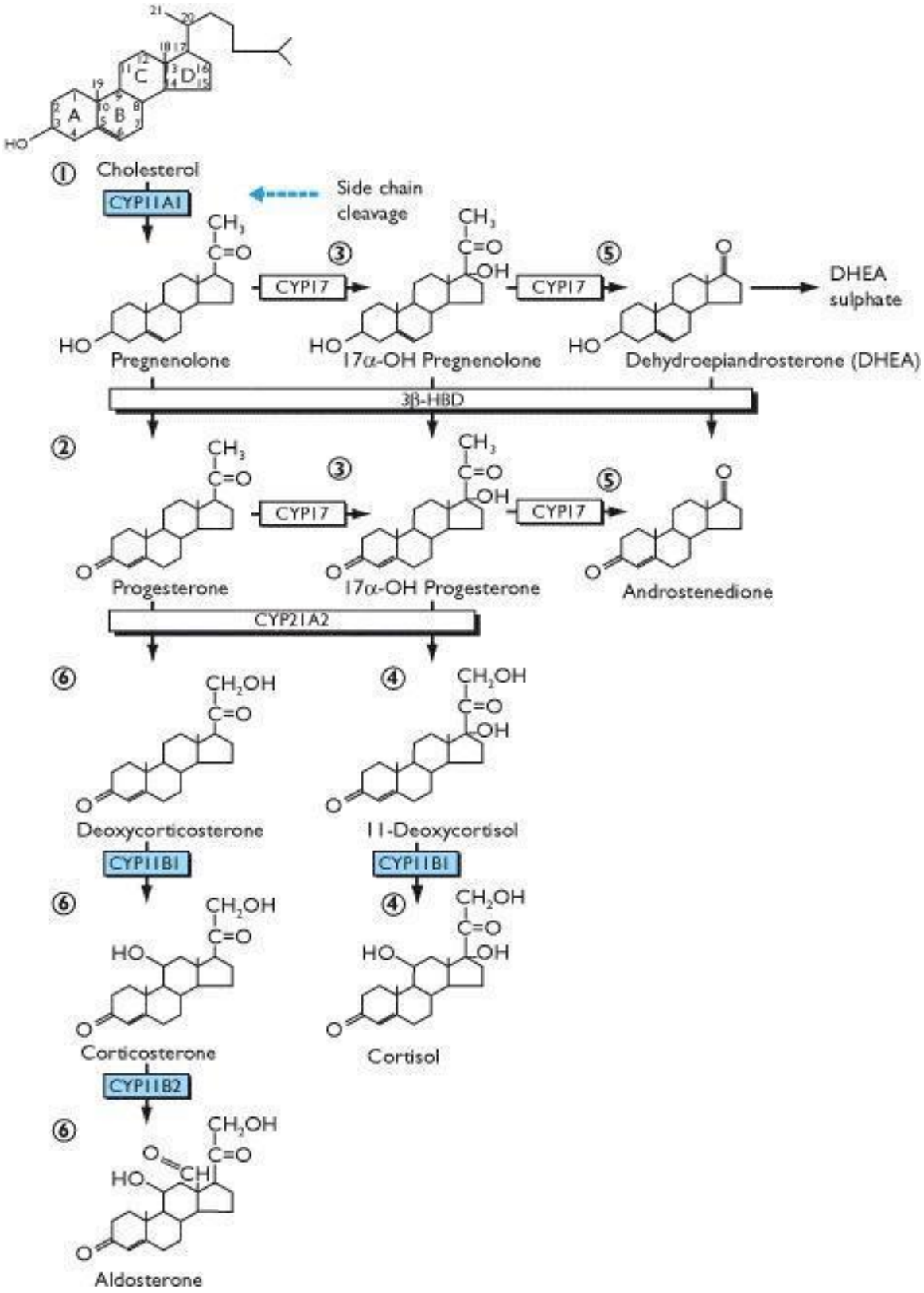

Figure 2.3: Synthesis of the major steroid hormones (excluding sex hormones) and the oxidative enzymes required for catalysis. Note that synthesis occurs in both the mitochondria (blue boxes) and the smooth endoplasmic reticulum. From Nussey, S.[18]

Stellenbosch University https://scholar.sun.ac.za

2.2.3 Plasma transport of the glucocorticoids

In accordance with the free hormone hypothesis by Carl M. Mendel [17], biological activity of a hormone is due to the presence of a free hormone as opposed to a hormone which is bound to a transport protein. Glucocorticoids produce pleiotropic effects, having a wide range of physiological consequences which require a large degree of physiological control. Plasma transport of the hydrophobic glucocorticoids, as well as the availability of free hormones is tightly controlled by the binding of hormones to transport proteins. In the human body, cortisol is bound primarily to corticosteroid binding globulin (CBG) [19], which accounts for between 80 and 90% of GCs within the bloodstream. In addition, about 5-10% of cortisol is non-specifically bound to albumin. Together, the CBG and albumin allow the transport of GCs throughout the human body, while maintaining a 5% fraction of free hormones for biological action [19].

The transport of hormones into the target cell is a passive process due to the lipophilicity of the GCs. Free hormones traverse the cell membranes of target cells where they interact directly with their cognate receptor, the glucocorticoid receptor (GR) [19].

2.3 The glucocorticoid receptor (GR)

2.3.1 The structure of the glucocorticoid receptor

The GR is an acidic protein and is part of the steroid/thyroid/retinoic super family of receptors. Specifically, such receptors are known as ligand mediated transcription factors. The activating ligand is species specific, with corticosterone being the endogenous GC in mice, whereas cortisol is the main GC in humans [15].

Various isoforms and splice variants of the GR exist [20], and each subtly modifies the regulatory effects of the GR. Most commonly mentioned are the GR-α and GR-β isoforms. Of

Stellenbosch University https://scholar.sun.ac.za

these isoforms the GR-α is a transcriptionally active isoform whereas the GR-β, while transcriptionally active generally receives less attention in the literature. The basic structure of the GR-α is described below. The GR is encoded by the *NR3C1* gene and consists of three major functional regions, the N-terminal domain (NTD), the DNA binding domain (DBD) and the ligand binding domain (LBD), respectively (**Fig. 2.4**).

The NTD contains the AF-1 domain, which provides transcriptional activation abilities to the GR that does rely on ligand binding. Of the three regions, it is the most variable, both in terms of sequence length, but also in terms of sequence variability [22,23].

The DBD is known to consist of a highly conserved amino acid sequence which is characterised by two zinc fingers, each consisting of four cystine residues interacting with a zinc atom. The arrangement allows the interaction of the GR with the glucocorticoid response element or the GRE [16]. Specifically, a small number of amino acids in the first Zinc finger in a region known as the proximal-box (P-box) are responsible for the interaction between the GR and its cognate GRE. On the other hand, the distal-box(D-box), located on the second zinc finger, plays a role in maintaining a dimerization interface between two DBD regions during GR oligomerization. The dimerization impaired GR mutant, the GRdim, for example, contains an A465T mutation in the D-Box of the mouse GR which impedes dimerization.

Finally, the LBD is moderately conserved regardless of species. It is separated from the DBD by a hinge region spanning 40 amino acids. The LBD allows interaction of the GR with a ligand and the binding of the GR with chaperone proteins, but it also plays an important role in receptor dimerization. Additionally, the LBD hosts the AF2 domain, which plays an important role in ligand-activated GR mediated transactivation [23]. Work by Bledsoe and colleagues on the crystal structure of the LBD has highlighted the role of the LBD in dimerization through the formation of an intermolecular beta sheet [23]. Mutations of I634A in the mouse GR have a severe reduction in the dimerization of the affected GR molecule, whereas a double mutation

Stellenbosch University https://scholar.sun.ac.za

of A465T in the DBD and I634A in the LBD of the same species has resulted in the formation of the novel, severely dimerization resistant GR mon [24].

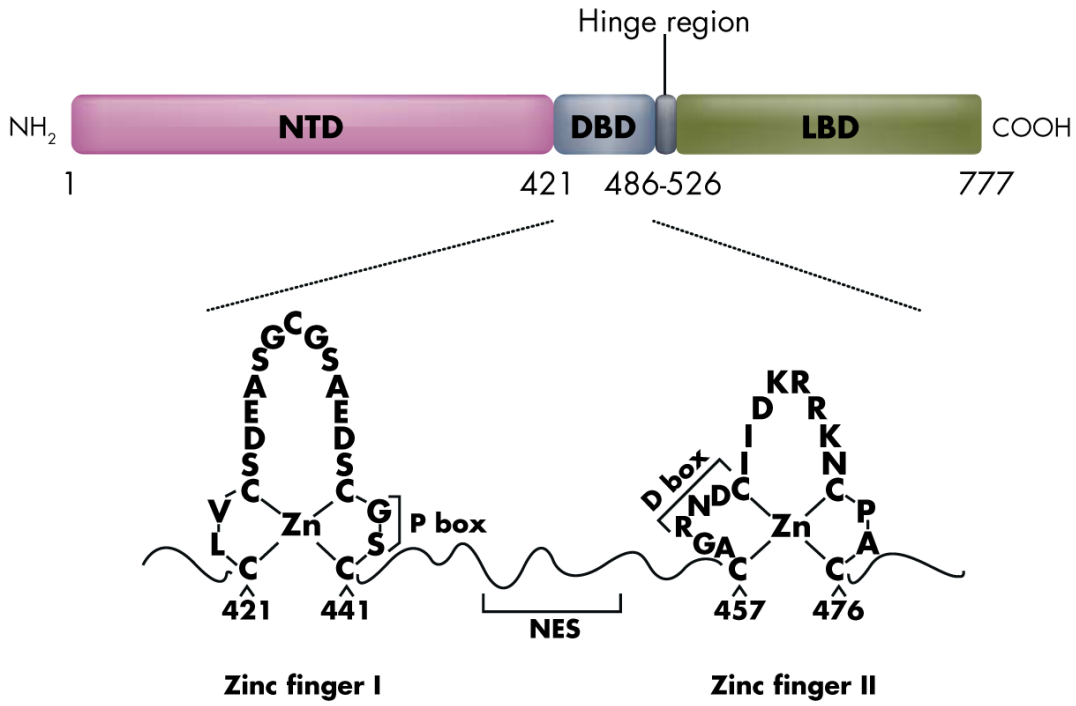

Figure 2.4: Structure of the human GR highlighting the structure of the DNA binding domain and the distinct zinc finger structure required for interaction with the glucocorticoid response element. Note the D box region in the second zinc finger, a region which affects dimerization of the GR. From Sofie Vandewyver *et al.* [20]

2.3.2 Activation pathway of the GR

The GR is an essential transcription factor, not only for normal function but for life, as experiments eliminating GR expression in transgenic mice, produced pups with severe lung deformities which expired shortly after birth [25]. Furthermore, the receptor acts as a ligand-activated transcription factor.

Prior to stimulation, the GR resides in the cytoplasm as a heteromeric complex bound to the acidic p23 protein, a dimer of the heat shock protein 90 (Hsp90), the heat shock protein 70 (Hsp70) as well as other chaperone proteins and immunophilins. Upon interaction with a GC,

Stellenbosch University https://scholar.sun.ac.za

the ligand creates a conformational change in the GR which in turn causes a change in the overall structure of the heteromeric complex, priming the protein for import into the nucleus, primarily mediated by the Hsp90 proteins within the complex [27,28].

The simplified, classical model of GR signal transduction is given in the figure below (**Fig. 2.5**). In this model, when the GR remains a monomer, it binds to transcription factors associated with the promotors of inflammation related genes. This tethering action is associated with the positive clinical effects of the GCs and is likely due to the crosstalk between the GR and other pro-inflammatory transcription factors such as NFκ-B and activator protein 1 (AP-1) that results in the transrepression of pro-inflammatory genes [28].

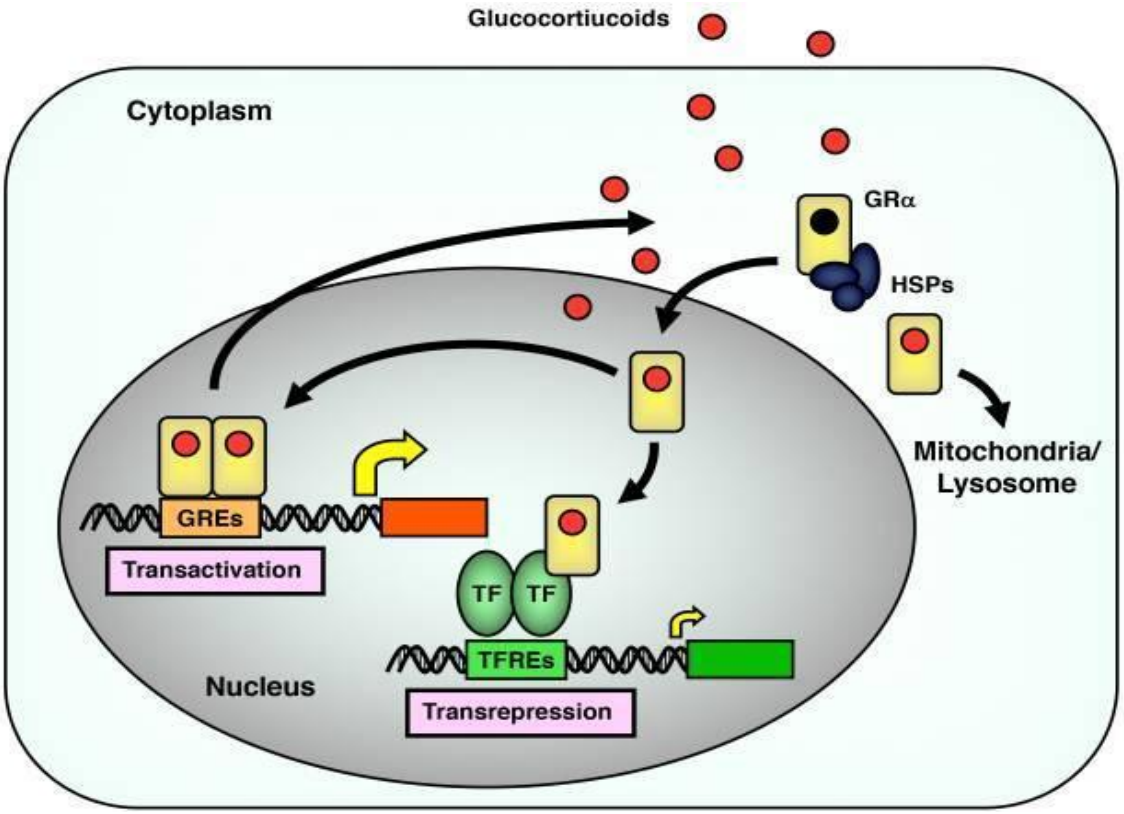

Figure 2.5: The classical pathway of GR signal transduction. The GR remains in the cytoplasm as a monomer until activation by the GCs occurs. Following activation, the GR separates from the heat shock protein complex and can function in one of two modes. As a monomer, the nuclear GR can tether pro-inflammatory transcription factors impeding transcription. In contrast, during trans-activation, the GR can dimerize and act as a transcription factor, activating pro-metabolic transcription.
[a]From Tomoshige Kino [29].

Stellenbosch University https://scholar.sun.ac.za

In contrast, the classical model also describes the GR as being able to mediate transcription via dimerization of the receptor. In this configuration, the GR can bind with its cognate response element, the glucocorticoid response element (GRE), which consists of two 6Bp palindrome sequences separated by a 3bp spacer [30]. Typically, however, this form of gene activation is associated with the negative side effects of the GCs such as various adverse metabolic disturbances [31].

Furthermore, research suggests that the GR is also able to bind to GRE half sites in conjunction with other secondary transcription factors as opposed to a strictly GR dimer while further evidence suggests that GR dimers can also cause gene suppression by binding to negative GREs which impede pro inflammatory gene expression [32].

Remarkably, the GR as a protein displays a degree of motif mismatch, allowing it to bind to a variety of GR binding sites in addition to the classical GRE motif within the genome. In doing so, the GR possesses an extraordinary ability to engage in crosstalk with various neighbouring transcription sites and exert an exceptional degree of control over the regulation of inflammation related genes [33].

2.3.3 Distribution of the GR throughout the human body

The GR is a protein which is almost ubiquitously expressed throughout the human body and is therefore found in almost every cell and tissue. Interestingly however, the distribution of GR varies greatly not only between various tissues, but also between the same tissues in different disease states. Furthermore, the distribution can be altered by various physiological conditions such as the age of the subject, level of fitness and various other parameters.

In terms of tissues, the concentration of the GR can be as low as 4.1 fmol GR/mg protein in peripheral blood mononuclear cells whereas concentrations can be as high as 893 fmol GR/mg protein in human skin cells [7].

Stellenbosch University https://scholar.sun.ac.za

Disease states can greatly alter the concentration of the GR within the same tissues. In skin for example, normal cells express the GR at a concentration of 893 fmol GR/mg protein [6], In contrast, biopsies of skin of AIDS patients have produced concentrations of 2777 fmol GR/mg protein, whereas Kaposi's sarcoma biopsies in AIDS patients have demonstrated concentrations as high as 4663 fmol GR/mg protein [7].

Low GR levels have been directly linked to GR insensitivity whereas high levels of GR have been associated with GR hypersensitivity [29]. It is therefore suggested that GR concentration plays an important role in mediating the differential effects of the GCs across a variety of tissues while plasma concentrations of the steroid remain constant throughout the organism [5,6].

2.3.4 Ligand independent dimerization and physiological relevance

Work by our laboratory has investigated the effects of the increase in GR concentration and described mechanisms of action for the GR based on concentration differences in the human GR. Studies by Robertson [1]. established a model for a spectrum of increasing GR concentrations relevant to physiological conditions. The model described by Robertson *et al.* defined low, medium and high concentrations of GR within the cell as 335 fmol GR/mg protein (low [GR]), 763 fmol GR/mg protein (med [GR]) and 1420 fmol GR/mg protein (high [GR]), respectively.

Promoter reporter assays using the above physiologically relevant GR spectrum revealed that increasing GR concentrations resulted in an increase of 3 and 10 fold, respectively for basal induction, and 4 and 12 fold when comparing efficacy to the low [GR] condition. Furthermore, potency increased 650 and 2600 fold for the med [GR] and high [GR], respectively.

Furthermore, work by Robertson [1] demonstrated the effects known as positive cooperative ligand binding by means of whole cell saturation binding. In these experiments, increasing GR

Stellenbosch University https://scholar.sun.ac.za

concentrations resulted in a decrease in the concentration of ligand required for half maximal binding (K_d) from 49.1 nM, 23.9 nM to 16.8 nM for the low [GR], med [GR] and high [GR], respectively, indicating an increase in ligand binding affinity as the GR concentration increased. Simultaneously, Hill slope data increased from a minimum of 1.08 at low [GR] to 1.72 at the high [GR] concentration, indicating positive cooperative binding at higher GR levels.

Using flag-tagged hGR and GFP-tagged GR, Robertson and colleagues [1] also convincingly demonstrated the spontaneous dimerization of the GR in the absence of the ligand dexamethasone at higher concentrations. These interactions were further confirmed by FRET analysis, showing a statistically significant increase in GR dimerization prior to ligand addition at higher GR concentrations. Specifically, the presence of dimeric GR increased from 37% for the low [GR] condition, to 60% and 63% for the medium [GR] and high [GR], respectively.

Taken together, these findings suggest that an increase in GR concentration results in an increase in the number of GR oligomeres present in the cell at a given moment, and increases the sensitivity of cells and therefore tissues to GC stimulation and may therefore account for the tissue-specific differences in ligand sensitivity. From these results, Robertson and colleagues [1] proposed the following model to describe concentration dependent GR dimerization (**Fig. 2.6**).

Of note, the GR can exist as either monomer or dimer and is capable of binding the ligand in either of these conformations. Ultimately, whether by the ligand independent dimerization pathway (**Fig. 2.6 C and D**), or by the ligand dependent pathway (**Fig 2.6 A and B**), both pathways are capable of producing a final product of ligand bound to a GR homodimer and the overall reactions must therefore have the same Gibbs free energy value. By extension, the products of the K_d of each individual step in the specific pathway should be equal to the K_{eq}.

Stellenbosch University https://scholar.sun.ac.za

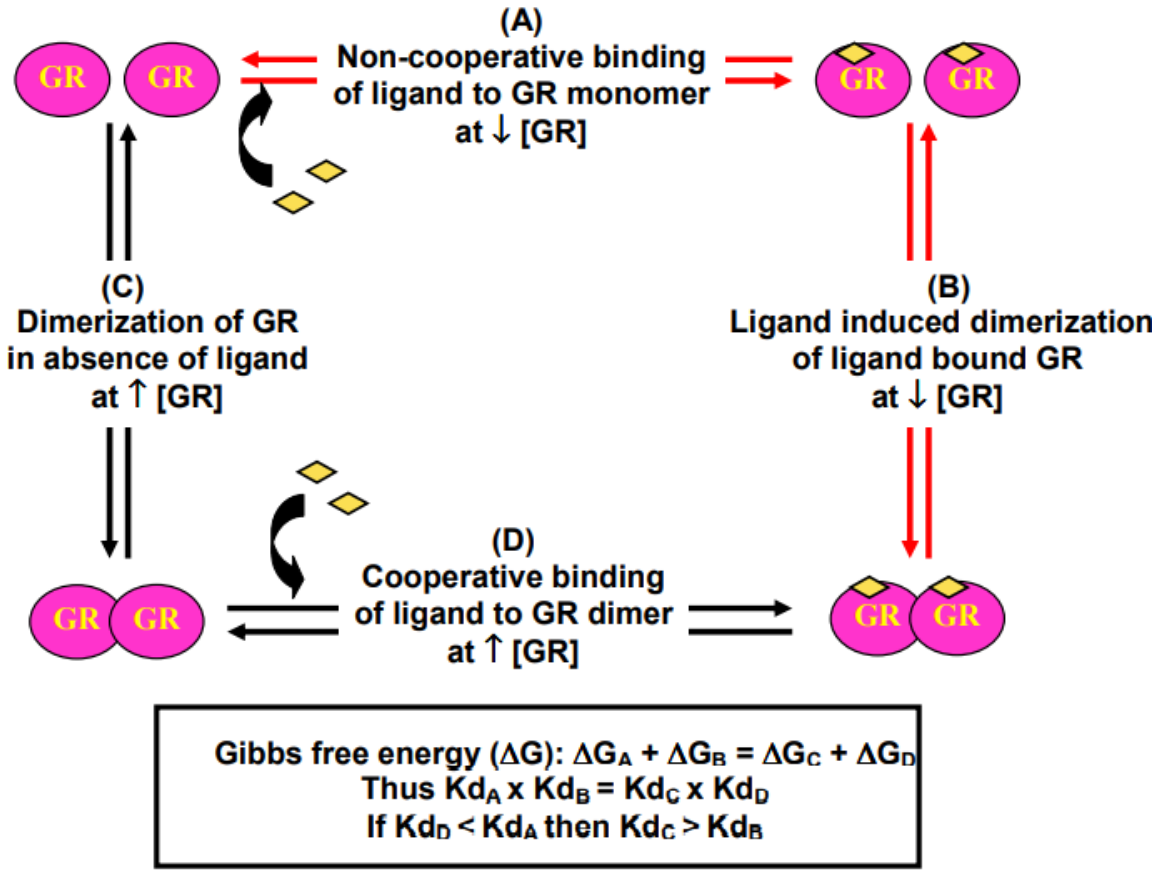

Figure 2.6: The concentration dependent GR dimerization model. In this model, the **A**) and **B**) pathways occur at low GR concentrations and are ligand dependent. The pathway illustrated by **C**) is at high GR concentrations at which the GR-monomer/GR- dimer equilibrium favours the homo dimer form. Ligand independent dimers pathway (**D**), present with a greater affinity for ligand and present with cooperative binding, thereby priming the cell for activation by low levels of GCs. From Robertson *et al.* [1].

Further work by Barry [2] sought to simulate the hGR dimerization cycle in the presence of the GR agonist dexamethasone *in silico* using laboratory based experiments. This project was able to replicate shifts in K_d particularly in step C of the independent dimerization model (**Fig. 2.6**) with the K_d increasing 13 fold in comparison to step D of the same model. Suggesting a conformation change in the GR molecule which drastically increases the affinity of the protein for its ligand. and suggested that differences in the K_d are dependent on concentration dependent shifts in the k_{off} while the k_{on} remained virtually constant [2]. This suggested that with increasing concentrations of the GR, the likelihood of the ligand escaping the ligand binding pocket is greatly reduced.

Stellenbosch University https://scholar.sun.ac.za

2.4: Biological functions of the GCs

The GR is a ubiquitous protein and influences the activity of nearly every cell in the body, with approximately 10% of genome expression being in some way influenced by GR activity. It is therefore implicated that the GR plays a major role in the regulation of various important physiological functions [30].

2.4.1 Metabolic effects

The GCs play an active role in glucose metabolism and this function is expanded upon below. The presence of high GC concentrations is in normal physiology accompanied by a marked increase in blood glucose concentration when the body has an increased requirement for energy. As such the affected systems all highlight a decreased ability in uptake of glucose while simultaneously promoting gluconeogenesis [32].

For example, in the liver, GCs act upon hepatocytes to induce gluconeogenesis from glucogenic amino acids, lactate and glycerol-3-phosphate derived from amino acids, while glycogen synthesis is simultaneously impeded. In skeletal muscle tissue, the GCs inhibit the uptake of and oxidation of glucose, ultimately reducing glycogen storage. The GCs also promote the breakdown of muscle for amino acid precursors required for gluconeogenesis. In white adipose tissue, the GCs similarly inhibit glucose uptake and oxidation, and furthermore activate lipolytic pathways to provide glycerol for gluconeogenesis requirements [34]. In the pancreas, the GCs inhibit insulin secretion by acting upon pancreatic $\boldsymbol{\beta}$-cells while conversely increasing glucagon hormone secretion by pancreatic α-cells. The negative effects of excessive glucocorticoid secretion on the glucose homeostasis are particularly highlighted in the state of insulin resistance brought about by obesity and hyperglycemia [35].

2.4.2 The effects of GCs on the immune system

We discuss three of the most important effects of GCs on innate immune response below.

Stellenbosch University https://scholar.sun.ac.za

Firstly, GCs are capable of inducing apoptosis in mature dendritic cells, which play a role as a liaison between the innate and adaptive immune system. In turn, the effect of the GCs on the dendritic cells allows for the prevention of pro-inflammatory responses, while simultaneously sparing the innate immunity of the patient [5]. GCs also minimise neutrophil migration to pro-inflammatory markers by repressing the ability of neutrophils to express pro-adhesion molecules. Simultaneously, GCs activate macrophage activity to increase the phagocytosis of neutrophils. This two-pronged approach ultimately limits the damage of neutrophils in autoimmune diseases by limiting the production of pro-inflammatory markers [5]. Finally, In T-Cells, the GCs are known to also induce apoptosis, preventing the signalling of pro-inflammatory markers and preventing the activity of neutrophils in the target tissue and subsequent tissue damage [32].

In terms of the adaptive immune system, GCs are known to affect the activity of B lymphocytes. In particular, they affect the B cells in two remarkable ways. First, GCs suppress the ability of B cells to express antibody production. Secondly, GCs are able to lower the number of viable B cells by moderately affecting each step of the B cell life cycle. For example, GCs are known to decrease the activation of B cells, but also lower the expression of Bcl-2, an anti-apoptotic protein [2, 33]. GCs therefore exert strong effects on both the innate and adaptive immune response, and it is for these reasons that GCs and their various synthetic agonists are the most widely prescribed treatment for autoimmune and rheumatological disorders.

2.4.3 The stress response

One of the most important roles of GCs is as part of the stress response [15]. In response to threats to the organism, the amygdala is stimulated to send a stress response to the hypothalamus and engages the downstream HPA-axis. In the short term, this increase in GCs provides the body with an influx of available energy in the form of glucose [36]. In the modern

Stellenbosch University https://scholar.sun.ac.za

work environment, however, patients are often exposed to chronic stress responses which can result in pathologies reminiscent of patients suffering from Cushing's syndrome or as it is also known, hypercortisolaemia [37]. These pathologies may include heart disease, atrophy of the muscle, osteoporosis (due to GC induced osteoblast apoptosis), hypertension, type 2 diabetes and suppression of the immune system [38].

2.4.4 Cognition and arousal

GCs are noted for having a remarkable effect on the development of memories and brain plasticity. In patients suffering from Cushing's syndrome as well as in patients suffering from steroid dementia, the chronic exposure to high levels of GCs strongly affects the hippocampus, the prefrontal cortex and hypothalamus [14]. These tissues exhibit exceptionally dense GR distribution and play critical roles in learning and memory retention. Patients suffer various cognitive impairments, including deficits in working memory, attention, sustained concentration and a decline in occupational or academic performance.

Studies in rats with chronically administered corticosterone [17], demonstrated a marked decrease in corticosterone receptors, which include the GR, and revealed a substantial depletion of hippocampal cells, similar to those of aged rats. This observation has given rise to the hypothesis that increases in GC expression are related to aging and it has contributed to a growing body of evidence that chronic GC use may lead to neurodegenerative disorders such as Alzheimer's and Parkinson's disease [39].

In normal physiology, high stress events and consequently high GC concentrations, lead to the formation of flashbulb memories, which are clear memories strongly associated with the stressor. In contrast however, very low levels of GCs, such as those associated with boredom or drowsiness, negatively affect learning and memory retention [39]. For memory retention of subjects unrelated to the stressor, a participant is required to endure moderate levels of stress.

Stellenbosch University https://scholar.sun.ac.za

2.5: Pharmacology

2.5.1 Clinical use of the GCs

Though inflammation is a beneficial part of the immune response, uncontrolled inflammation is not and can be highly debilitating if not fatal to the patient. Diseases such as asthma for example, affect approximately 21.9 million adults and 8.9 million children in the U.S. alone. Furthermore, approximately 8.5 million Americans suffer from auto-immune diseases such as rheumatoid arthritis, type 2 diabetes and Grave's disease. According to the WHO approximately 20% of all deaths in the per year are attributable to sepsis, an auto-immune condition brought about by systemic infection. In the U.S. for example, sepsis affects approximately 700 000 patients each year with 30% of patients succumbing to the disease [10].

GCs are widely administered for the treatment of various inflammatory and auto-immune disorders, hematological cancers and following organ transplants to prevent negative inflammatory effects. These GCs are administered by a variety of means and can be applied as ectopic creams, in tablet form or as inhaled sprays [40]. They are able to exert pharmacological effects either through direct genomic interaction, or by means of indirect action. As mentioned previously, classical GR pathways refer to the genomic interactions of the GR with the DNA by transactivation or transrepression with transactivation effects being considered to be a direct genomic effect, requiring the direct interaction of the GR dimer with the genome. Transactivation is associated with many of the negative metabolic side effects of the GCs however, also with the anti-inflammatory gene expression of genes such as secretory leukocyte protease inhibitor (SLPI) and lipocortin 1 [41]. In contrast, one of the means by the GR is able to affect transrepression of pro inflammatory genes is by directly interacting with pro-inflammatory transcription factors such as NFκB and AP-1, sequestering the pro-inflammatory transcription factors in the cytosol and preventing the transcription of pro-inflammatory genes [41].

Stellenbosch University https://scholar.sun.ac.za

2.5.2 Side effects and selective GR agonists

The long term use of GCs is not without detrimental effects and patients vary significantly in their responses to GC treatment. The side effects are numerous and are often a consideration when administering the GCs for long term use. Commonly, the negative side effects of the GCs are associated with the classical path of transactivation, and particularly the metabolic effects which accompany gene activation. These include effects such as muscle wastage [42], hyperglycaemia and steroid induced diabetes [43]. Long term GC usage can also negatively affect concentration and memory formation, a condition known as steroid dementia. Furthermore, long term use of the GCs can lead to osteoporosis, brought about by the effects of the GCs on osteoblasts driven bone formation [44].

Classical treatment strategies such as with the potent GR agonist dexamethasone, indiscriminately activate both the transrepression and transactivation pathways of GC mediated stimulation. As most of the negative metabolic side effects are associated with the transactivation pathways of the GR homodimer, more recent treatment strategies have begun to place emphasis on the development of selective GR agonists/modulators (SEGRMs). An example is Compound A, a plant derived non-steroidal compound which limits GR transactivation by binding to the GR reversibly [45]. CpdA induces abrogation of GR dimers and as a result is unable to activate transactivation pathways via GREs, while simultaneously promoting the transrepression of pro-inflammatory genes via monomeric GR-Ligand complexes.

2.5.3 GC resistance

Resistance to GCs is also of concern. 25% of difficult-to-control asthma patients are resistant to GC treatment. Furthermore, approximately 30% of patients suffering from rheumatoid arthritis, lupus erythematosus and ulcerous colitis exhibit resistance to GC treatment.

Stellenbosch University https://scholar.sun.ac.za

Resistance is observed for each step of the activation pathway, in other words, resistance can occur prior to GR activation, due to deficiencies of the receptor itself, but also downstream of in the activation pathway due to affected target genes of the GC [10].

GC resistance may be associated with the activation of the splice variant GR-β in response to IL-2 IL-4, IL-8 and TNF-α mediated stimulation. The GR-β isoform inhibits GR-α activity by binding as a heterodimer to the GRE, inhibiting the anti-inflammatory gene expression. Peripheral blood mononuclear cells (PBMCs) in the airways of GC resistant asthma patients express significantly higher levels of the GR-β isoform than those of healthy subjects. This problem is compounded by the fact that the half-life of the GR-β is double that of the GR-α leading to a disproportionate accumulation in target cells. GR-β accumulation has been associated with GC resistance in patients suffering fatal asthma, as well as in nasal polyps, patients with nocturnal asthma and ulcerative colitis [46].

Another important factor for GC resistance can be attributed to the amount of available GR. GC resistance can be characterized as systemic or acquired, with the latter being characterised by its effect on GR levels in specific tissues or cell types. In many disease states, but also following GC mediated treatment, the available GR α pool available for activation by ligand decreases dramatically in acquired GR resistance [46]. The reduction in available GR is mediated on multiple levels, ranging from the methylation of the GRα promotor, nGRE regulation of the promotor leading to reduced transcription of the GRα, post transcriptional destabilization of the GRα mRNA and GRα regulation and ubiquination leading to degradation of the GRα protein. The level of GR concentration in a cell or tissue type, is therefore of utmost importance in considering treatment options for patients at risk of developing GC resistance [46]. Furthermore, post association of the GR with ligand, abnormalities in the immunophilins, RAP-46 and BAG-1 have been shown to prevent the GC induced apoptosis of mouse s49 leukaemia cells. Similarly Mutations in AP-1 and NFK-β transcription factors have also been implicated in disrupting the effects of the GR via tethering pathways [46].

Stellenbosch University https://scholar.sun.ac.za

2.6: Observation of the GR and tools

2.6.1 Dimerization variants of the GR

Currently, a major advantage for research into the kinetics underlying GR dimerization is the advancement of available GR variants for experimentation, especially in the mouse model. Various forms of the GR isoform occur naturally. However, the GRα is considered the prototypical form of the GR when it is discussed in related literature and is also the most transcriptionally active. Alternative forms of the GR such as the GRβ and GR**γ** for example, do play important physiological roles, both exerting dominant negative effects on GR regulated genes in glucocorticoid resistance studies [47].

A dimerization deficient mutant of the GR, GRdim, refers to a mutant form of the GR with a mutation within a 5 amino acid region of the DNA binding domain known as the D-loop (**Fig. 2.4**). The GRdim was originally reported as being unable to dimerize and therefore suggested to be able to separate the effects of transrepression from that of transactivation. Experimentation, however, suggests that the GRdim is in fact not incapable of dimerization, with our laboratory [8,49] as well as others [24] reporting varying degrees of dimerization. The GRdim is available for the mouse model with the A465T mutation [24].

In response to the work showing that the GRdim is capable of some degree of dimerization, Presman and colleagues [24]developed the novel monomeric form of the GR, GRmon for further experimentation. This variant of the mouse GR contains two mutations, one in the DBD at A465T as well as in the LBD at the location I634A. This GR variant has proven resistant to dimerization even at high concentrations (1 μM) of dexamethasone.

Stellenbosch University https://scholar.sun.ac.za

2.6.2 Shortcomings of the K_d as an indicator of drug target effectiveness

Historically, pharmacological drug affinity has been measured in terms of its equilibrium dissociation constant K_d as an indicator of ligand target occupancy under equilibrium conditions. However, recent years have seen an increasing recognition of the complexity of in vivo conditions, particularly due to large attrition rates of therapeutics from in vivo to in vitro experimentation, where reactions are rarely in a state of equilibrium [50,51]. More recently, a premium has been placed on successful drug discovery that emphasises the role of both the thermodynamics and the kinetics of drug target interactions and acknowledges the effects of conformational adaptation of drug targets to improve the residency time of the ligand on the protein of interest. This view is especially relevant to drug targets such as the GR, where receptor concentration directly affects the residency time of the ligand.

2.6.3 Fluorescence correlation spectroscopy

In this subsection we offer a brief overview of fluorescence correlation spectroscopy and its use in the observation of oligomers, furthermore, we discuss in particular the number and brightness method which can be used for the observation of receptor dimerization over time, thereby offering valuable insight into receptor kinetics.

Fluorescence correlation spectroscopy (FCS) refers to a family of microscopy techniques which are employed for the observation of dynamic molecular interactions in solution. A common characteristic of FCS is a small, clearly defined sample volume (in the order of femtoliters) and a monochromatic light source for excitation. As a result, a small number of molecules (approximately 10^3) diffuse through the observation volume in a given time and allow for the observation of fluctuations in fluorescent signal strength following laser excitation, while minimizing background noise [52]. In practice, FCS techniques are advantageous as hardware requirements are affordable for most institutions. FCS can be subdivided into further

Stellenbosch University https://scholar.sun.ac.za

techniques, the most relevant of these the Number and Brightness technique developed by Digman *et al.* [3] for the accurate estimation of oligomerization state of fluorophore-tagged proteins of interest within living cells. This technique, as well as the basic principles underlying FCS in general, are further expanded upon in Chapter 4.

In conclusion, this chapter has encapsulated a basic overview of the structure, biosynthesis and the complex mechanisms of delivery of the GCs to target cells. Furthermore, the chapter has highlighted the interplay between the GCs and their cognate receptor, the GR, in effecting various physiological outcomes, whether normal, or pathological though the complex modulation of gene transcription. The chapter in particular highlighted an overlooked aspect of GC action, that of GR concentration, a topic which may yet hold serious implications in pharmacological applications as GR concentration is strongly implicated in modulating GC effectiveness in various tissues and disease states. We finally briefly introduced the number and brightness method, a novel method with which to describe the underlying kinetic data of receptor dimerization and elucidate the effects of increased GR concentration on ligand residency time described by the k_{off}.

In the next chapter, a method for producing COS-1 cells transfected with eGFP-tagged GR of physiologically relevant concentrations is demonstrated and provides practical information for when considering initial transfection concentrations and cell harvest times. After this, chapter 4 incorporates the information gained in these experiments as a means to optimize a single cell experimental system using COS-1 cells of physiologically relevant concentrations while observing the oligomerization of fluorescently tagged mGR proteins under different conditions over time. Finally, the conclusions of this dissertation are summarized in chapter 5.

Stellenbosch University https://scholar.sun.ac.za

Chapter 3

Optimizing transfection conditions for the Number and Brightness assay

In this chapter the transfection profile over time of the mouse GR variants: mGRwt, mGRmon and mGRdim is explored in depth. The chapter begins by first expanding upon the rationale for the methodology of the experiment. Next the chapter introduces the results and places the results into context. In particular, the potential uses of these findings in the field of GR kinetic studies, and potential shortcomings introduced by the use of the traditional assumptions of transfection is emphasized. Finally, the relevance of the results obtained in this chapter for further experimentation is examined.

3.1 Introduction

The central objective of this research project is the quantification of the rate of GR dimerization at increasing concentrations of mouse GR.

To approach this, the literature as well as unpublished work from our laboratory was screened to determine the range of endogenous GR concentrations, which exist in both normal and perturbed physiology. In addition, a method for duplicating these GR concentrations in an experimental system was investigated [49].

A review of the literature on the physiologically relevant concentrations of GR indicated that expression values ranged from as little as 4.1 fmol GR/mg protein in peripheral blood mononuclear cells (PBMCs) [53] to as much as 16200 fmol GR/mg protein in epithelial stem cells (cytotrophoblasts) [57,58]. In addition, fluctuations in GR concentration are not only found in the same healthy tissue biopsies [56,57], but also when comparing healthy tissues of different individuals. Furthermore, comparing healthy to diseased tissues, such as in those

Stellenbosch University https://scholar.sun.ac.za

affected by cancer [7], indicate significant differences in GR expression. A clear example is the increase in GR expression from 893 fmol GR/mg protein in healthy skin to 4663 fmol GR/mg protein in biopsies of skin with Kaposi's sarcoma in AIDS patients.

Prior to the current study, a model containing a range of physiologically relevant GR concentrations was developed by Robertson *et al.* [49], which selected and optimized a system of human GR (hGR) expression in the COS-1 cell line. The cell line in question was selected on the basis that it is inherently deficient of the GR protein [49]. The authors transfected $2x10^6$ COS-1 cells per 10 cm plate with the human GRwt and GR dim (hGRwt and hGRdim) variants at 40 ng, 400 ng and 12000 ng of plasmid DNA, followed by saturation ligand binding to determine the concentration of GR (fmol GR/mg total protein). An average transfection efficiency of 20% was estimated by fluorescence spectroscopy as the constructs were tagged with GFP. With transfection efficiency of 20% considered and applied to the observed protein concentrations, the original transfections of 40, 400 and 12000 ng DNA (designated low, medium and high, respectively), produced 3 statistically different GR concentration cell subpopulations ranging from 335 to 1420 fmol GR/mg protein [49].

This spectrum of GR concentrations obtained by Robertson *et al*. [49] was argued as being physiologically relevant. For example transfection of low (40 ng DNA) concentrations of mGRdim and mGRwt expressing plasmid produced 209 and 335 fmol GR/mg protein respectively, which equates to the expected expression observed in mononuclear white blood cells of 191 fmol GR/mg protein [12].The transfection of medium (400 ng DNA) concentrations of mGRdim and mGRwt, producing 721 and 763 fmol GR/fmol respectively, were shown to correlate closely with the GR expression of 893 fmol GR/mg protein in healthy skin [7]. Finally, the transfection of high (12000 ng DNA) concentrations of the mGRwt expressing construct, expressing 1420 fmol GR/ng protein, was found to be satisfactorily below the range of 4663 fmol GR/mg protein observed in biopsies of cancerous keratinocytes in AIDS-related Kaposi's sarcoma [7] and certainly below the 16200 fmol GR/mg protein in healthy cytotrophoblasts

Stellenbosch University https://scholar.sun.ac.za

(epithelial stem cells) observed in normal physiology [54].

Using these three distinct GR concentration containing populations, Robertson *et al.* [49], performed saturation ligand binding with tritiated dexamethasone and revealed positive cooperative ligand binding, with Hill slopes increasing from 1.08 to 1.72 as the GRwt concentration increased. In addition, these studies revealed an increasing affinity of the GRwt for the ligand dexamethasone, with K_d values for ligand binding decreasing from 49.1 to 16.8 nM as the GRwt concentration increased [8]. In contrast, the Hill slope and binding affinity was not significantly affected by increasing concentrations of the GRdim variant.

Having shown positive cooperative ligand binding (Hill slope > 1) at the higher levels of GR expression [8], an attribute which would require more than one binding site, further experimentation was done by Robertson *et al*. [8] to evaluate the ligand independent dimerization potential of the GR at increasing concentrations. The FRET technique using YFP and CFP tagged human GR constructs, which were co-transfected at the low, medium and high GR levels, produced similar GR expression levels when compared to their untagged human GR expressing counterparts. To maintain internal consistency during FRET, cells with low, medium or high transfections of GR were scrutinized individually for their fluorescence intensity and were observed to produce statistically different CFP-GR relative intensity values after 30 min of dexamethasone stimulation. Subsequently, Robertson *et al.* [8] defined these GR populations as low ranging between 0-600 rlu (relative light units), medium between 600-1200 rlu and high >1200 rlu. Using these definitions, FRET data was used to establish ligand-independent dimerization, which increased progressively with increasing GR concentration.

To further investigate the role of ligand independent ligand dimerization, Robertson *et al.* [8] made use of Flag tagged GRwt in conjunction with GFP-GR. Remarkably, it was found that in control samples treated with the solvent (ethanol), dimerization of the GR increased significantly when compared to the low and medium GR concentrations. Furthermore, it was

Stellenbosch University https://scholar.sun.ac.za

observed that high and medium GR concentrations had reached a level of maximal dimerization prior to being stimulated with dexamethasone. It was also found that the GRdim was able to partially dimerize at higher concentrations of the GR, suggesting that the construct is indeed dimerization impaired as opposed to entirely dimerization deficient [8].

The work by Robinson *et al.* [8] generated further questions regarding the mechanisms underlying ligand-independent dimerization and in particular its effects on the K_d of ligand binding were highlighted. The equilibrium constant K_d, in addition to being an indicator of ligand binding affinity, also comprises of the kinetic descriptors k_{on} and k_{off} with $K_d = k_{off}/k_{on}$. Briefly described, k_{on} refers to the second order rate constant, which describes the rate at which the binding reaction between the protein and ligand occurs in $M^{-1} \cdot s^{-1}$. In contrast, the first order rate constant k_{off}, measured in s^{-1}, describes the life span of the ligand protein complex and can by extension be used to determine both the mean lifetime and half-life (t½) of the complex [8,50,58]. Both the k_{on} and k_{off} are therefore essential descriptors of duration of receptor activation and ligand residence time and have become especially useful in pharmacological fields for the evaluation and development of compounds in open biological systems susceptible to progressive ligand removal [51,59].

In order to describe the effects of increased GR concentrations on these kinetic parameters and to produce an effective time dynamic *in silico* model incorporating ligand-independent dimerization, Barry [2] endeavoured to improve upon the use of the whole cell binding technique (WCB) by combining WCB with fluorescence activated cell sorting (FACS) to observe the effects of increased GR concentration of the human GRwt and human GRdim expressing constructs. The coupling of these techniques could hypothetically allow the concentration of GR in the chosen cells to be more tightly controlled than in the Robertson study [8] by selecting only for cells of a known concentration at a far greater accuracy than previously possible. This could result in a greater resolution of not only the K_d, but also the underlying k_{on} and k_{off} kinetic parameters. A crucial feature of the study by Barry's study was

Stellenbosch University https://scholar.sun.ac.za

the use of a standardised eGFP tag attached to the hGRwt and hGRdim constructs, allowing for the use of the fluorescent signal as proxy for GR expression [24].

This fluorescent tag permitted the translation of previous CFP (Fdon: fluorescent donor) emission values, used to determine the definitions of low, medium and high GR expressing cells in the FRET work of Robertson *et al.* [8], to be unambiguously translated to FACS. The CFP-GR low (40 ng), medium (400 ng) and high (12000 ng) groups, providing CFP Fdon measured in relative light units (rlu) values of 0-600 rlu, 600-1200 rlu and >1200 rlu respectively, were thus translated to the eGFP-human GR system. Here transfection with 40 ng, 400 ng and 4000 ng DNA of GFP-GR expression plasmid DNA provided low values for a signal strength from $10^{2.5}$ to $10^{3.3}$, medium values $10^{3.3}$ to $10^{4.2}$ and high equivalent expression for values above $10^{>4.2}$ of relative FITC-A forward scatter [6]. Hereafter these definitions for the FACS system will be referred to as low (40 ng), medium (400 ng) and high (4000 ng) concentrations of DNA. Using this system, sorting for WCB was, however, shown to be problematic due to mechanical stresses on the transfected cells and the inability to provide sufficient population sizes for the envisioned experimental procedure. As a result, unsorted populations transiently transfected at low, medium and high plasmid DNA concentrations were used to determine the kinetic parameters of k_{on}, k_{off} and K_d for each GR plasmid concentration. However, the ability to scrutinize the transfected cellular populations by FACS and the process of optimization provided insights into both the mechanism of transfection efficiency and the distribution of transfected cells into subpopulations. Specifically, Barry [2] determined that transient transfection with the human GR produces a peak transfection efficiency at 48 to 72 hours after transfection, which scales with the initial plasmid DNA concentration. In addition, his results suggested that the transfected populations are not homogenous with respect to GR expression. Instead, the transfected populations reorganise into subpopulations of increasing GR concentration in a fixed ratio when only the transfected population is observed.

Stellenbosch University https://scholar.sun.ac.za

3.1.1 Aims

Aim 1: Investigate parameters affecting the global transfection efficiency (TE):

To achieve this aim, mouse eGFP tagged constructs, mGRwt, mGRdim and mGRmon were used, with the eGFP tag as a proxy for GR levels in each individual cell.

Objective 1: Investigate the effect of GR plasmid concentration and GR variant on global TE: As per definition by Barry [6], cells were transiently transfected at either low (40 ng), medium (400 ng) or high (4000 ng) concentrations of plasmid DNA. Cells were then analysed by means of FACS to establish the degree of global transfection using the definition of a transfected cell (above a FITC-A reading $10^{2.5}$) as established by Barry [2].

Objective 2: Effect of time after transfection on global TE**:**

This objective is to observe the effects of time on the global transfection efficiency for the different constructs. In this instance attention was given to the initial transfection concentration i.e. 40, 400 or 4000 ng of plasmid DNA as well as the specific mouse GR construct transfected. Global transfection efficiency was analysed over a 120 hour period at 24 hour intervals following transfection. Comparisons were used to determine the similarities in transfection behaviour between the various constructs.

Aim 2: Investigate the distribution of GR expression levels (low, medium and high) of cells transfected with different concentrations of GR plasmid DNA and GR variants.

The second aim of this study was directed at the distribution of the GR expression levels of cells within the transfected population to determine whether transfected cells produce homogenous subpopulations of comparable GR concentration. Specifically, the cells scrutinized for GR concentration included not only transfected cells but also the non-transfected fraction of the population. Two objectives were therefore two-fold:

Stellenbosch University https://scholar.sun.ac.za

Objective 1: Investigate relative distribution of GR concentration subpopulation expression levels relative to the total cell population.

Objective 2: Investigate absolute distribution of GR concentration subpopulation expression levels relative to the transfected cell population

To achieve these objectives, the eGFP-tag was again used as a proxy for GR concentration in COS-1 cells transfected with mGRwt, mGRdim and mGRmon expressing plasmids at increasing concentrations (40, 400 and 4000 ng DNA, respectively). Furthermore, to include the effect of time readings will be taken for a period of 120 hours following transfection, at 24 hour intervals. Cellular expressed GR concentration were analysed for fluorescent intensity and defined as either high, medium or low expression in terms of the definitions proposed by Barry [6], where low, medium and high GR concentrations were observed at $10^{2.5\text{-}3.3}$, $10^{3.3\text{-}4.2}$ and $10^{>4.2}$ relative FITC-A forward scatter, respectively.

3.2 METHODS

3.2.1 Cell Culture

Monkey kidney fibroblast cells (COS-1 cells) obtained from ATCC (Virginia USA), were cultured in supplemented DMEM containing 44 nM of sodium bicarbonate and 1 mM sodium pyruvate, all of which were purchased from Sigma Aldrich (St Louis, Missouri, USA). Supplemented DMEM also contained 10% (v/v) fetal bovine serum (FBS), 100 g/mL streptomycin as well as 100 IU/mL penicillin, purchased from Merck (Darmstadt, Germany). Cells were maintained at a pH of 7.4, 37˚C with 5% CO_2. Passage numbers ranged from 14 to 30. Cells were regularly tested for mycoplasma infection and only mycoplasma negative cells were used.

Stellenbosch University https://scholar.sun.ac.za

3.2.2 Plasmids

The mouse GR variants pEGFP-GR (mGRwt), pEGFP-GR^{A465T} (mGRdim) and pEGFP-GR$^{A465T/I634A}$ (mGRmon), were a kind gift from Martin Stortz (Universedad de Buenos Aires, Buenos Aires, Argentina). The eGFP-mGR^{A465T} was generated form pEGFP-mGR by means of site directed mutagenesis by Top Gene Technologies (Quebec). Mutation of the variant pEGFP-mGR$^{A465T/I634A}$ was generated by site directed mutagenesis by the Stony Brook Cloning facility (Stony Brook University, New York, USA) [60]. The empty pGL2-basic vector was purchased from Promega (Madison, USA). Plasmid purification was performed by use of the Nucleobond®Xtra Maxi plasmid extraction kit according to the manufacturer's instructions. Plasmid identity was confirmed through the use of restriction enzyme digests. All GR plasmid variants were digested by means of *Sal-1* digestion, while digestion of pGL2-Basic was performed by using *BamH1* purchased from Fermentas (Waltham, USA). Only supercoiled plasmid DNA was used for transfection.

3.2.3 Transfection

For transfection, the diethylaminoethyl (DEAE)-dextran method [60] was used: 10 cm plates were seeded with 1x10^6 COS-1 cells/plate, 24 hours prior to transfection. Cells were incubated in supplemented DMEM at 37˚C. The following day, the medium was aspirated and a transfection mix, consisting of unsupplemented DMEM with 1% DEAE (v/v) and 0.1mM chloroquine, was added. The total plasmid DNA amount was kept at 4000 ng and the transfection mix was applied for 4 hours. DNA mixtures contained the mouse GR expressing constructs pEGFP-GR, pEGFP-GR^{A465T} and pEGFP-GR$^{A465T/I634A}$ at 40, 400 or 4000 ng DNA (low, medium and high DNA concentrations, respectively). The pGL2-Basic was used as a non-expressing construct to ensure each transfection mix contained 4000 ng of total plasmid DNA. Following the 4-hour incubation period, the transfection mixture was replaced with 10% (v/v) DMSO (Sigma Aldrich) in PBS for 5 minutes. Finally, the DMSO mixture was replaced with supplemented DMEM for 24 hours.

Stellenbosch University https://scholar.sun.ac.za

3.2.4 Fluorescence activated cell sorting (FACS)

FACS was employed to determine global transfection efficiency as for the first aim, but also to determine the distribution for GR containing concentration subpopulation prevalence as for the second aim. GR presence was observed by use of the prosthetic eGFP-group attached to the mGRwt, mGRdim and mGRmon variants by means of the BD FACS Aria system (BD-Biosciences, San Jose, California, United States). Following transfection, cells were replated into 6-well plates at a density of $2x10^5$ cells per well. Untransfected COS-1 cells were used to differentiate between transfected and untransfected cell lines, whereas fluorescein isothiocyonate (FITC) beads (BD-Biosciences, San Jose, California, United States) were used as an internal standard to maintain sorting gate consistency. In all instances, time was considered as a factor. Collection times began 24 hours after transfection, with 24-hour collection intervals occurring to a maximum of 120 hours following transfection.

For the first aim, focus was given to the overall or global transfection efficiency of a sampled cell population of $10x10^3$ cells. In this instance cells were stimulated with a 488 nm laser to excite the eGFP tag inherent to the GR constructs to produce a green emission peak at 509 nm [61]. FITC signals registering above $10^{2.5}$ were selected as being successfully transfected [2].

For the second aim, attention was given to the concentration distributions of GR containing cell subpopulations. To this end, sorting gates were again selected to match previous work by Barry [6] and as such transfected cells were defined as having a FITC-A signal in excess of $10^{2.5}$. Low expression (low [GR]) was defined as populations with a relative FITC-A signal between $10^{2.5}$ to $10^{3.3}$. Medium expression (medium [GR]) was defined as FITC-A signals between $10^{3.3}$ to $10^{4.2}$. High expression was defined as FITC-A signal above $10^{4.2}$ (high [GR]). An example of this procedure is given in Addendum A.

Stellenbosch University https://scholar.sun.ac.za

The prevalence of low [GR], medium [GR] and high [GR] cell subpopulations was determined and presented in one of two ways: either as relative or as absolute distribution. Relative distribution was presented as a percentage of the transfected cell population, as was acquired directly from the FACS data. Absolute distribution presented the high [GR], medium [GR] and low [GR] subpopulations as a percentage relative to the total cell population and was calculated as follows:

$$(\text{Subpopulation\%}) \times (\text{Global transfection efficiency}) = \text{Absolute Subpopulation Distribution}$$

3.2.5 Statistical analysis

Statistical analysis was performed by means of Prism 5 (GraphPad) software.

For the first aim: The relationship between global transfection efficiency and time was determined by one-way ANOVA followed by Bonferroni's multiple comparison post-test. Two-way ANOVA followed by Bonferroni's multiple comparison test was employed to observe the relationship between different mGR variants, but also to determine the effects of time on observed global transfection efficiency. To perform linear fit for transfection efficiency, plasmid concentrations were first transformed logarithmically after which a linear fit was performed using GraphPad Prism software. Predictive capability was determined as an R-Squared value for the straight line function using Graph-pad Prism software.

For the second aim: mGR concentration subpopulations of different mGR plasmid variants were compared using one-way ANOVA followed by Bonferroni's multiple comparison test for each time point.

To determine the relative mGR concentration subpopulation distribution within the transfected population (relative distribution) as well as the distribution of subpopulations within the entire cell population (absolute distribution), the underlying subpopulations were compared according to their subpopulation class by one-way ANOVA followed by Bonferroni's multiple

Stellenbosch University https://scholar.sun.ac.za

comparison post-test.

In all instances, values of $p<0.05$ were deemed statistically significant whereas values of $p<0.005$ and $p<0.001$ were deemed highly significant.

3.3 Results

3.3.1 Initial plasmid DNA concentration affects the observed global transfection efficiency irrespective of mGR construct employed

To investigate the parameters affecting global transfection efficiency (Aim1) the first objective was to investigate the effect of mGR plasmid concentration and mGR variant.

Initial consideration of only the mGRwt construct at increasing initial transfection of high, medium and low concentrations of plasmid DNA over a total time span of 120 hours following transfection (**Fig. 3.3.1 A**) revealed that irrespective of the initial plasmid DNA concentration, the initial global transfection efficiency (the percentage of cells transfected in the total cell population) increased rapidly from 24-48 hours and was statistically significantly ($p<0.05$). From 48 hours onwards, the transfection efficiency plateaued up to the 120 hour time point.

Comparison of global transfection efficiencies at 48 hrs indicated a statistically significant ($p<0.01$) increase in the mGRwt global transfection efficiency from 12% at low, to 28% at medium and 41% at high plasmid DNA concentrations (**Table 3.1**). In similar fashion, scrutiny of global transfection efficiency trends for the mGRdim (**Fig. 3.3.1 B**) and mGRmon (**Fig. 3.3.1 C**) constructs closely correspond to those observed for the mGRwt with a significant ($p<0.05$) increase in transfection efficiency as the mGR plasmid DNA concentration increased (**Table 3.1**).

The constructs under investigation contain the same peGFP plasmid backbone and vary only in terms of the final expression of an mGR variant that differs due to individual amino acid

Stellenbosch University https://scholar.sun.ac.za

substitutions [14]. When differences in the global transfection efficiency of the mGR variants were compared at equivalent concentrations of plasmid DNA transfected (**Table 3.1**), no significant ($p>0.05$) differences in transfection efficiency between the mGRwt, mGRdim and mGRmon were observed suggesting that irrespective of the construct employed the transfection efficiency at a particular plasmid DNA concentration would be similar.

Having shown that the global transfection efficiencies of the constructs were not significantly different at the same concentration of plasmid DNA, it was therefore possible to generalise a ratio of global transfection efficiency relative to initial concentration of plasmid DNA transfected. Thus, despite the fact that the ratio of plasmid DNA transfected for low (40 ng), medium (400 ng) and high (4000 ng) was 1:10:100, the ratio of global transfection efficiency was only 1:2:2.8.

Table 3.1: Comparison of global transfection efficiency at 48 hrs of mouse GR variants at increasing concentrations of DNA plasmid transfected.

Transfection condition (ng DNA transfected)	% Average Global Transfection efficiency ± SEM, n=3		
	mGRwt	mGRdim	mGRmon
Low (40)	11.7 ± 3.1%^{ns}	14.5 ± 3.3%^{ns}	13.5 ± 5.0%^{ns}
Medium (400)	27.8 ± 6.4 %$^{ns;\ **}$	31.0 ± 6.2% $^{ns;\ *}$	33.3 ± 4.9% $^{ns;\ **}$
High (4000)	41.3 ± 7.3% $^{ns;\ ***}$	46.9 ± 7.7% $^{ns;\ **}$	45.9 ± 1.8% $^{ns;\ ***}$

COS-1 cells were transiently transfected with increasing concentrations of GR plasmid DNA of the mouse GR expressing plasmid variants, mGRwt, mGRdim and mGRmon. The eGFP tag was used as a proxy for GR expression, which was monitored by FACS and recorded at 48 hours. Presented are the AVG ± SEM of three independent biological repeats done in triplicate. Statistical analysis was performed by (1) Tukey's multiple comparison test comparing mGRwt to the mGRdim and mGRmon at a specific concentration of plasmid DNA, with "ns" representing non-significant statistical results or (2) by Dunnett's multiple comparison test comparing medium and high to low transfection condition within a GR plasmid variant with *= $p<0.05$, ** = $p<0.01$ and *** = $p<0.001$.

Stellenbosch University https://scholar.sun.ac.za

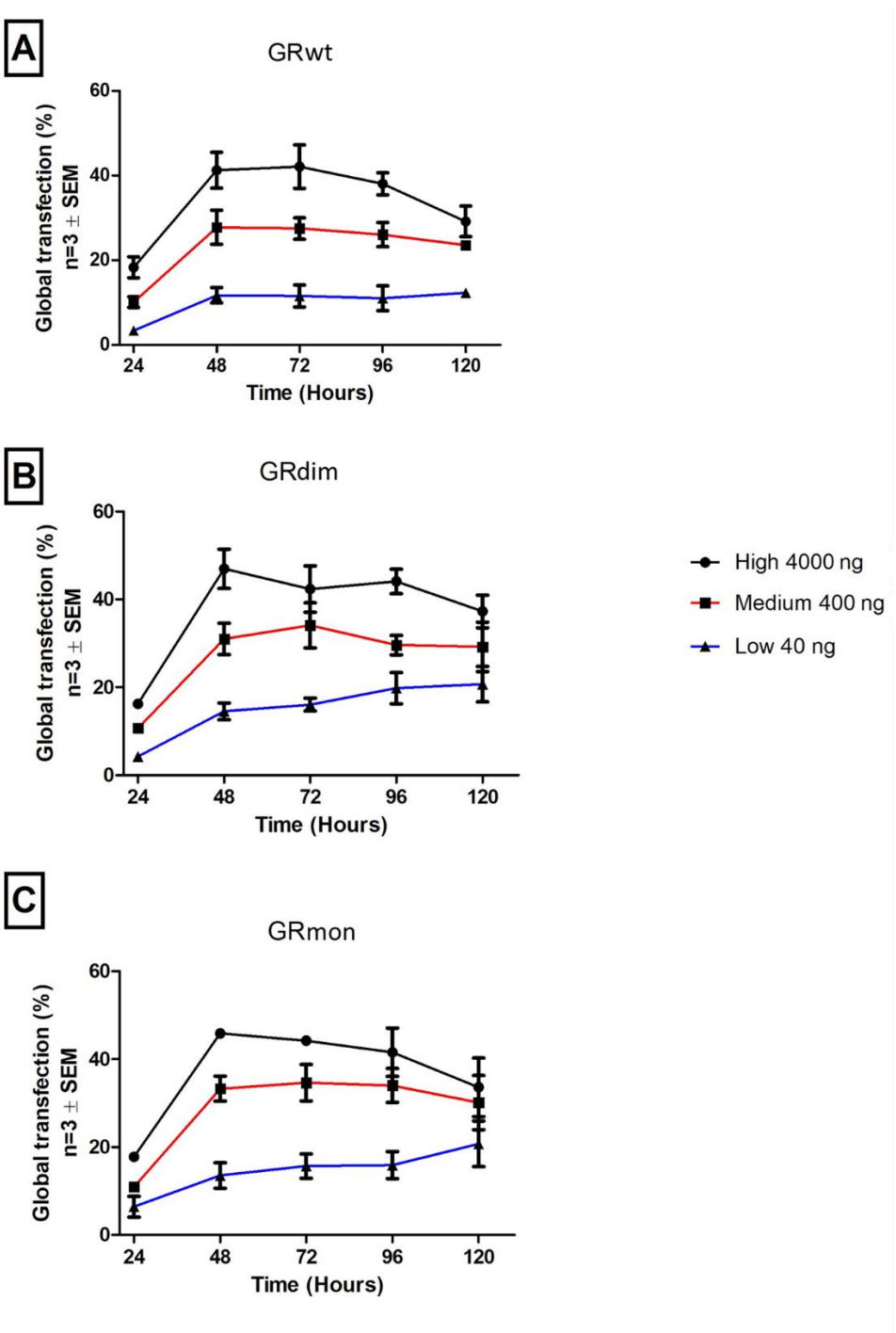

Figure 3.3.1: Global transfection efficiency following transfection with increasing concentrations of mGR expressing plasmids over 120 hours. A, **B** and **C** represent cells transfected with mGRwt, mGRdim and mGRmon, respectively at increasing GR concentrations. Black lines represent cells transfected at the high concentration (4000 ng), whereas blue and red lines represent cells transfected at concentrations of 400 and 40 ng GR plasmid DNA, respectively. Three biological repeats were performed per GR variant. Data was acquired from three biological repeats for each variant.

Stellenbosch University https://scholar.sun.ac.za

3.3.2 Time affects global transfection efficiency and is not reliant on plasmid variant under investigation

The second objective of Aim 1 considered the effects of time for each initial plasmid DNA concentration on global transfection efficiency.

Initial considerations accounted for the trends of the global transfection efficiency of the three different mGR constructs, the mGRwt, mGRdim and mGRmon at the high GR plasmid concentration (4000 ng plasmid DNA and **Fig. 3.3.2 A**). At this DNA concentration, all three constructs behaved in a similar manner, with an initial abrupt increase in global transfection efficiency from the 24 to 48-hour time period, which was maintained up to 96 hours. Thereafter, global transfection efficiency decreased substantially as the 120-hour time point was reached.

Next, the initial transfection concentration was changed to 400 ng plasmid DNA (**Fig. 3.3.2 B**). For all variants, a general trend emerged with global transfection efficiency increasing rapidly from the 24 to 48-hour time point as also seen with 4000 ng plasmid. Following this time point, the global transfection reached a plateau, which was mostly sustained up to the 120 hour time point. Finally, at a concentration of 40 ng plasmid DNA (**Fig. 3.3.2 C**) the initial increase in global transfection efficiency from 24-48 hours as seen with DNA plasmid concentrations of 4000 ng and 400 ng was once again observed. Interestingly however, and in contrast to previously mentioned results, the global transfection efficiency continued to increase until the 120 hour time point.

Two-way ANOVAs with Bonferroni's post-test considered the effects of both time as well as GR variant (Table 3.2).The GR variant had no statistically significant effect on the outcome of global transfection efficiency (all $p>0.05$). In contrast, time as a factor for affecting global transfection efficiency following the initial transfection, was shown to be highly significant ($p<0.0001$).

Stellenbosch University https://scholar.sun.ac.za

Overall, irrespective of initial transfection conditions, the mGR variant did not show any statistically significant influence on observed global transfection efficiency. In contrast, analyses consistently highlighted the effects of time as a significant factor in determining the global transfection efficiency (**Table 3.2**).

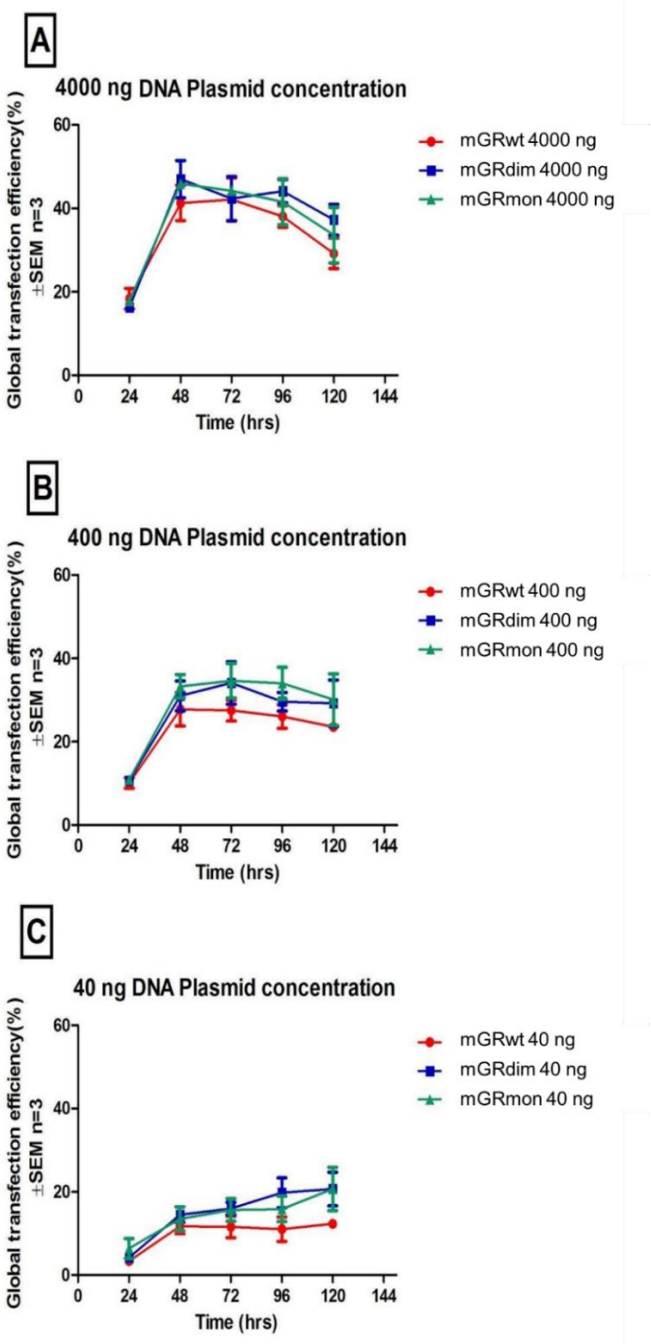

Figure 3.3.2: Effects GR variants and initial transfection concentrations on global transfection efficiency over a time period of 120 hours. Figures **A, B** and **C** represent transfection at either 4000, 400 or 40 ng of plasmid DNA respectively. The same experiments as per **figure 3.3.1** were used.

Stellenbosch University https://scholar.sun.ac.za

Table 3.2 Summary of statistical outcomes for factors affecting observed global transfection efficiency.

	Factors affecting global transfection efficiency	
GR plasmid Concentration	**mGR variants**	**Time**
4000 ng	n.s.	****
400 ng	n.s.	****
40 ng	n.s.	****

COS-1 cells were transfected with the mGR variants, mGRwt, mGRdim or mGRmon. Global transfection efficiency was recorded at 24 hour intervals up to a total time of 120 hours following initial transfection. Two-way ANOVA followed by Bonferroni's multiple comparisons test was used to elucidate the significance of either the factor of mGR variant, or time on the observed global transfection efficiency. Significance is indicated as "****" for $p<0.0001$ and "n.s." for not significant. The same experiments as per **figure 3.3.1** were used.

3.3.3 Observed global transfection efficiency is affected by time and can be defined as a logarithmic function of concentration

In the following sub-section, the observed global transfection efficiency of the GR constructs as depending on both time and initial plasmid concentration is described in an attempt to bring together the two objectives of Aim 1. GR behaviour in terms of global transfection efficiency was analysed only on the basis of plasmid DNA concentration as opposed to GR variant, as previous analysis showed that observed variant differences were not statistically significant.

When the GR variant values were pooled a trend of increasing global transfection efficiency from 5% at 24 hours, to a final maximum value of 18% at 120 hours was revealed for the low (40 ng) concentration of GR expressing plasmids (**Fig. 3.3.3**). Statistical analysis using one-way ANOVA followed by Bonferroni's multiple comparison test highlighted a statistically significant ($p<0.05$) increase in expression at all time points when compared to 24 hour expression.

The medium (400 ng) concentration of GR plasmids resulted in an increase in global

Stellenbosch University https://scholar.sun.ac.za

transfection efficiency from 11% at the 24 hour time point to a peak expression of 32% at the 72 hour time point, which gradually diminished to 28% at 120 hours. It is worth noting that the 48 hour time point produced a global transfection efficiency of 32%, a value higher than the global transfection efficiency observed for the low GR at both the same time point (14%) and the maximum global transfection efficiency of 18% observed at 120 hrs. Statistical analysis using one-way ANOVA followed by Bonferroni's by multiple comparison post-hoc test, indicates a statistically significant increase ($p<0.001$) in global transfection efficiency for all time points when compared to the 24 hour time point as also seen with the low concentration of GR (40 ng).

The high (4000 ng) concentration of GR plasmids transfected revealed an increase in the global transfection efficiency from 17% at 24 hours to a peak of 45% at the 48 hour time point. Subsequently, global transfection efficiency progressively decreased to 33% at the 120 hour time point. In comparison, the global transfection efficiency at the 48 hour time point of the high GR (45%) was higher than the 48 hour time point observed for the medium and low transfection conditions of 35% and 14%, respectively, and was also the highest global transfection efficiency observed for any transfection condition. Post-hoc analysis of the high GR transfection condition by one way ANOVA followed by Bonferroni's multiple comparisons test revealed significant ($p<0.001$) increases in the global transfection efficiencies of all other time points when compared to the 24 hour time point. However, statistically significant differences ($p<0.01$) were revealed when comparing the 48 hour transfection efficiency to that of the 120 hour group, as well as for the expression of the 72 hour point in comparison to the 120 hour time point. In both instances the 120 hour global transfection efficiency was lower.

To analyse the relationship between global transfection efficiency and logarithmically scaled plasmid DNA concentration linear regressions were performed. Linear regressions showed statistically relevant increases (24, 48, 72 and 96 hours $p<0.0001$; 120 hours $p<0.0002$) and produced strong positive slopes of increasing transfection efficiency with increasing plasmid DNA concentration in all instances, with R^2 values ranging from 87% at 48 hours, which

Stellenbosch University https://scholar.sun.ac.za

diminished to 43% at 120 hours.

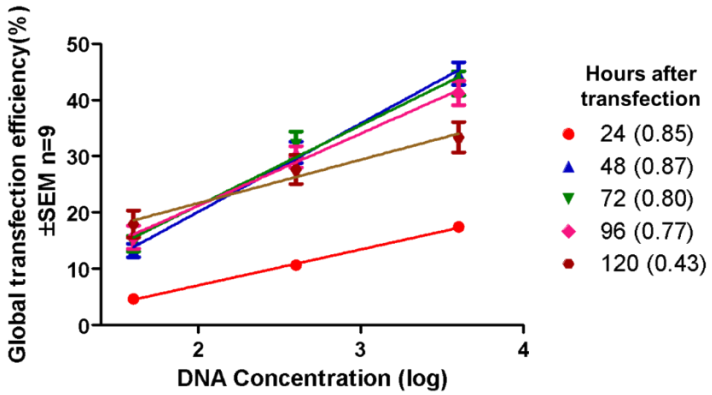

Figure 3.3.3: The relationship between time, initial plasmid DNA concentration (log ng) and observed mGR global transfection efficiency of pooled mGR variant values. COS-1 cells were transiently transfected with increasing concentrations (40, 400 or 4000 ng) of eGFP-GR expressing mGR. The eGFP-tag was used as a proxy for GR expression by means of FACS at 24-hour intervals for a period of 120 hours. Transformation of concentration data to logarithmic scale and linear regression analysis was performed using GraphPad Prism software. R^2 values are presented in brackets next to the indicated time point. The same experiments as per **figure 3.3.1** were used, with all variants pooled to increase statistical resolution.

3.3.4 Transfection of GR variants produces subpopulations with similar absolute levels of GR expression

To investigate the distribution of GR concentration subpopulation expression levels (Aim 2) in cell populations transfected at increasing GR DNA concentrations and to also optimize the FACS system for later number and brightness (N&B) experimentation (Chapter 4) the prosthetic eGFP tag attached to mouse variants of mGRwt, mGRdim and mGRmon was used as a proxy for GR expression. After transfection with either low (40 ng) medium (400 ng) or high (4000 ng) concentrations of plasmid DNA, cell populations were characterised as containing either low [GR], medium [GR] or high [GR] based on their reported fluorescence signal (FITC-A) and relative GR-containing subpopulation distribution (Aim 2, Objective 1) expressed as a percentage relative to the whole cell population (**Fig. 3.3.4**).

Stellenbosch University https://scholar.sun.ac.za

Initially, focussing on the 4000 ng DNA transfection concentration condition, the GR variants were compared in terms of the behaviour of their subpopulations, high [GR], medium [GR] and low [GR] at each time point (**Fig. 3.3.4 A**). Analysis by one-way ANOVA followed by Bonferroni's multiple comparisons test revealed no statistically significant ($p>0.05$) differences between the GR variants (mGRwt, mGRdim and mGRmon) at the high GR (4000 ng) transfection condition. Similarly, statistical analysis of the 400 ng DNA transfection concentration condition (**Fig. 3.3.4 B**) and the 40 ng DNA transfection concentration (**Fig. 3.3.4 C**), indicated that there were no statistically significant differences between the GR variants at each time point.

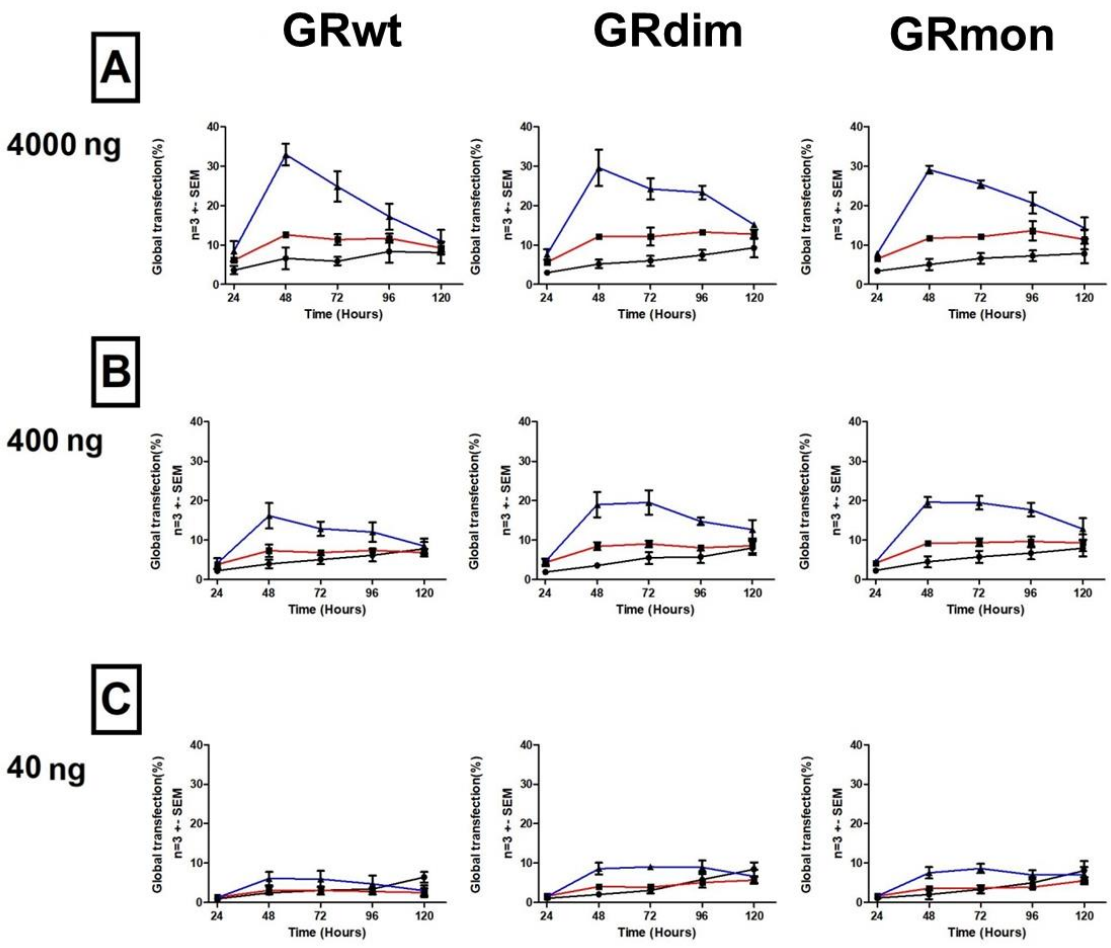

Figure 3.3.4: GR variants produce GR-concentration subpopulations with similar absolute GR expression. (**A**), (**B**) and (**C**) indicate transfection with 40, 400 or 4000 ng DNA of the eGFP-GR expressing variants mGRwt, mGRdim and mGRmon. High [GR], medium [GR] and low [GR] subpopulations are denoted by blue, red and black lines respectively. Three independent experiments were performed per GR variant.

Stellenbosch University https://scholar.sun.ac.za

Together, these findings indicate no significant differences between the GR variants in terms of their observed distribution into GR concentration expressing subpopulations, which suggests that, rather than the GR variant, the initial GR concentration is a determining factor in absolute distribution of GR concentration subpopulations. Therefore, for the following subsections GR subpopulation distributions were pooled for the GR variants and were considered in terms of initial GR plasmid concentration transfected, as opposed to GR subtype transfected.

3.3.5 Increasing GR plasmid DNA concentration affects the relative distribution of GR concentration subpopulations over time.

Having determined that GR variant did not affect GR concentration subpopulation distribution in the relative pool of transfected cells, we continued to evaluate which factors do (Aim 2, Objective 1), by evaluating results of pooled GR variant populations.

First the effects of time on GR concentration subpopulation relative distribution were investigated. For the 4000 ng GR plasmid DNA transfection condition, the effects of time on GR concentration subpopulation (**Fig. 3.3.5 A**) revealed the following: For the 24-hour time point, statistical analysis showed strong significant differences ($p<0.01$) between the low [GR] and medium [GR] , as well between the low [GR] and high [GR] subpopulations. However, the differences between the medium [GR] and high [GR] were not statistically significant. In contrast, the time intervals from 48-96 hours showed strongly significant differences ($p<0.01$) between all GR concentration subpopulations. By the 120-hour time point, however, the difference in distribution had weakened, and showed statistical difference ($p<0.05$), only when comparing the low [GR] to the high [GR].

Next, the distribution of absolute GR containing subpopulations of the 400 ng GR plasmid DNA transfection condition were analysed (**Fig. 3.3.5 B**). As for the 4000 ng condition, a rapid

Stellenbosch University https://scholar.sun.ac.za

statistically significant redistribution into distinct subpopulations was observed between the 24 to 48 hour time point with the high [GR] subpopulation, statistical differences between the subpopulation groups were not as pronounced as for the 4000 ng DNA concentration with statistical significance between groups being entirely lost by 120hours. Finally, the distribution of [GR] subpopulations of the 40 ng DNA transfection condition was investigated (**fig 3.3.5 C**). In comparison to the 4000 ng and 400 ng transfection conditions. The 40 ng transfection condition displayed a further diminishing of distribution into [GR] subpopulations, significant differences between groups lost entirely by 96 hours. All three concentration conditions showed a disproportionate presence for the high [GR] which was significantly higher than the low [GR] and medium [GR] in most instances.

In summary, irrespective of the initial transfection concentration or the time period in these experiments, transfection with the GR produced three distinct physiological GR containing groups low [GR], medium [GR] and high [GR] with the high [GR] commonly being most prevalent in most instances. Notably, higher transfection concentrations lead to higher transfection efficiencies whereas time affected peak transfection efficiency at 48hours.

Next, the relative distribution of GR concentration subpopulations and its relationship to the initial GR plasmid DNA concentration transfected was investigated (**Fig. 3.3.6**).
For the 24-hour time point (**Fig. 3.3.6 A)**, statistical analysis revealed that initial GR plasmid DNA concentrations transfected had statistically significant ($P< 0.05$) effects when comparing the prevalence of low [GR], medium [GR] and high [GR] subpopulations in terms of absolute GR concentration subpopulation expression. The greatest statistical difference observed in all cases was between the 40 ng and 4000 ng concentrations, with the 4000 ng concentration producing the higher percentage of the relative distribution in each instance. Increases in absolute population when increasing initial concentration from 40 ng to 400 ng were 3 fold for the low [GR], 4 fold for the medium [GR] and 5 fold for the high [GR], respectively.

Stellenbosch University https://scholar.sun.ac.za

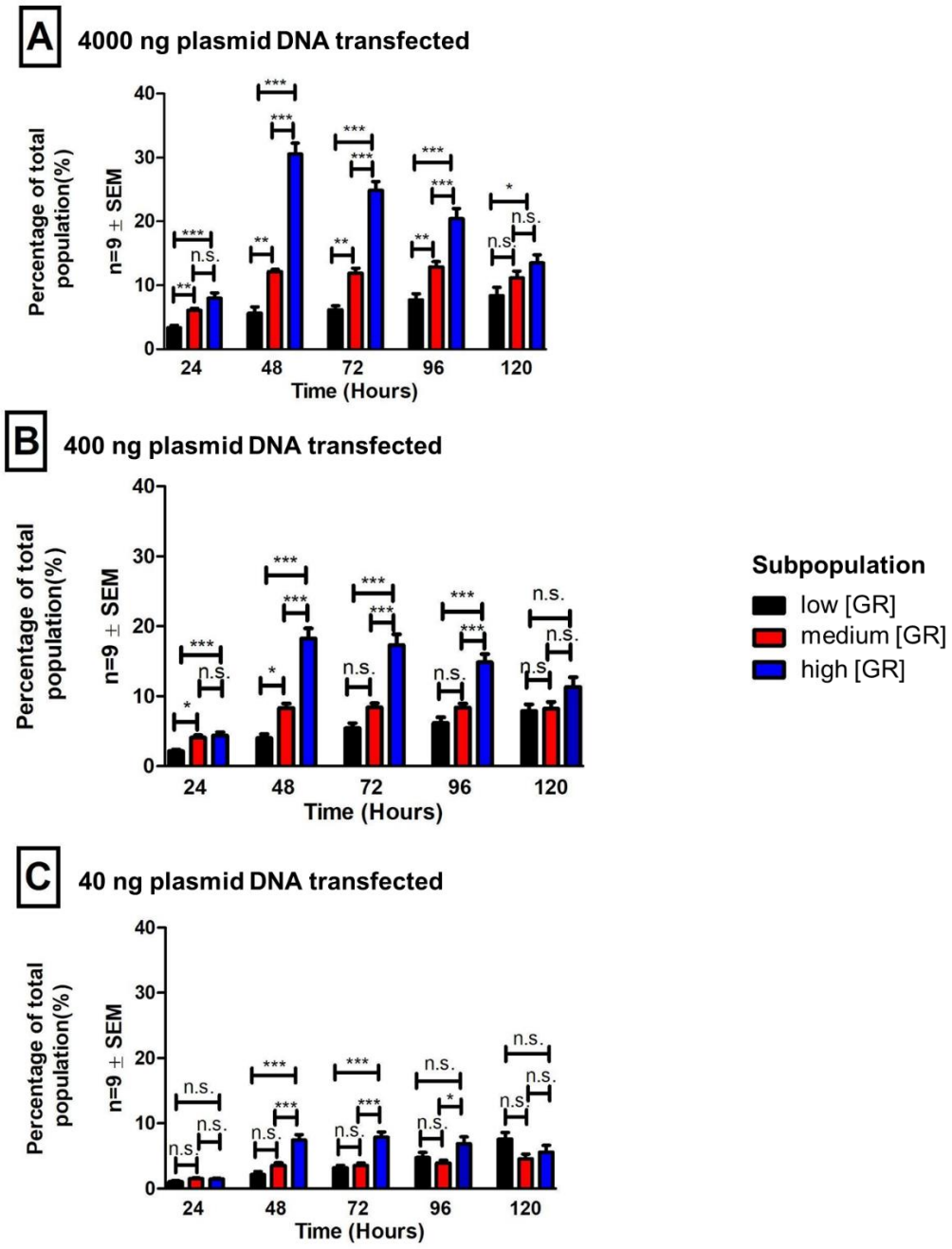

Figure 3.3.5: Time dependent comparison of relative subpopulation distribution patterns with increasing plasmid concentration. Pooled data for COS-1 cells transiently transfected with increasing concentrations of eGFP tagged mGR variant expressing plasmid DNA. Transfection concentrations of 4000 ng are represented by figure A, 400 ng by figure B, and 40 ng by figure C. Using the eGFP tag as proxy for GR expression, subpopulation distribution was evaluated and compared at each time point. Statistical analysis compared the low [GR], medium [GR] and high [GR]. ***, **, * and "n.s." represent statistically significant differences of ($p<0.001$), ($p<0.01$), ($p<0.05$) and not significant, respectively. Three independent experiments were performed per GR variant.

Stellenbosch University https://scholar.sun.ac.za

For the low [GR] subpopulation at 48 hours (**Fig. 3.3.6 B**), an increase in absolute population was observed for all subpopulations when compared to the 24 hour time point. However, increasing transfection concentration lead to a change in relative expression of the subpopulations. In all instances, the 4000 ng transfection condition expressed as a higher percentage irrespective of subpopulation, with differences between 40 ng and 4000 ng for the low [GR] being approximately two fold and the high [GR] populations for the same concentration approximately four fold.

From the 72 to the 120 hour time point. (**Fig 3.3.6 C-E**) the differences in expression between the 40, 400 and 4000 ng transfection conditions were mostly maintained, however, the proportional differences observed for the various subpopulations diminished as time progressed. Notably, by the 120 hour time point, no statistically significant differences were observed in the low [GR] population whereas the statistical significance in difference between the 40-4000 ng condition diminishes for the medium [GR] and high [GR] subpopulation.

Taken together, the trend over all time points indicated that transfection of the 4000 ng GR plasmid concentration condition resulted in a higher observed percentage of relative GR-concentration subpopulation expression. Furthermore, time was shown to affect the percentage of relative expression.

The relative distribution GR-concentration by subpopulation for the 48 hour time period was summarized in **Table 3.3**. The 48 hour time point was selected as it showed both the highest overall transfection efficiency, and also the highest absolute expression of the subpopulations low [GR] medium [GR] and high [GR]. Interestingly all three transfection concentrations(40, 400 and 4000 ng DNA respectively) produced statistically significant distributions of subpopulations of the GR. However, the 4000 ng condition also produced a higher overall transfection efficiency and therefore a higher absolute population of transfected cells.

Stellenbosch University https://scholar.sun.ac.za

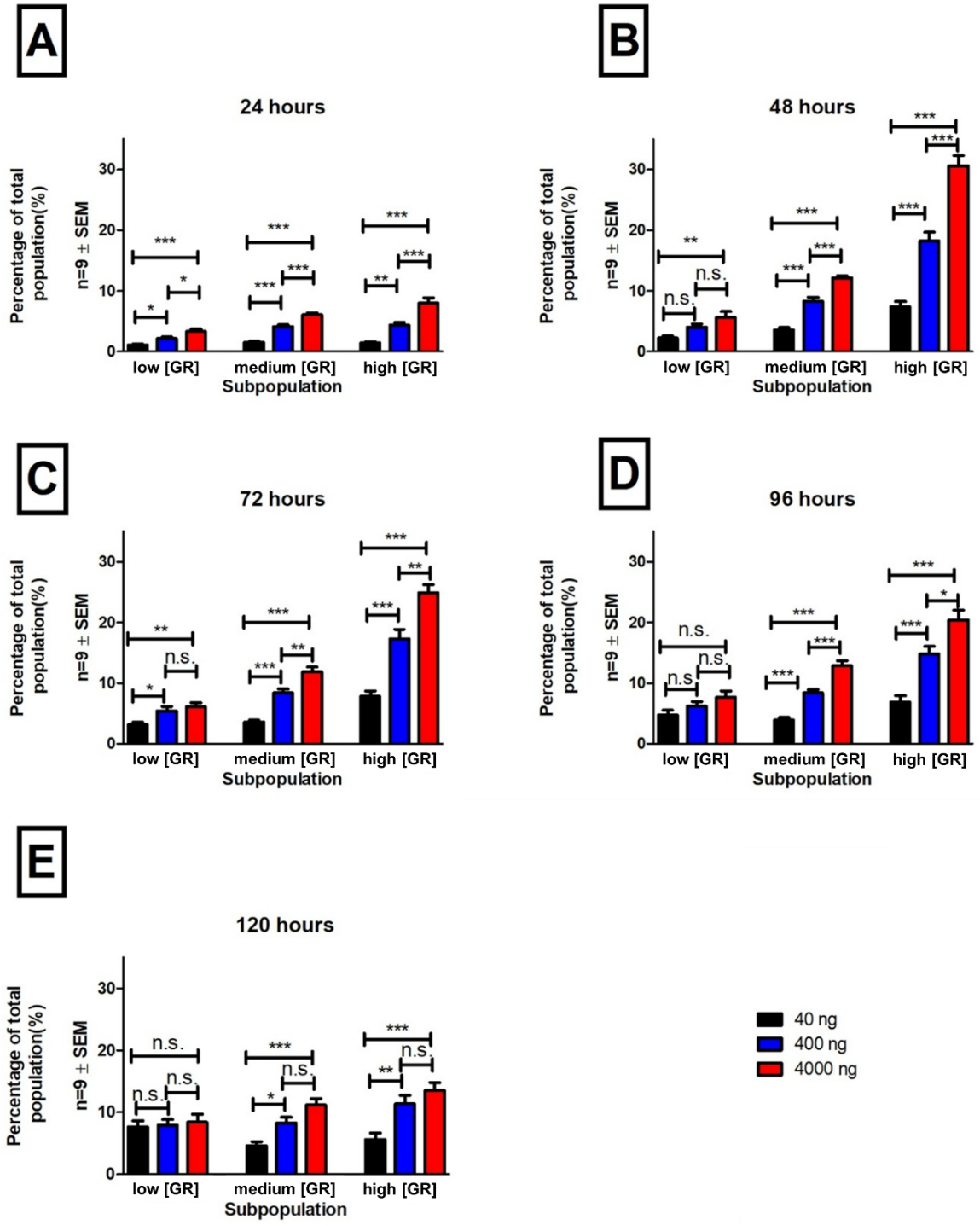

Figure 3.3.6: Prevalence of relative GR expressing subpopulations, when initial GR plasmid DNA concentration is increased. FACS sorted populations are indicated as either low [GR], medium [GR] or high [GR]. Initial transfection conditions are indicated as 40, 400 or 4000 ng by the colours, black blue and red respectively. The letters A through E indicate graphs produced for the individual collection time points 24, 48, 72, 96 and 120 hours respectively. *, **, *** and “n.s.” indicate results of statistically significant values of ($p<0.05$), ($p<0.01$), ($p<0.001$) and nonsignificant respectively. Three independent experiments were

Stellenbosch University https://scholar.sun.ac.za

performed per GR variant.

Table 3.3 Comparison of relative GR concentration subpopulation distributions at 48 hours points in relation to increasing GR DNA plasmid concentration.

48 hours				
Condition	**4000**	**400**	**40**	**Statistically significant?**
high [GR] (%)	30.5	18.3	7.4	***
medium [GR] (%)	12.2	8,3	3.6	***
low [GR] (%)	5.6	4.0	2.2	**
Global TE	**48.3**	**30.6**	**13.2**	***

COS-1 cells were transiently transfected with increasing concentrations of eGFP-mGR with FACS used to quantify subpopulations according to GR expression. Statistical analysis compared average absolute sub-population percentages at increasing GR concentrations. “n.s.”, ***, ** and * signify not significant ,$p<0.001$, $p<0.01$ and $p<0.05$ respectively, with the lowest degree of significance selected between different conditions selected. “Total TE” represents total transfection efficiency. Three independent experiments were performed per GR variant.

3.3.6 Absolute distribution of GR subpopulations within transfected cell lines

Having determined that the effects of concentration of GR plasmid DNA time on relative GR concentration subpopulation distribution, the parameters affecting the absolute distribution of GR concentration subpopulations within the transfected cell population were evaluated.

Evaluation of the absolute distribution of the 4000 ng GR plasmid DNA transfection condition was shown in (**Fig. 3.3.7 A**). Initial 24-hour readings when expressed relative to the low GR concentration subpopulation showed a 2.3 fold increase for the high [GR] and a 1.8 fold increase for the medium [GR] subpopulations. The high [GR] subpopulation was mostly

Stellenbosch University https://scholar.sun.ac.za

maintained over the time span of 120 hours, however, maximal differentiation between [GR] subpopulations was observed at 48 hours (**Table 3.3**) when a 5.3 fold increase for the high [GR] and a 2.1 fold increase for the medium [GR] was measured relative to the low [GR]. From 48 hours on, the dispersion of GR subpopulations decreased over time and at 120 hours the differences in distribution of the different subpopulations converged with only a 1.6fold increase for the high [GR] and a 1.3 fold increase for medium [GR] when compared to the low [GR].

Compared to the high (4000 ng) transfection condition, the medium (400 ng) transfection (**Fig. 3.3.7 B**) revealed the following. 24 hour dispersion was less pronounced than for the 4000 ng concentration. Peak dispersion was similar to that of the 4000 ng transfection condition (**Table 3.3**), occurring at 48 hours, though slightly less pronounced between the medium [GR] and low [GR]. In contrast to 4000 ng, the 120 hour time point showed a reduced dispersion in the presence of the subpopulation groups. With the medium [GR] and low [GR] groups being expressed in approximately the same ratio.

For the 40 ng transfection (**Fig. 3.3.7C**), differences in the proportional expression of the different GR subpopulations were the least pronounced of the three concentrations. As with previous conditions. A trend of maximal dispersion occurred at 48 hours and once again (**Table 3.3**) proportional differences decreased until the 120 hour time point. Notably and in contrast to the previously mentioned transfection concentration conditions, the 40 ng condition produced a low [GR] condition which was far more prominent than the medium other subpopulations, with the high [GR] and medium [GR] expressing 30% and 40% lower than the low [GR] respectively.

Comparisons of the distributions of the three different initial transfection concentration groups are highlighted in (**Table 3.3**). Notably individual comparisons of the percentages of high [GR], medium [GR] and low [GR] present for the different initial transfection periods were not found

Stellenbosch University https://scholar.sun.ac.za

to be significantly different between either subpopulation or 48 or 72 hour time point. Interestingly however, the ratio of the 4000 ng transfection condition at the 48 hour time point was approximately 5:2:1 (high [GR] : medium [GR] : low [GR] respectively) and decreased to a minimum of 3:1:1 (high [GR] : medium [GR] : low [GR] respectively) at the 40 ng transfection condition for the same time point. This decrease in dispersion was also observed for the 72 hour time point and appeared to be concentration dependent.

In summary, both transfection concentration and time affect absolute subpopulation dispersion, however these effects had subtle differences. Initial plasmid concentration produced three distinct groups, with higher concentrations leading to higher expression of the high [GR] and medium [GR] subpopulations when compared to the low [GR]. On the other hand, time lead to an exacerbation of the initial expression differences, with the first 48 hours being the most pronounced. After this, the proportional differences between GR subpopulations become less pronounced as time progresses.

Table 3.4 Comparison of absolute GR subpopulation distribution at the 48 and 72-hour time points with increasing initial transfection concentration. COS-1 cells transfected with increasing plasmid concentration were analysed by means of FACS at 48 and 72 hours using the eGFP tag as proxy for GR expression. Subpopulation distribution per condition is expressed as a measure relative to the low [GR] subpopulation. Analysis was performed by one way ANOVA followed by Bonferroni's multiple comparison test. Results which were not found to be statistically significant ($p>0.05$) and are indicated by n.s.

	4000 ng		**400 ng**		**40 ng**		**Statistically significant?**
Time point	48 hours	72 hours	48 hours	72 hours	48 hours	72 hours	
high [GR] (%)	63	56	59	55	55	52	n.s.
medium [GR] (%)	25	27	27	27	26	24	n.s.
low [GR] (%)	12	15	14	17	18	23	n.s.
Ratio H:M:L	**5:2:1**	**4:2:1**	**4:2:1**	**3:2:1**	**3:1:1**	**2:1:1**	

Stellenbosch University https://scholar.sun.ac.za

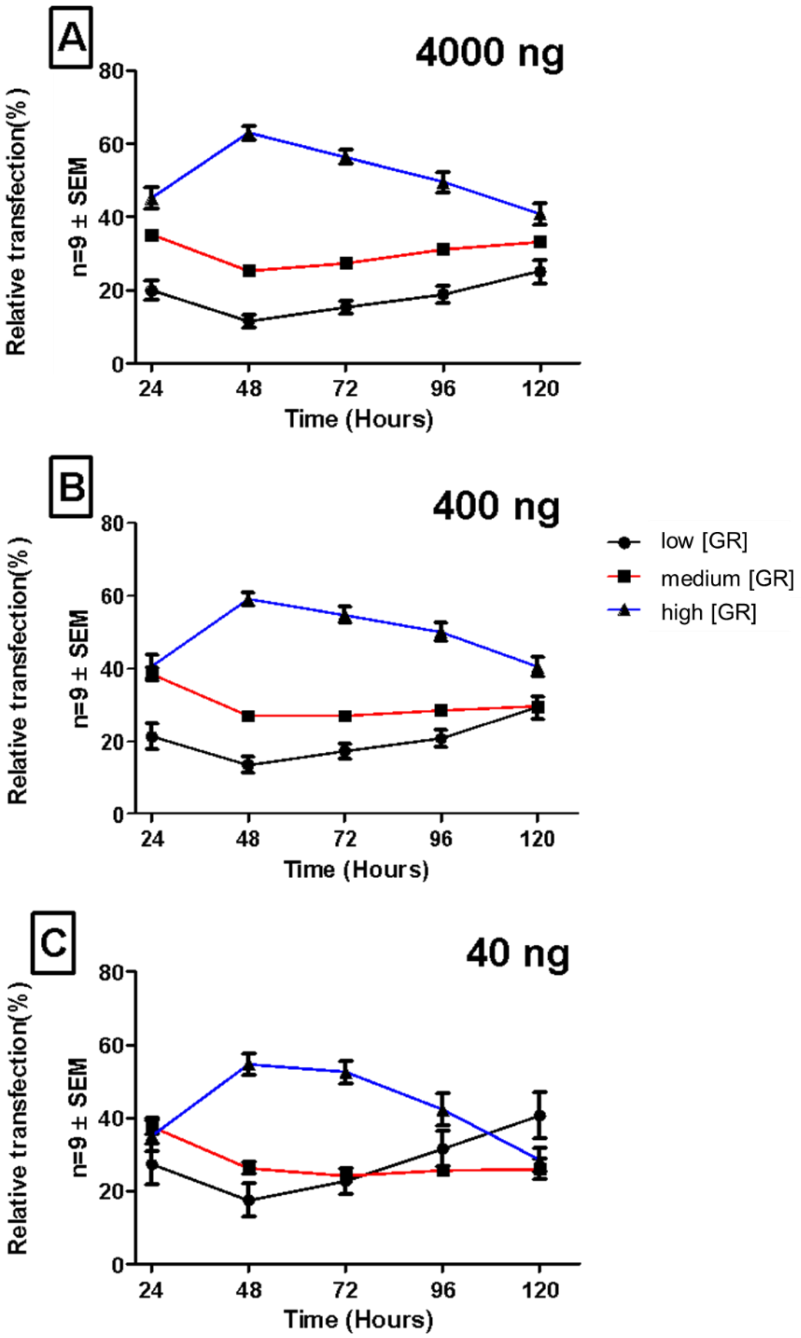

Figure 3.3.7: Absolute prevalence of GR expressing subpopulations following transfection with increasing concentrations (40, 400 and 4000 ng) of plasmid DNA over a time period of 120 hours. Figure A represents the distribution of GR subpopulations at a transfection condition of 4000 ng, whereas figures B and C represent the distribution of subpopulations at 400 ng and 40 ng initial DNA transfection respectively. For all figures, blue represents the high [GR] subpopulation whereas the red and black lines represent the medium [GR] and low [GR] respectively. Three independent experiments were performed per GR variant.

Stellenbosch University https://scholar.sun.ac.za

3.4 Discussion

This study consisted of two aims, the first of which was related to the parameters affecting global transfection efficiency, namely time and GR DNA plasmid concentration transfected. The **first aim** specifically investigated the roles of time and initial plasmid concentration on transfection efficiency. The results showed that an increase in GR-DNA plasmid concentration of the eGFP-tagged mouse GR variants mGRwt, mGRdim and mGRmon, yielded a consistent outcome for global transfection efficiency during transient transfection where irrespective of the GR variant employed, it was shown that a higher concentration of GR plasmid DNA transfected consistently produced a higher global transfection efficiency (**Fig. 3.3.1 and Table 3.1**). This is illustrated by the conserved trend of high concentrations (4000 ng) of GR plasmid DNA transfected consistently producing global transfection efficiencies which were on average 2 fold higher than those produced by the medium concentration (400 ng) and 3 fold higher than the low concentration (40 ng) of GR plasmid DNA.

Furthermore, time and its effects on global transfection efficiency was also considered and it was shown that there was a fluctuation in global transfection efficiency over time (**Fig. 3.3.1**), highlighting a dynamic element to transient transfection. The findings showed that maximum global transfection efficiency could be isolated between 48 and 72-hours points for the medium [GR], and high [GR] plasmid DNA concentration conditions. The trends observed correspond to those obtained with the human GR constructs by Barry [6], who also demonstrated an increase in global transfection efficiency at both increased concentration of GR plasmid DNA, and also between the 48 to 72 hour time span. In comparison work by Tseng [62], using the GFP construct GFP(S65T) illustrated a similar trend with maximal transfection efficiency being achieved at the 48 hour time point. Furthermore, this study also showed that transfection efficiency gradually diminished from the 72hour time point onward. Tseng also illustrated the effect of plasmid concentration, with increases in transfected GFP(S65T) concentration leading to an increase in transfection efficiency. However, in contrast to our current findings, work by Todd [63], also using liposomal transfection methods in mammalian HeLa and CV-1

Stellenbosch University https://scholar.sun.ac.za

cell lines with the pGL plasmid produced remarkably different results. Work in these cell lines [63] achieved in excess of 80% transfection efficiency in HeLa 1 cells after 6 hours of transfection and 40% in CV-1 cells respectively. The variations in findings from different sources, using different combinations of plasmid constructs and cell lines may therefore suggest that differing abilities of plasmid uptake and rates of protein expression exist depending on construct and the cell of interest, the maximum transfection efficiency attained may differ accordingly [60], [64].

In **figure 3.3.3** it was suggested that it may be possible to accurately describe transfection efficiency as a line fitted to the log function of the initial DNA transfection concentration. Interestingly, R^2 values for the fitted functions diminished substantially as the time post transfection passed the 72 hour time point. This aberration may be explained by an increase in spontaneous plasmid ejection as time progresses or may be due to DNA degradation [62,65]. A criticism of this finding is that the number of iterations used was quite low, in addition, the range of concentrations was rather limited resulting in lower than desirable R^2 values. In future, a more refined statistical result may be obtained by both increasing the number of iterations of experiments performed, but also by means of increasing the range of DNA concentrations employed for the experiment.

Previous work by Robertson [1] reported a maintained estimate of 20% in global transfection efficiency despite increasing plasmid concentration. These findings differ not only from our study but also those from Barry and others [2, 65]. The technique employed to estimate the global transfection efficiency values in the previous study relied on fluorescence microscopy as opposed to FACS, inherent technical variations in the techniques used may account for the differences observed. To illustrate this point, the fluorescence microscopy method estimates transfection efficiency on the basis of the number of cells expressing the green fluorescent protein, GFP-GR as a percentage of the total nuclear stained cells. The sample sizes

Stellenbosch University https://scholar.sun.ac.za

mentioned as representative for microscopy estimations were stated as 131 and 261 cells for the medium and high plasmid concentrations, respectively and offered a transfection efficiency approximated to be 20% in each instance. In contrast, FACS-based sorting as used in the current study provided a data pool of 10 000 cells per data collection point, resulting in greater statistical resolution and reduced error.

An implication of the findings in this study therefore suggests that fmol GR/mg protein estimations reported for saturation binding by Robertson *et al* [1] are likely to have been underestimated. Our findings here(**Table 3.3**) show that the 40 ng transfection condition had a global transfection efficiency of 13.2% , nearly half that estimated using the microscopy technique. On the other hand, the high 4000 ng transfection condition produced a transfection efficiency of 48.3%, more than double that estimated by microscopy for the Robertson study. The implication would be that the calculated protein levels per cell lie between 507 fmol GR/mg protein for the low GR condition and 588 fmol GR/mg protein for the high GR. A further consideration, is that the current study made use of the DEAE transfection method due to cost considerations. Liposomal transfection methods have been reported to provide higher levels of transfection efficiency across various cell lines and may also affect the outcome [66].

The **second aim** for this study was concerned with the distribution of physiologically relevant GR subpopulations within the transfected population and these were observed either in terms of an absolute percentage of the total cell population as per **objective 1**, or as an relative percentage within the transfected cell population alone per **objective 2**.

For **objective 1** transfection of COS-1 cells with increasing concentration of the eGFP-GR expressing variants (**Fig 3.4 & 3.5**) were scrutinized both in terms of time and initial plasmid concentration. Irrespective of initial plasmid concentration, it was shown that three physiologically relevant GR expressing subpopulations could be sorted from the overall cell

Stellenbosch University https://scholar.sun.ac.za

population suggesting that during transfection, the transfected plasmid is not integrated into the transfected population uniformly. This non-uniform uptake is in agreement with work by Materna *et al.* [67] investigating the uptake of pSM-EYFP and pSM-ECFP in the Jurkat cell line, in which the uptake of plasmid was shown to be taken up in a Poisson-like fashion. As shown previously (**Fig 3.2**), concentration affected the total transfection efficiency, and comparing subpopulations also highlighted that transfection concentration affected the composition of GR containing cells within the transfected population. Time was also shown to be a critical factor. In all instances, maximum expression of the GR was observed at the 48 hour time point. Notably, we also compared the individual effects of the various eGFP-GR variants individually (**Fig. 3.3.2**), however, they were not found to have any statistically significant effect on the dispersion on the distribution of the GR-expressing subpopulations. These findings are in agreement with previous work by Barry [6] who similarly found a redistribution of the GR into the three physiologically relevant GR containing subpopulations post transfection using an eGFP-hGR construct. These findings therefore suggest that the various eGFP-GR constructs similarly redistribute into GR expressing subpopulations following transfection and are likely attributable to the fact that the mouse and human GR are similar in structure [68].

For **objective 2** of **Aim 2** we emphasized the effects of concentration and time on the absolute composition of the transfected population and is shown in **figure 3.3.7** and **Table 3.3**. In terms of concentration, higher initial plasmid concentrations resulted in a higher dispersion in the absolute numbers of GR subpopulations. Progression of time resulted in a redistribution of the observed GR-subpopulations to the medium [GR] and high [GR] containing populations. These findings are in agreement with previous work by Barry [2], who observed a similar distribution over time in the hGR construct. This suggests that following transfection, cells containing plasmid require time to express the eGFP-GR protein and initially, cells with a high concentration of plasmid may be identified as a low [GR] containing cell. Peak expression is

Stellenbosch University https://scholar.sun.ac.za

then achieved at 48hours following transfection, after which expression diminishes due to cell division or other factors.

3.5 CONCLUSION

The two aims for this study have allowed for the following conclusions:

First, transfection at a higher concentration i.e. 4000 ng, resulted in the highest gross transfection of cells. Second, the time required for maximum transfection efficiency was at the 48 hour time point. Next, it was demonstrated that at the 4000 ng transfection condition, the transfected population redistributed into three physiologically relevant GR containing subpopulations, i.e. the low [GR], medium [GR] and the high [GR]. Finally, it was demonstrated that relative to the transfected population, the ratio of the low [GR] to medium [GR] and high [GR] subpopulations were not significant when comparing 40 ng,400 ng and 4000 ng initial transfection conditions 48 hours following transfection. Therefore, transfection with 4000 ng of eGFP-GR for a period of 48 hours, would provide the highest yield of transfected cells and still provide sufficient variation in terms of the physiologically relevant GR subpopulations required for further N&B experiments.

Stellenbosch University https://scholar.sun.ac.za

Chapter 4

Validation of the Number and Brightness assay for the observation of oligomerization in the GR mouse model

Overview

In the following section various methods to detect differences in oligomerization species, which may produce valuable observations for kinetic studies, by means of fluorescence correlation spectroscopy (FCS) are briefly discussed. Specifically, this section highlights the use of the Number and Brightness (N&B) technique in live cells. The use of this technique in prior research to determine the formation of protein structures within living cells, and particularly, the role of N&B in determining essential regions of the GR protein required for dimerization is stressed. Focus is then shifted to the use of the N&B assay in the context of GR concentration-dependent dimerization studies. Application of the N&B technique to the determination of the dissociation constant and underlying kinetic parameters of dimerization is emphasised. Following this, difficulties in clearly defining populations of GR expressing cells at specific levels of protein expression are highlighted.

With this background in mind, the translation of physiologically relevant concentrations of GR containing COS-1 cells to the Confocal microscope is described. Following this, the optimization of the N&B technique is presented and the application of the technique to analyse ligand independent dimerization and a 30 min oligomerization visualization routine is introduced.

Stellenbosch University https://scholar.sun.ac.za

The chapter then proceeds by introducing the results of these endeavours and concludes with a discussion of the implications of these results.

4.1 Introduction

4.1.1 Brief introduction into fluorescence correlation spectroscopy and the methods employed for oligomerization quantification.

A challenge in the field of molecular biology has been the development of a system which is capable of determining the level of oligomerization of proteins with a high degree of accuracy. The system in question should be able to analyse oligomerization in live cells, which would equate to accurate measurements regardless of the nominal fluctuations in protein concentrations which accompany cellular compartmentation. Advances in modern microscopy hardware have led to ever increasing detector sensitivity to fluorescent signals, whereas advances in optics have led to ever smaller observation volumes, capable of resolving interactions between individual molecules. On another front, advancement of modern molecular biology techniques allows for near limitless opportunities to modify proteins of interest to carry a variety of fluorescent tags, suitable to various applications.

Fluorescence correlation spectroscopy (FCS) refers to a variety of microscopy techniques capitalizing on the use of both these advancements in microscopy and biochemical techniques to acquire information about molecular interactions within a solution. A common feature of all correlation spectroscopy techniques is the use of a very small optical volume (≤1 femtolitre) and a monochromatic light source. A small volume is preferred for two reasons, first, the number of molecules (≈10^{-3}) moving into and out of the observation volume is limited, leading to large fluctuations in fluorescent signal intensity. Second, the amount of background signal is drastically reduced [69–72]. The optics required to observe diffusion within the observation volume usually consist of a high numerical aperture objective, a barrier filter and a dichroic

Stellenbosch University https://scholar.sun.ac.za

beam splitter [52]. The specificity of the end volume is resolved by the use of either two-photon laser techniques or a pinhole system native to confocal microscopy [52]. These systems of discrimination tightly control the observation volume and eliminate background noise. The light source for FCS work is required to be a constant source of monochromatic radiation to ensure that the observed fluctuations in signal are attributed primarily to the photo-physics of the fluorophore under investigation [52]. To this end, laser radiation is often employed as a stable light source. As a final hardware consideration, the system requires an effective device for measurement of the fluorescent signal emitted by the stimulated fluorophore. Multiple solutions are available to address this particular requirement with various photomultiplier tube (PMT) and avalanche photodiode (APD) detectors available [52].

An advantage of these hardware requirements is that they are similar to those for standard confocal microscopy. As a consequence, FCS work can frequently be performed on a standard confocal system, which may require little or no modifications to hardware depending on the desired application. As for data collection, a simple software package, such as the SIM4FCS package developed by Gratton [73] (Laboratory for Fluorescence Dynamics, Irvine, California, USA) is sufficient for the analysis of a wide variety of fluctuation-based spectroscopy techniques. This combination of hardware, which is reasonably accessible, as well as software, which is relatively inexpensive, results in a system that is able to accurately describe molecular kinetics in a manner which avails itself to the common researcher, even in laboratories which may otherwise lack the resources required for highly specialized microscopy equipment. These traits therefore make various FCS techniques novel and accessible to the African context, where access to expensive techniques often limits options for research.

4.1.2 The underlying principle of fluctuation-based spectroscopy

Fluctuation-based spectroscopy primarily relies on, but is not limited to, the observation of the

Stellenbosch University https://scholar.sun.ac.za

Brownian motion [74] of fluorescent particles through an observation volume. Such movements lead to fluctuations in the observed intensity is detected within the observation volume [69, 70].

An early iteration of fluctuation-based spectroscopy, which is currently enjoying a resurgence in both chemical and biochemical fields, is image correlation spectroscopy (ICS) [75, 76]. ICS differs fundamentally from FCS in its niche of application. ICS is better suited for slow diffusion processes such as the diffusion of molecules through a cell membrane [76]. In this instance the collection of sufficient data for statistics from a single point may take an impractical amount of time. ICS overcomes this problem by collecting data from multiple spatial points at the same time to satisfy the necessary statistical component of standard FCS [76]. Both FCS and ICS rely on the motion of a small number of particles through a clearly defined optical volume, with the assumption that particle behaviour strictly adheres to a Poisson distribution [77]. In this method a short series of intensity measurements are taken over a given time span (**Fig. 4.1.1**), thereby producing a series of intensity values which fluctuate around the population equilibrium value.

In FCS, it is necessary to clearly define the ellipsoidal illumination volume (point spread function or PSF). However, it is common practice to attain these parameters by using a fluorophore of a known diffusion rate as opposed to determining the values directly [78]. Combination of both the spatial parameters of the illumination volume, as well as the intensity data transformed by correlation function allows for the description of both the diffusion characteristics of the molecule being observed, and the molecular concentration.

In theory, the FCS method can therefore be applied to acquire the diffusion rate of different fluorescent species through a perturbed medium relative to that of these same species in a known medium [79]. In addition, it also allows the researcher to acquire the concentration of

Stellenbosch University https://scholar.sun.ac.za

these different molecular species based on their occupancy of the observation volume. In practice, however, the FCS method suffers limitations in the resolution of protein aggregate species, in particular those which consist of monomers and dimers, as the differences in diffusion rates between the observed proteins is too low to accurately discriminate between species [79].

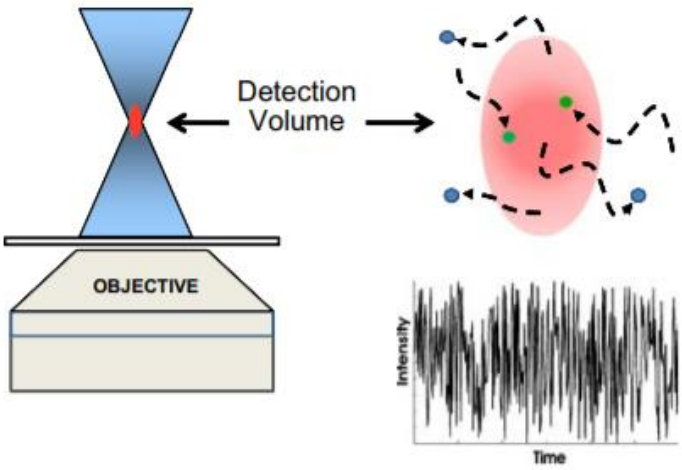

Figure 4.1.1: A graphical representation of fluorophores in a small observation volume typical of FCS. The inset graph is a typically expected data pattern, in which observed emission intensity values fluctuate over time as fluorophores diffuse through the observation volume (From Jameson *et al.* [52]).

4.1.3 The Photon Counting Histogram Method

The resolution limitations of the FCS method for aggregation analysis, is however elegantly solved by simply changing the manner in which the series of intensity fluctuations are analysed. Instead of relying on the temporal observation of fluctuations to which one applies an autocorrelation function in order to discern chemical kinetics, such as is found in the FCS method, it is possible to analyse fluctuations on the basis of moment analyses. In doing so, the observed intensity readings can be represented as an intensity distribution plot or histogram of the acquired photon counts [80] and is shown in **Figure 4.1.2**. Given a sufficiently large data acquisition time to generate a Poisson distribution of intensity readings, the technique capitalizes on the molecular occupancy of molecules diffusing through a small

Stellenbosch University https://scholar.sun.ac.za

confocal or two photon observation volume to determine the brightness of the individual molecules. This approach was first postulated by Palmer and Thompson in 1987-1989 [80] and shortly afterwards demonstrated experimentally by Qian and Elson in 1990 [69] Subsequently, expansions upon these initial demonstrations led to the simultaneous development of the photon counting histogram (PCH) approach by Chen *et al.* [70],as well as the fluorescence intensity distribution analysis (FIDA) by Palo *et al.* [81]. Both these methods rely on the allocation of a photon count per second per molecule (CPSM), which defines the molecular brightness of the molecule (ε). These approaches were, however, initially produced for solutions and did not consider the cellular context.

In light of this limitation, Chen *et al.* [82] demonstrated the practical applications of this system in live cell systems containing proteins tagged with increasing concentrations of either eGFP or eGFP2 (two eGFP tags per protein) (**Fig. 4.1.2**).

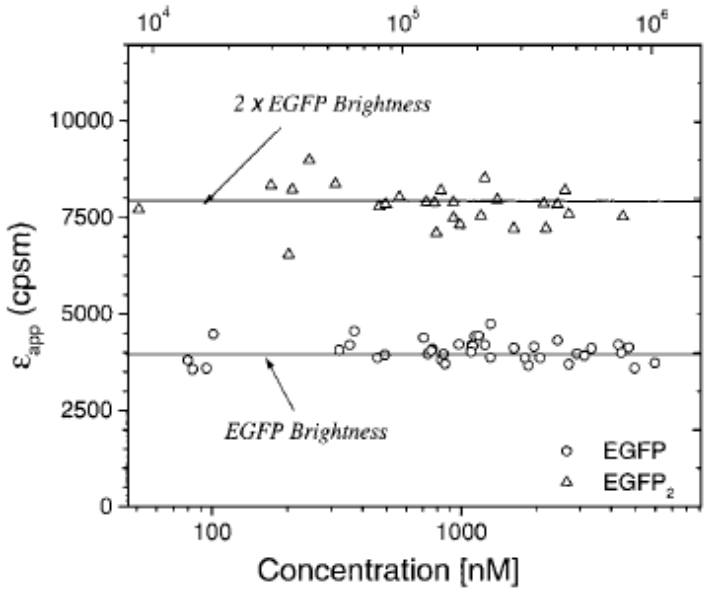

Figure 4.1.2: Demonstration of the efficacy of the photon counting histogram (PCH) method to distinguish between monomeric and dimeric molecules at a single point. Circles represent single EGFP molecules whereas triangles for EGFP2 represent two fused EGFP molecules. Datapoints represent the measurement brightness in individual cells expressing either EGFP or EGFP2. Note that the brightness of EGFP2 is consistently double that of the EGFP irrespective of the concentration of the molecules added. From Chen *et al*. [82].

Stellenbosch University https://scholar.sun.ac.za

The demonstration successfully illustrated the ability to overcome the limitations of FCS in terms of cellular compartmentalization as the observed aggregation states were clearly resolved regardless of the increasing concentration of the eGFP. However, the PCH method still has a shortcoming: its limited resolution.

4.1.4 Number and Brightness Technique

The N&B technique is a variation of the PCH distribution analysis method, which has instead been adapted for observation at a higher spatial resolution. The differences between the PCH technique and the N&B technique are easily understandable. The PCH method acquires the statistics needed for brightness calculations from a small area (single pixel) for an accurate estimation of molecular brightness. The drawback of the PCH method is that it is not well suited for the analysis of large regions of interest, with the computational algorithm and time required per pixel being too long to be practically feasible.

The N&B technique sacrifices the point to point accuracy afforded by PCH, instead generating the average intensity over a larger region [73].This trait of the N&B method provides the advantage of accurately and conveniently investigating the aggregation state of a fluorescently tagged molecule within a discrete region of interest such as the cytoplasm or nucleus without the requirement of imaging each pixel individually as would be the case for PCH.

The N&B technique also benefits from additional traits, which are due to its pedigree as a PCH derivative. For example, the technique is not dependent on the concentration of occupying fluorescently tagged molecules due to the photophysics of the fluorophore being investigated [82]. This makes the technique well suited to the highly compartmentalized cellular interior, treating each region as a microcuvette in its own right. In addition, and in a manner similar to PCH, the technique is a form of moment analysis, averaging the brightness at each independent moment per pixel and is therefore different from the temporal data collection method which is native to FCS when determining the diffusion rates of fluorescent species.

Stellenbosch University https://scholar.sun.ac.za

An inherent advantage of N&B as a technique, is that with growing interest the technique has been specifically adapted for use on standard confocal or TIRF microscope setups [83]. This characteristic in itself makes the technique more accessible to researchers as the equipment required is commercially available and does not require the building of an in-house microscope system. Hardware modifications may typically be required on a case to case basis. However, data processing can be performed via relatively affordable software such as the SIM4FCS package mentioned previously. The number and brightness technique can also be adapted for use on analogue detection systems [73], allowing the application of the technique to a broader base of users.

4.1.5 N&B theoretical background

In the N&B method, brightness is determined on a pixel by pixel basis, by means of intensity (*I*) analysis over a series of temporally disconnected image sequences. For acquisition of the image it is important to consider the pixel dwell time t_d (also referred to as bin time) [84], which is required to be less than the diffusion rate of the molecule of interest through the observation volume.

In the biological context, diffusion rates are between ~0.01 and 30 μm^2/sec for proteins, whereas typical ranges for dwell times within the confocal system are between 0.01 and 10 μm^2/sec [52]. A dwell time which exceeds the diffusion rate of the molecule of interest will result in an acquisition artefact known as temporal averaging [73], a phenomenon wherein diffusion, photophysical processes or the process of isomerization nullify the observed fluctuations. Total acquisition time of the N&B process is determined by the resolution of the image which affects the scan time required for each image, as well as the total number of images (stack), which are required to produce a Gaussian distribution at each pixel [73].

It is important to note that the N&B method, as with traditional PCH/FIDA methodology, creates

Stellenbosch University https://scholar.sun.ac.za

a data set which relies solely on fluctuations in measured intensity caused by fluorophore diffusion through the observation volume [73]. The temporal order of these fluctuations is irrelevant. In other words, a data set of the same acquired but randomly arranged images, will produce the same observations as data collected in time sequence.

The subroutine as used in the Sim4FCS package determines the brightness in the following manner:

To determine variance (σ^2), average intensity (<*I*>) is first determined as the average pixel intensity in the complete stack, which is given as the total number of images (*K*).

$$< I >= \frac{I_1 + I_2 + I_3 \ldots + I_K}{K} \tag{1}$$

Finally, the variance (σ^2) can be determined as a variance of a fluorescent signal:

$$\sigma^2 = \frac{\sum_k \quad (I_k - < I >)^2}{K} \tag{2}$$

In this instance the formula assumes that variation is solely due to emission from the target molecule and as such hardware considerations such as detector shot noise, detector saturation limit, physical description of the observation volume and detector efficiency are considered to be sufficiently accounted for.

In such an instance, the true brightness (ε) is given as the ratio of the variance (σ^2) to average intensity (<I>) also called apparent brightness with the symbol B minus 1. When the molecules are immobile this ratio describes the instrument noise (σ^2 = <*I*>). When interpreted an ε=0 value therefore refers to observation of the immobile fraction. A value of ε=1 would refer to observation of a monomer and higher orders, such as ε=2 and ε=3 would lead to the

Stellenbosch University https://scholar.sun.ac.za

observation of dimers and trimers respectively.

$$\varepsilon = \frac{\sigma^2}{< I >} - 1 = B - 1 \tag{3}$$

Therefore, any pixel in which the variance (σ^2) is equal to the average intensity (<I>), in other words, in a scenario where the variance in fluctuation in fluorescence is equal to the average intensity, such as is the case in an immobile fraction, the value of the true brightness (ε) will be equal to zero.

Careful observation of the underpinning formulas for N&B data analysis clearly illustrates that intensity variance is related to the average intensity of the same observation volume in which the fluctuations are captured. For this reason, the brightness is not related to the concentration of molecules contained within the microcosm in which it is observed. This phenomenon is also explained in the standard PCH method, and as such has been well documented by Chen *et al.* [70].

4.1.6 Practical examples of the N&B technique in literature

Despite the novelty of the N&B technique, it has already been employed in various studies prior to the current study. Examples include the use of the N&B technique to establish the degree of brightness in the focal adhesions of eGFP-tagged Paxillin transfected CHO-K1 cells [73] (**Fig. 4.1.3**). Similarly, Clark *et al.* [85] demonstrated the use of the N&B method for analysing the oligomerization of eGFP-tagged SHORTROOT proteins in the stem cells in *Arabidopsis* roots.

Stellenbosch University https://scholar.sun.ac.za

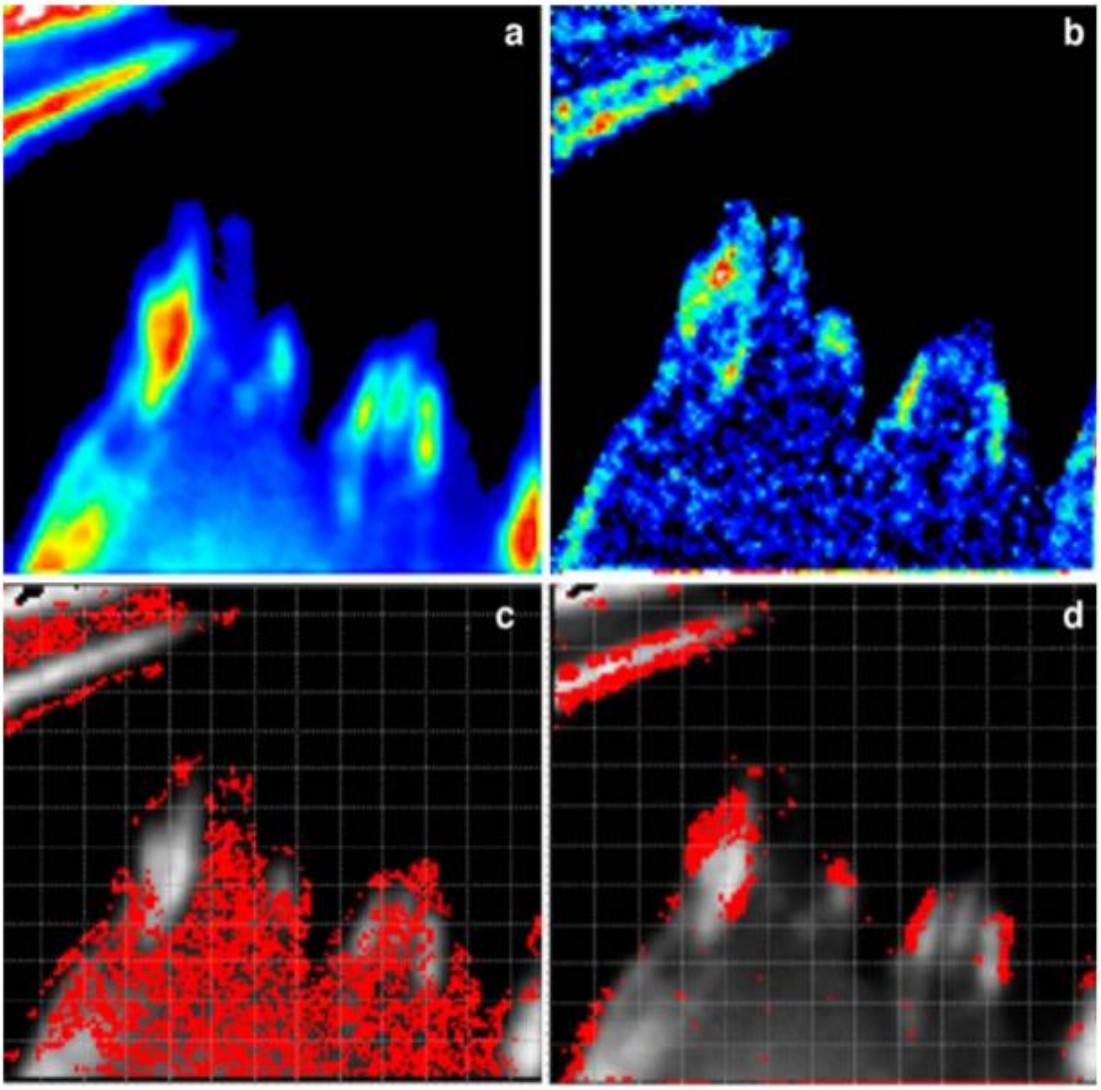

Figure 4.1.3: A practical example of the N&B technique in CHO-K1 cells transfected with EGFP-tagged Paxillin. A) The image intensity map illustrates a clear accumulation of EGFP tagged Paxillin at focal adhesions. B) The brightness map reveals increasing brightness values along the borders of select focal adhesions. C) With the brightness value of the monomer selected, 1150 csm, the distribution of the monomeric EGFP molecules can be shown. D) In contrast, with a brightness value of 11500 csm selected, it is possible to observe the accumulation of oligomerized proteins along the borders of some focal adhesions [3].

Most applicable to the current study, however, the use of the N&B technique has also been extended to glucocorticoid receptor (GR) related work. A critical example of such use was demonstrated by Presman [24], who employed the technique during an investigation into the relationship between GR domains and dimerization. In this series of experiments, the research

Stellenbosch University https://scholar.sun.ac.za

team employed the novel eGFP tagged GRmon mouse variant in baby hamster kidney cells (BHK). The N&B was used to show not only the dimerization potential of the GRwt under different stimulatory conditions (**Fig. 4.1.4 A**), but also the ability of the GRmon to strongly resist dimerization even at high dexamethasone concentrations (**Fig. 4.1.4 B**).

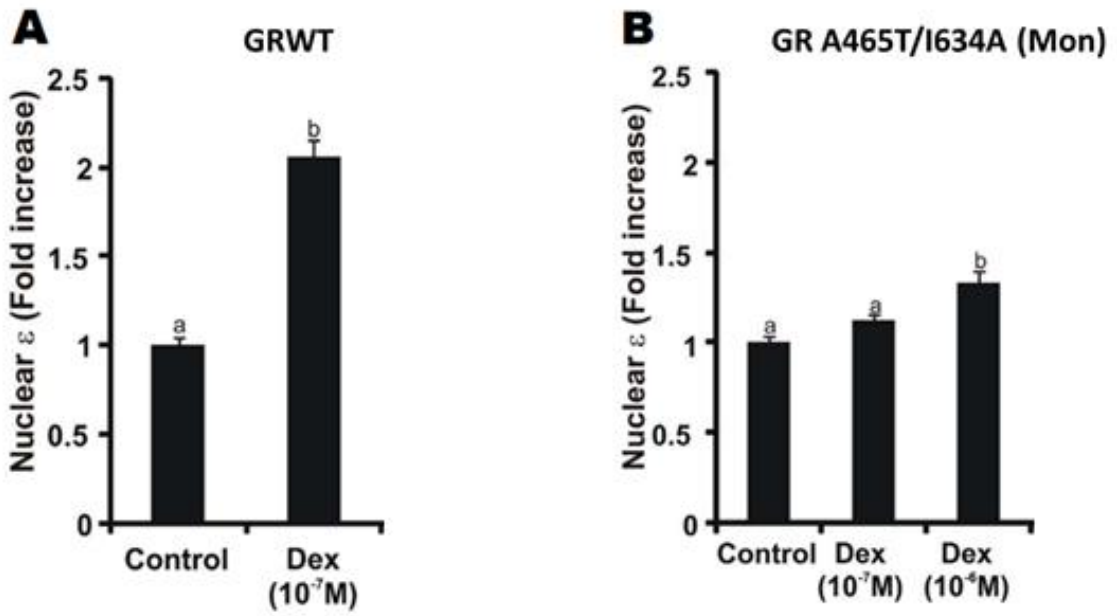

Figure 4.1.4: Use of the N&B technique for the observation of GR dimerization in the nucleus of baby hamster kidney cells (BHK) transfected with either the wild type mouse GR (pEGFP-mGRwt) or the monomeric mouse GR (pEGFP-mGRmon). (**A**) Following stimulation by dexamethasone for at least 30 min, the observed brightness (ε) of the GRwt increased two-fold when compared to the control condition indicating dimerization of the molecule. (**B**) In contrast, the observed brightness of the novel monomeric GR variant GRmon, was shown to be resistant to dimerization even at high (10^{-6}M) dexamethasone concentration. Modified from Presman *et al.* [24].

In the examples of N&B use above, it should be noted that the employed methodology relied solely on single time point measurements of data for the purposes of quantifying the oligomerization state of the molecules under observation at a specific time. These studies were not focussed on resolving the kinetic parameters which underlie the oligomerization processes. As touched upon in the introductory chapter of this dissertation, time is an important but commonly overlooked parameter of ligand binding which affects the residence

Stellenbosch University https://scholar.sun.ac.za

time of the ligand within the receptor [49, 59]. Additionally, for GR related work in particular, GR concentration within the cell is not often considered as an important parameter when investigating ligand-dependent dimerization. This omission is quite baffling as the literature generously provides examples of fluctuation in GR concentration not only within different tissues, but also when comparing healthy and diseased tissue types. The biological function of this spectrum of GR concentrations is mostly unexplored. Observations by Robertson *et al* [49], as well as work by Barry [2] in COS-1 cells transfected with GR constructs of human origin suggest that the GR concentration affects not only the ligand-independent dimerization potential of a receptor, but also the affinity of the receptor for the ligand by the mechanism of positive cooperative ligand binding which relies on *a priori* receptor dimerization. Interestingly, Barry [2] identified that changes in K_d are underpinned by changes in the k_{off}, rather than k_{on}, which may indeed point to differences in residence time as a consequence of GR concentration.

Ultimately, information garnered from these studies led to the development of the model for ligand independent dimerization as postulated by Robertson *et al* [49], (**Fig 2.6**) whereas later unpublished work by Barry [6] developed an *in-silico* representation of the model.

4.1.7 Aims

Aim 1: Translation of FACS GR concentration parameters to the confocal microscope

The **first objective** of this aim endeavoured to translate the sorting parameters utilised during fluorescence activated cell sorting (FACS) conditions (from Chapter 3) to confocal microscopy. To achieve this, COS-1 cells transfected with the eGFP tagged GRwt construct, were sorted according to the previously mentioned definitions with FACS FITC-A values of low [GR] between $10^{2.5}$-$10^{3.3}$, medium [GR] between$10^{3.3}$- $10^{4.2}$ and high [GR] above $10^{4.2}$.

Stellenbosch University https://scholar.sun.ac.za

After sorting, the intensity readings for the cells of the different GR concentration subpopulations were analysed in terms of their average fluorescence intensity values on the confocal microscope. In doing so, clear intensity parameters for the confocal microscope which were functionally equivalent for the low [GR], medium [GR] and high [GR] subpopulations of FACS were established.

Aim 2: Observation of ligand-independent dimerization in the mouse GR model

The second aim of this research project was to observe whether or not ligand independent dimerization, as seen in the human GR model, was observable in the mouse model. Ultimately, the intended application of the technique relied on the accurate determination of the oligomerization state of the GR. For this reason, as a **first objective**, the dimerization potential of a monomeric form of the eGFP (pmeGFP) was investigated, both at the lowest and highest range of concentrations expected for the experiment and served as a monomer reference against which to observe GR dimerization. Next, as a second **objective**, the dimerization state of GRwt containing cells from the low, medium and high GR concentration subpopulations was observed to determine the effects not only on dimerization, but also on the K_d related to GR-GR interactions at increasing GR concentrations.

Aim 3 Observation of oligomerization behaviour following time course stimulation by dexamethasone

The third and final aim of this investigation was to use the newly developed technique to observe the effects of different [GR] on GR dimerization over time in the presence of the ligand dexamethasone.

To achieve this, the effects of the addition of the ligand, dexamethasone, to cell lines expressing increasing GR concentrations were observed. This final step additionally validated whether the methodology could be effectively employed over time to observe trends or kinetic parameters in dimerization.

Stellenbosch University https://scholar.sun.ac.za

4.2 Methods

4.2.1 Preparation of the monomeric eGFP control

The pmeGFP-C1 was purchased from Addgene (Addgene plasmid #36412) and expresses the enhanced monomeric (A206K) eGFP as used in the following publications [84,85]. COS-1 cells ($1x10^6$ cells/10 cm dish) were transfected by means of the DEAE dextran method (see Section 3.2.3) at the high (4000 ng) DNA concentration. After 24 hours, cells were replated into 8-well microscopy plates at a confluence of $7x10^4$ cells per well in 10% charcoal stripped FCS DMEM supplemented with 100 g/mL streptomycin and 100 IU/mL penicillin. Cells were incubated at 37˚C for 24 hours to allow for cellular adhesion to occur. Following incubation, cells were imaged by the Z stack method (see Section 4.2.3.2) to analyse cellular intensity, after which the number and brightness method was applied as described in section 4.2.4.

4.2.2 Translation of FACS (Fluorescence activated cell sorting) sorted GR concentration subpopulations parameters to the confocal microscope.

4.2.2.1 Fluorescence activated cell sorting.

Four 10 cm dishes of COS-1 cells were transfected as per Section 3.3.3 for the high condition (4000 ng DNA) of eGFP mouse GRwt. An additional dish of COS-1 cells, which was not transfected, was prepared as a control for standardisation of the FACS sorting system. Following 48 hours of incubation at 37˚C in DMEM supplemented with 10% foetal bovine serum (FBS), 100 g/mL streptomycin and 100 IU/mL penicillin, medium was aspirated and the cells washed with PBS. PBS was then aspirated and 2 mL of trypsin was added per dish prior to 5 min of incubation at 37˚C. Following incubation, trypsin was neutralised with 10% charcoal stripped FBS supplemented DMEM, after which the contents of each dish were aliquoted and centrifuged at 650 RCF for 5 minutes to collect cells. Supernatant was subsequently aspirated and the remaining pellet resuspended in 20% charcoal stripped FBS containing PBS in

Stellenbosch University https://scholar.sun.ac.za

preparation for sorting. Post sorting collection vials were specifically prepared with a 20% charcoal stripped FBS supplemented DMEM for each sorting condition to increase cell viability post-sorting.

The FACS ARIA system was calibrated and the sorting mode prepared as described in Section 3.2.4. Following sorting procedures, collected samples were mixed by inversion of collection tubes before being aliquoted and centrifuged at 650 RCF for 10 min. Collected cells were subsequently resuspended in a 20% charcoal stripped FBS supplemented DMEM medium at a confluence of $7x10^4$ cells per well in an 8-well microscopy plate and allowed a time period of 3 hours to adhere to the plate.

4.2.2.2 Translation of FACS sorted GR subpopulation parameters to the confocal microscope.

To classify GR concentration subpopulations, samples collected by FACS were optically sectioned during a Z stack procedure. A Zeiss LSM 780 confocal microscope (Carl Zeiss inc.) was used at the Central Analytical Facility (Stellenbosch University). To maintain cell viability, an in-microscope incubation chamber set to 37˚C with a CO_2 concentration of 5% was used. The excitation source employed was a multi-line argon laser set to 488 nm with fluorescence detection by means of a GaAsP array detector set to the photon counting mode. Image resolution was 1024x1024 pixels at a zoom of 1.1, through a 63x oil immersion objective (1.4 numerical aperture), producing a pixel area of 128.4x128.4 µm. In each instance the cell was sectioned into 7 sections with a Z axis displacement of 0.5 µm between each sectioning. Finally, focus was achieved by setting the pinhole to 52 µm.

Cellular intensity of GFP was analysed post imaging using Zen software (Carl Zeiss inc.). This was done in the median intensity mode applied to the entire overlaid image stack. The cell of interest was then analysed by enclosing the cellular perimeter with the Bezier option to acquire

Stellenbosch University https://scholar.sun.ac.za

the mean intensity value. A representative acquisition is illustrated in Addendum B. Acquired mean intensity values were finally imported into Prism 5 Software (Graphpad) for statistical analysis with a one-way ANOVA followed by the Neuman-Keuls multiple comparison test.

4.2.3 N&B

N&B was performed on the LSM 780 confocal microscope system. A 63x oil immersion objective (1.4 numerical aperture) was used. The laser used as an excitation source was a multi-line argon laser which was set to 488 nm for the excitation of the green fluorescent protein. The emission of green fluorescence was detected with a GaAsP array photo-detection system set to the photon counting mode at 510 nm. Images were taken at a resolution of 256x256 pixels at a zoom of 5.1, resulting in a pixel area of 26.36 µm x 26.36µm per pixel. The dwell time for each pixel was set at 12.6 µs, an acceptably short bin time which is not likely to produce any temporal averaging artefacts while simultaneously being long enough to observe fluorophores in the observation volume [84]. The focal plane was maintained by a pinhole aperture of 34 µm. To prevent drift of focus, the autofocus function was engaged for the duration of sample acquisition. A stack consisted of 155 frames per 5 minutes of analysis. The total number of stacks would therefore be dependent on the duration of the experiment. For example, an experiment with 35 minutes of imaging would yield 1085 individual images which were separated into 7 stacks for analysis.

Individual stack analysis was performed by means of the “Globals for images” software package developed by the Laboratory for Fluorescence Dynamics (UCI, Irvine, California, USA), using the number and brightness subroutine for RICS images.

4.2.4 Reagents

Dexamethasone (Sigma D4902; Mr 392.46) was dissolved in ethanol to a concentration of either 10^{-7} or 10^{-5}M for the stimulation experiments.

Stellenbosch University https://scholar.sun.ac.za

4.2.5 Statistical analysis

Statistical analysis was performed by GraphPad Prism 5 (Graphpad) software.

For the first aim, One-way ANOVA followed by Neuman-Keuls multiple comparisons tests were performed for the purpose of identifying non-overlapping GR subpopulations for relative light intensity based cell sorting by means of the confocal microscope. Differences were regarded as significant at $p<0.05$. 33% and 67% percentiles were calculated from the collected light intensity values for each subpopulation. Consequently, cells were selected from mixed populations and evaluated to ensure that the sorted population conformed to the desired specifications.

For the second aim, to account for differences in sample sizes two tailed Mann-Whitney tests were performed on the meGFP transfected COS-1 cells in order to detect whether the relative light intensities of the high [GR] subpopulations were significantly different from that of the low [GR] equivalent. Differences were regarded as significant at $p<0.05$ [88].

Similarly, Mann-Whitney tests were performed into order to verify whether increases in GR concentration affected ligand independent dimerization of the GRwt. Differences were regarded as significant for $p<0.05$.

For the third aim, One-way ANOVA followed by Tukey's multiple comparisons tests were employed, first to determine whether the addition of the ligand dexamethasone influenced ligand dimerization of the mGRwt at increasing GR concentrations, then to determine performance over time. Differences were regarded as significant at $p<0.05$.

In all instances, values of $p<0.05$ were deemed statistically significant whereas values of $p<0.005$ and $p<0.001$ were deemed highly significant.

Stellenbosch University https://scholar.sun.ac.za

4.2.6 Determination of K_d for ligand independent reactions.

Calculation of the K_d for the ligand independent dimerization step of the GR was performed as a comparison to previous work in our laboratory.

To determine the ratio of monomers to dimers, a relative to meGFP brightness value of two was assumed to be indicative of complete dimerization of the eGFP tagged, whereas a value of one was assumed to be indicative of a completely monomeric population.

The percentage of monomeric GR was determined as follows:

$$\%\text{Monomeric GR} = ((\text{relative meGFP brightness} - 1)\text{x}100 \quad (1)$$

The dimerized GR fraction was then determined by the following formula:

$$\%\text{Dimeric GR} = 100 - \%\text{monomeric GR} \quad (2)$$

To determine the K_d of the unliganded GR dimerization reaction, the following mass action form the association was employed:

$$K\text{d} = {[\text{GR monomeric}]^2}/{[\text{GR dimeric}]} \quad (3)$$

GR concentrations for the GR at low [GR],medium [GR] and high [GR] were acquired from previous tritiated dexamethasone (^{3}H-Dex) ligand binding experiments performed by Robertson *et al*. [49] and assumed a 20% transfection efficiency increasing the transfected cell GR concentration five fold. The concentrations used for input into the mass action formula were therefore 54 nM, 123 nM and 229 nM for the low [GR] medium [GR] and high [GR] equivalents respectively.

Stellenbosch University https://scholar.sun.ac.za

4.3 Results

4.3.1 Conversion of FACS GR concentration parameters to the confocal microscope.

Having previously established that transfection does not produce homogenous populations of GR concentration subpopulations (Chapter 3), as a first aim a method for translating FACS data to the confocal microscope was investigated.

The first objective was to utilize FACS sorted GR concentration subpopulations to establish mean intensity values from confocal microscopy (**Fig. 4.3.1**). The mean values acquired were 19.2 for the low [GR], 39.9 for the medium [GR] and 59.8 for the high [GR]. Statistical analysis of FACS sorted GR concentration subpopulation mean intensity values from the confocal microscopy revealed a statistically significant difference when comparing the low [GR] to the high [GR] subpopulation ($p<0.005$). The statistical differences between the subpopulations low [GR] and med [GR], as well as the medium [GR] and high [GR] were less pronounced, yet still statistically significant ($p<0.05$).

Relative light intensity (from here on reported as RLUs) values and/or ranges from the confocal microscopy would provide parameters for three non-overlapping GR concentration subpopulations that correspond with the low [GR], medium [GR] and high [GR] subpopulations obtained during FACS. The three FACS sorted populations had mean confocal microscope RLUs of 19.2, 39.9 and 59.8 for low [GR], medium [GR] and high [GR], respectively. Initially, separation was considered in terms of the 25 and 75 percentile ranges of each sorted cell subpopulation and, with column statistics applied, produced groups with intensities as follows: low [GR] 9.1 to 30.9 RLUs, medium [GR] 30.7 to 45.4 RLUs and high [GR] 39.6 to 79.4 RLUs. Overlap of the groups was observed between the low [GR] and the medium [GR] parameters as well as the med [GR] and high [GR] parameters, however not between the low [GR] and

Stellenbosch University https://scholar.sun.ac.za

the high [GR] parameters. In contrast, column statistics that applied percentiles between 33% and 67% produced selection groups (**Fig. 4.3.1 Table insert**) with intensities between: low [GR]: 12.8 to 25.2, medium [GR]: 38.0 to 42.1, high [GR]: 43.0 to 67.4. In this instance, no overlaps between the parameters were observed.

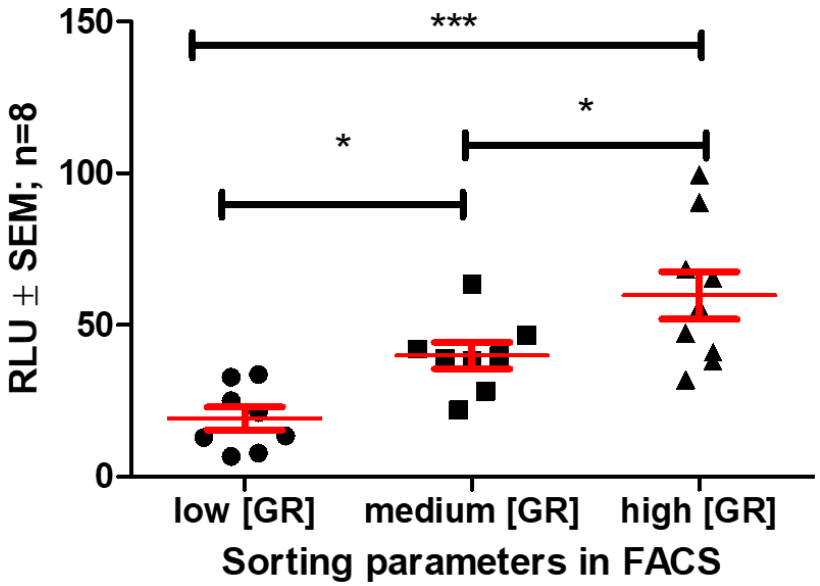

	low [GR]	medium [GR]	high [GR]
33% Percentile	12.8	38.0	43.0
67% Percentile	25.2	42.1	67.4
Mean	19.2	39.9	59.8

Figure 4.3.1: Translation of FACS sorting parameters to relative intensity units of the confocal microscope by using FACS sorted GR concentration subpopulations. COS-1 cells were transfected with high concentrations (4000 ng) of eGFP tagged mouse GRwt. 24 hours following transfection, sorting was performed by means of FACS into previously described sorting gates for low [GR], med [GR] and high [GR] subpopulations. Sorted cells were allowed a time span of 3 hours to ensure adhesion after which confocal microscope intensity values were extracted by Z stack mean intensity analysis. The table (inset) illustrates confocal microscope intensity values representative of the lower 33% and higher 67% percentile of recorded intensities per GR concentration subpopulation. Analysis was performed by means of one-way ANOVA followed by Neuman-Keuls multiple comparison tests. Error bars denote the standard error of the mean. Asterisks represent significant statistical differences with * representing $p<0.5$ and *** representing $p<0.001$.

Stellenbosch University https://scholar.sun.ac.za

Taken together, the percentile ranges of 33% and 67% were selected as the upper and lower limit of selection criteria so as to maintain three distinct GR concentration populations in future experiments.

4.3.2 Application of confocal microscope intensity measurements to unsorted cell populations transfected with GR.

The feasibility of selecting individual cells of a specific GR concentration subpopulation from an unsorted population of mGRwt transfected cells was investigated as the second objective of the first aim (**Fig. 4.3.2**). Cells were selected from a mixed unsorted population in accordance with the 33-67% percentile limits described in the previous section and produced three groups with means of 52.4, 40.5 and 17.7 RLUs for the high [GR], medium [GR] and the low [GR] subpopulations, respectively (**Fig. 4.3.2**). Statistical analysis revealed that these three different GR concentration subpopulations were statistically significantly different ($p<0.001$).

The average intensity of each sorted subpopulation was then compared to the FACS sorted subpopulations described previously (**Fig. 4.3.1**). The averages between the sorted and unsorted groups were not significantly different.

For the sorted low [GR] subpopulation, a parameter of 12.8 to 25.2 was established to prevent possible overlap of collected cells. For cells collected as representative of the low [GR] concentration, intensity values ranged from a minimum of 13.0 to 23.5 RLUs with an SEM=± 1.07 from the mean, well within the acceptable definition for the low [GR] subpopulation.

Similarly, for the sorted medium [GR], a parameter of 38.0 to 42.1 was established to prevent overlap. Again, representative cells collected from the mixed population were shown to range from a minimum of 38.5 to a maximum of 41.6 RLUs with SEM=±0.4, again well within our

Stellenbosch University https://scholar.sun.ac.za

required parameters.

Finally, we repeated analysis for the high [GR] subpopulation. The acceptable parameters for the sorted high [GR] population ranged between 43.0 and 67.4 RLUs. The intensity values of cells sorted from the mixed cell population, showed a minimum value of 45.6 to a maximum of 60.2 with a SEM=±1.3.

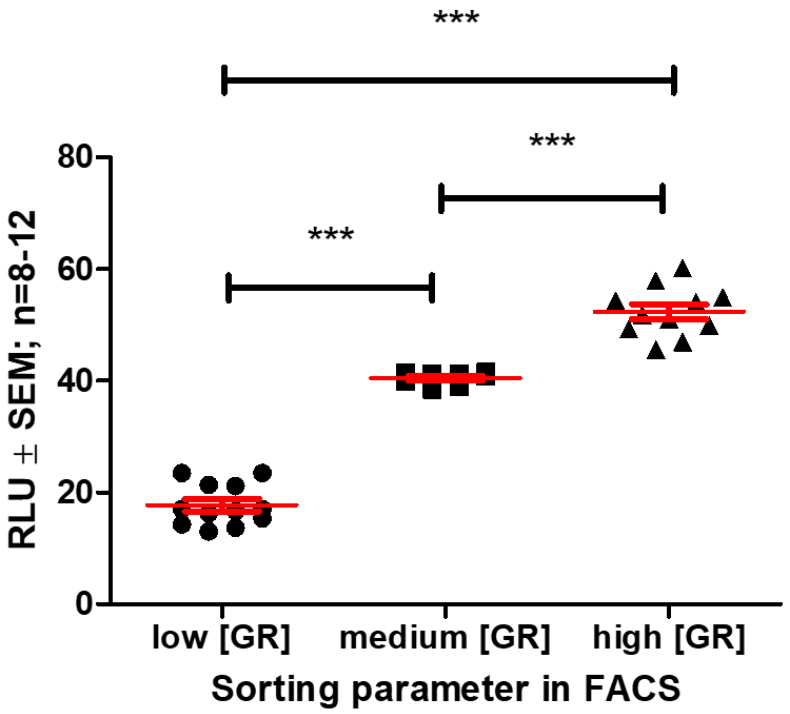

	low [GR]	medium [GR]	high [GR]
25% Percentile	14.6	39.2	49.3
75% Percentile	21.2	41.4	54.9
Mean	17.7	40.5	52.4

Figure 4.3.2: RLU based selection of individual cells of desired GR concentration equivalents from unsorted populations of transiently transfected eGFP GRwt. COS-1 cells transfected with the eGFP-tagged mouse GRwt construct at the high concentration (4000 ng) were analysed with the confocal microscope using the Z stack method to acquire average RLU as a product of eGFP tag fluorescence. Statistical analysis as for **Figure 4.3.1**.

Stellenbosch University https://scholar.sun.ac.za

4.3.3 Stability of monomeric eGFP at high concentrations

N&B was performed across a large spectrum of GR containing cells with increasing GR concentrations to observe the process of GR dimerization in the GRwt. As such it was necessary to have a stable control, which is not subject to dimerization even at high concentrations, for comparison as part of **Objective 2** for the **second aim.**

Naturally occurring eGFP, as derived from *Aequorea victoria*, is known to dimerize at high concentrations [86]. However, the A206K of the protein produces an electrostatic repulsion via lysine which inhibits dimerization even at high concentrations, while having minimal effects on spectroscopic observations of the protein. In this section, the stability of the monomeric nature of the A206K variant was verified using the N&B method over the ranges of GR concentrations planned for our experiment (**Fig. 4.3.3**).

Cells transfected with 4000 ng monomeric eGFP and selected for RLUs that were equivalent to that of the high [GR] and low [GR] subpopulations were compared in terms of the relative brightness of the low [GR] GR equivalent meGFP containing cells (**Fig. 4.3.3**). The high [GR] equivalent meGFP concentration showed a 0.98ε SEM ± 0.08 fold increase in brightness when compared relative to the low [GR] equivalent meGFP transfected subpopulation, however, these results were not shown to be statistically significant ($p>0.05$). Thus, indicating no observable difference in the oligomerisation state of the monomeric eGFP when comparing the high [GR] to low [GR] concentrations. The monomeric eGFP therefore presents as a suitably stable reference point against which to observe oligomerization of the GR in further experiments.

Stellenbosch University https://scholar.sun.ac.za

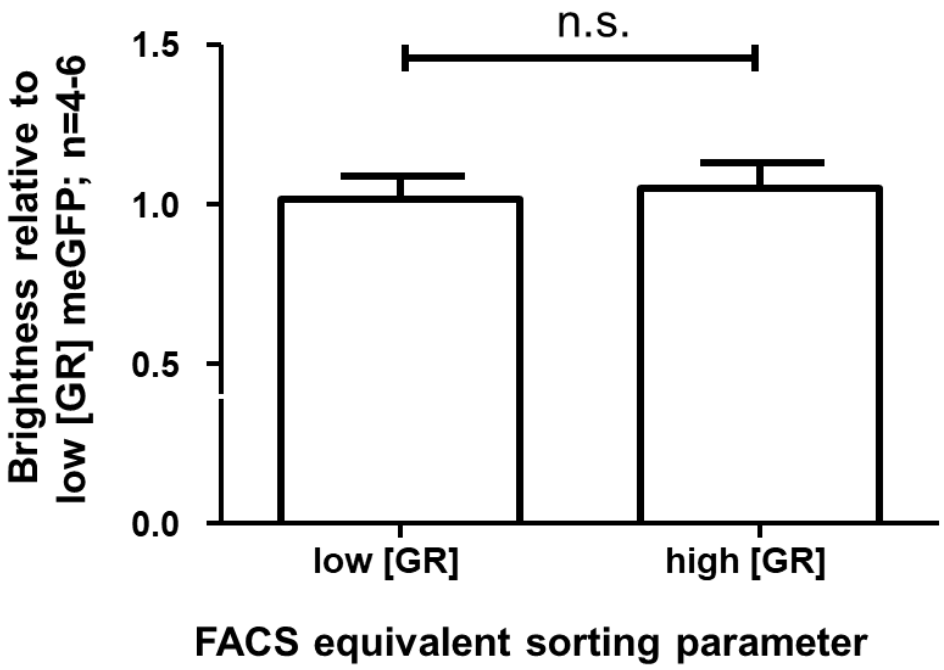

Figure 4.3.3: Comparison of the relative brightness of the monomeric eGFP control at extreme of concentrations expected for analysis for a period of 5 minutes. COS-1 cells were transiently transfected with 4000 ng of DNA of the meGFP construct and were selected as equivalent to either low [GR] or high [GR] based on RLU. “ns” indicates results which are not statistically significantly different ($p>0.05$).

4.3.4 Ligand-independent GR dimerization

Having established the stability of the meGFP monomeric control over the expected spectrum of concentrations of interest we were curious to, as our **second objective** of our **second aim**, observe the dimerization state of unstimulated GR containing cells at low, medium and high GR concentrations relative to meGFP (**Fig. 4.3.4**).

The low [GR] cells produced a brightness value of 1.12ε ± 0.07, which was not found to be statistically ($p>0.05$) different when compared to the meGFP control. For the medium [GR] sample set, the average brightness was 1.20ε ± 0.05, whereas the high [GR] group produced an average brightness of 1.49ε ± 0.05. Both were found to be statistically ($p<0.05$) different from the low [GR] sample.

Stellenbosch University https://scholar.sun.ac.za

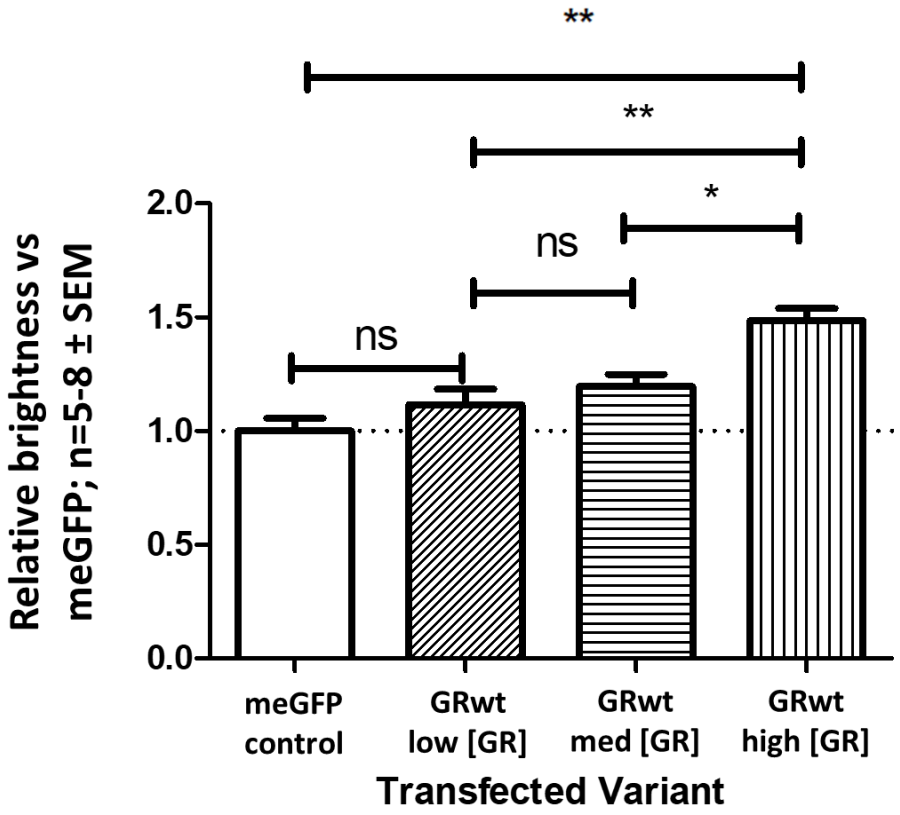

Figure 4.3.4: Ligand-independent dimerization of GR in cells at higher GR concentrations. COS-1 cells were transiently transfected with 4000 ng DNA of either the meGFP-GRwt or the meGFP construct. Low [GR], med [GR] and high [GR] expressing cells were selected by confocal microscope RLU based on previous parameters (section 4.3.1) . N&B performed on unstimulated cells obtained brightness values after 30minutes. “ns” refers to results which revealed no statistical difference whereas * and ** indicate results which are statistically significant with values of $p<0.05$ and $p<0.005$ respectively.

Furthermore, we analysed the effects of increasing GR concentration on GR-GR binding affinity, described by the K_d (**Table 4.1**). Of the three protein concentrations, the low [GR] condition most favoured the monomeric state of the GRwt with 88% of protein being in the monomeric state, and 12% forming a dimer complex. In comparison, the med [GR] showed an increase in dimerization to 20% whereas the high [GR] condition produced the highest dimerization state with 51% of the GR dimerized. K_d remained similar at lower GR concentrations with a K_d of 348 nM and 394 nM for the low [GR] and medium [GR] respectively however a K_d of 108 nM was determined for the high [GR].

Stellenbosch University https://scholar.sun.ac.za

Table 4.1: Oligomerisation state of GR and K_d at increasing cellular GR concentration.

Concentration	%GR monomers	%GR dimers	[GR] Monomers	[GR] Dimers	K_d (nM)
low [GR]	88	12	48	6	348
medium [GR]	80	20	98	25	394
high [GR]	49	51	112	117	108
				Average K_d	283

4.3.5 The effects of the ligand, dexamethasone, on the dimerization status of cells expressing different GR concentrations

The final set of experiments, and **Aim three**, in the development and validation of the N&B technique for our purposes required addition of dexamethasone to observe the effects of the compound on ligand stimulated oligomerization. **Figure 4.3.5** compares the effects of ligand dependent oligomerization at a time point prior to stimulation (0 min) and after stimulation (30 min) with dexamethasone at increasing GR concentration subpopulations. Statistical analysis revealed no statistical significance in the differences in oligomerization state for cells treated with dexamethasone (10^{-7} or 10^{-5}M) compared to untreated cells. However, despite these results, an interesting trend appeared across all data sets for the higher dexamethasone concentration (10^{-5}M) wherein the observed dimerization of the liganded-GR was consistently higher than that of the unstimulated GR. For example, with 10^{-5}M dexamethasone, the oligomerization of the low [GR] (**Fig 4.6A**) showed a mean increase from 1.08-fold to 1.30-fold in brightness compared to meGFP, while med [GR] (**Fig. 4.3.5 B**) saw an increase in average brightness from 1.19 ± 0.05 to 1.33 ± 0.19 and high [GR] (**Fig. 4.3.5 C**) saw an increase in the mean from 1.40 ± 0.05 to 1.80 ± 0.13.

Finally, the effects of dexamethasone at a concentration of 10^{-5}M over a complete 30 min time course are illustrated in **Figure 4.3.6**. Statistical analysis revealed statistically significant ($p<0.05$) changes in the oligomerization state of the low [GR] subpopulation from 1.1-fold to

Stellenbosch University https://scholar.sun.ac.za

1.4-fold for the 0 and 15 min time points, respectively (**Fig. 4.3.6 A**)

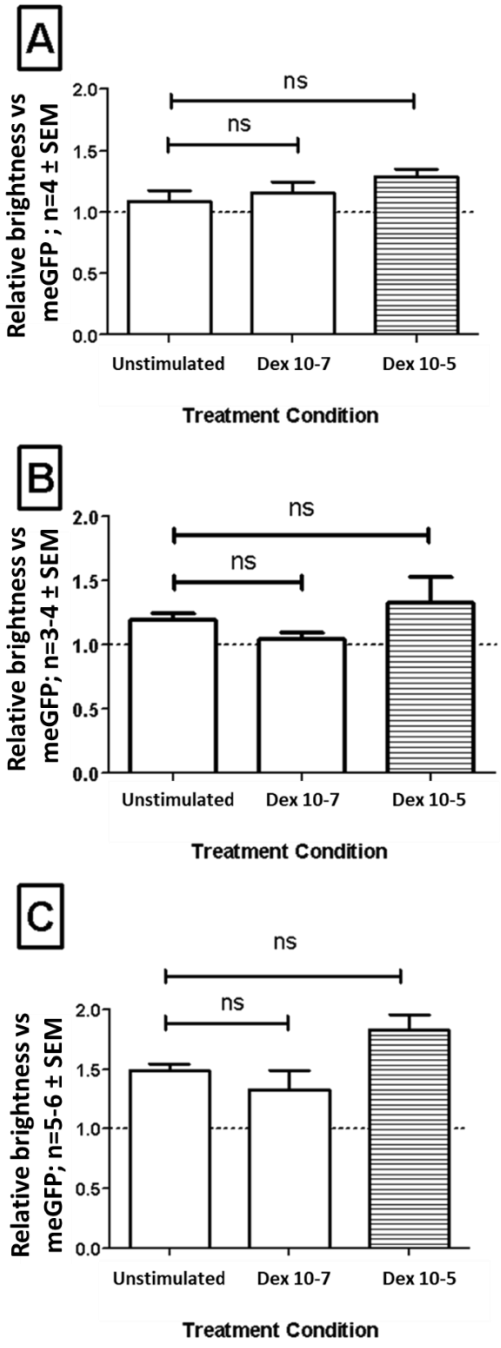

Figure 4.3.5: Brightness following the addition of dexamethasone to COS-1 cells containing increasing concentrations of the eGFP tagged mouse GR. COS-1 cells were transfected with 4000 ng of GRwt and selected by mean of RLU to reflect (**A**) low [GR], (**B**) medium [GR] or (**C**) high [GR] prior to stimulation. Cells were stimulated by dexamethasone at a concentration of either 10^{-5}M or 10^{-7}M with the results illustrating the effects after 30 minutes of stimulation Statistical analysis was performed by means of one-way ANOVA followed by Tukey's multiple comparison test. "ns" refers to results which revealed no statistical differences. The dotted line refers to the meGFP control value.

Stellenbosch University https://scholar.sun.ac.za

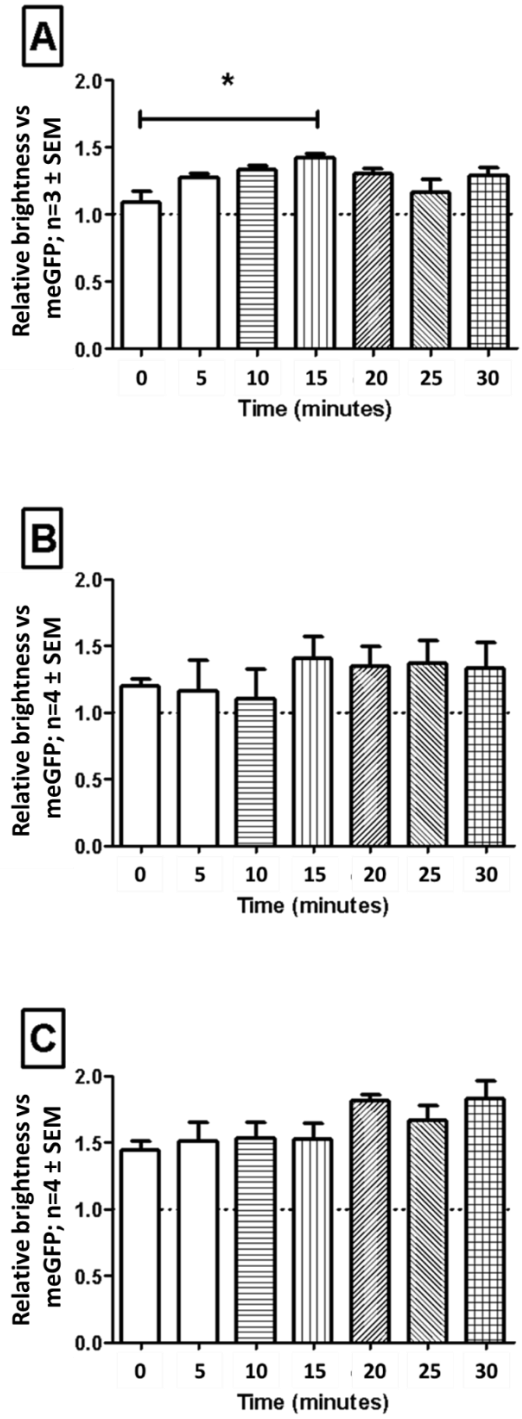

Figure 4.3.6: The effects of stimulation by dexamethasone on the brightness of cells with increasing GFP-tagged mouse GR over time. Cells defined as either low [GR], medium [GR] or high [GR] were incubated with 10^{-5}M dexamethasone and N&B brightness readings were taken every 5 minutes for 30 minutes. * refers to a statistical relevance of $p<0.05$ whereas the dotted line refers to the value of the monomeric eGFP control.

Stellenbosch University https://scholar.sun.ac.za

4.4 Discussion

Aim 1: Translation of FACS GR concentration parameters to the confocal microscope.

Our first aim was to translate FACS sorted GR concentration subpopulations to the confocal microscope in terms of their relative light intensity. GR cells transfected with eGFP tagged mouse GR were sorted by FACS in to the low [GR], medium [GR] and high [GR] subpopulations, which using the Z stack method yielded RLUs on the confocal microscope corresponding to three non-overlapping GR concentration groups.

The RLU ranges established to distinguish between the various [GR] containing populations were 12.8-25.2 RLU for low [GR], 38.0-42.1 RLU for medium [GR], and 43.0-67.4 RLU for high [GR]. In addition, we also demonstrated that by using these criteria it is possible to effectively distinguish between cells of different [GR] subpopulations in a mixed unsorted parent group.

Previous work [1,2,6,7], have emphasized a spectrum of physiologically relevant GR concentrations both within healthy and diseased tissues. Our technique has allowed for the discrete selection of GR containing cells within physiologically relevant concentrations for further experimentation. Additionally, fluorescence based concentration determination is a reliable and widely used source of concentration determination [88, 89]. Fluorescence intensity is known to scale to the concentration of the fluorescent molecules available.

Conversion of FACS data to mean intensity values for confocal microscopy was a convenient and fairly rapid process. With intensity ranges established for confocal microscopy, the procedure was employed routinely prior to the N&B technique and GR concentration of cells as either low [GR], medium [GR] or high [GR] could be ascertained rapidly, in 3 minutes, prior to committing to further experimentation. This technique may find use in future in dimerization kinetic studies comparing GR variants, such as GFP-tagged mGRmon and mGRdim, to the GRwt, but also in comparative studies between the behaviour of mGR and human GR's kinetic

Stellenbosch University https://scholar.sun.ac.za

behaviour.

Aim 2: Observation of ligand-independent dimerization in the mouse GR model

The second aim was to find suitable monomer as a control for the study and perform and to observe ligand independent dimerization in cells containing increasing concentrations of the GR.

Our **first objective** involved the use of the monomeric form of the eGFP containing the A206K mutant, which prohibits the formation of dimers through electrostatic repulsion even at high concentrations [89]. This is achieved without compromising fluorescent performance of the molecule making it a promising candidate as a monomeric control against which to reference the dimerization of the mGR variants at increasing concentrations**.** N&B analysis of cells containing monomeric eGFP concentrations comparable to the classifications of low [GR] and high [GR], the lowest and highest concentrations expected for the N&B experiment, yielded no statistically significant differences in observed monomeric eGFP brightness, suggesting that the monomeric eGFP could be employed as a stable reference point for a monomeric protein against which to compare the dimerization potential of the mGR at increasing GR concentrations. The monomeric eGFP therefore shows promise as a monomeric reference against which to compare not only the mGRwt variant, but also variants such as the mGRdim and mGRmon, which are expected to have lower dimerization capabilities [24, 48].

The importance of a stable monomeric fluorescent reference protein such as the meGFP cannot be overstated. Specifically, unmodified eGFP, as acquired from *Aequorea victoria* is known for its ability to dimerize under increasing GR concentrations [91] which can lead to undesired artefacts [92] such as false positive FRET imaging or inappropriate oligomer interactions in fluorescent imaging techniques. Thus, meGFP offers an alternative control for future work, which is stable across a wide variety of GR concentrations without the risk

Stellenbosch University https://scholar.sun.ac.za

dimerization and is inferred to be more suitable for dimerization studies than unmodified eGFP. Work by Presman [24] for example, employed eGFP as a reference protein, however, the research did not consider the effects of cell to cell variation in eGFP concentration on the potential dimerization of the protein. Unfortunately, due to time constraints, a direct comparison between the eGFP and meGFP was not possible. It may however prove useful as a topic for future research into control selection for dimerization studies.

The **second objective** of this aim was related to observing the dimerization state of the GRwt at increasing cellular concentrations of unliganded GR. The current study illustrated that, as the cellular concentration of the GRwt in COS-1 cells increased, so too did the observed brightness and dimerization state.

The current study made use of the N&B technique coupled with previously acquired saturation binding data obtained by Robertson [1]. We observed a K_d of 283 nM, for ligand independent dimerization step when considering the High[GR] population, whereas the low [GR] and medium [GR] populations produced K_d values of 348 nM and 394 nM respectively.

The disparity in K_d between the higher and lower concentrations may be due to the lower reported degree of oligomerization for the High[GR] by the N&B method when compared to Co-IP work by Robertson [1], which reported full oligomerization, as compared to 50% oligmerization as reported in this research. This finding may suggest the need for further calibration in future N&B research. Taken together however, these findings overall suggest that the dimerization state of the GR increases spontaneously with increasing GR concentrations, which is in corroboration with previous work by both Barry and Robertson [1,2]. The K_d values from this study have been shown to be quite different from the reported CFP-GR and YFP-GR FRET data however, with an average K_d of 83 nM provided by Barry [2]**.** However, the findings presented here were in close agreement with previous *in vitro* FCS work by Kino *et.al.* which provides K_d values of 410-416 nM for unliganded GR [29, 93]. These

Stellenbosch University https://scholar.sun.ac.za

differences therefore suggest that the observed differences in K_d between Kino and Barry are likely attributable to the techniques employed. Fluorescence cross correlation spectroscopy (FCCS) distinctly differs from FRET in that it does not have distance limits for protein interactions as the proteins of interest are simultaneously illuminated by two different laser light sources. Dimerization is determined as increased cross correlation due to complex formation when compared to independent molecules and offers superior resolution of the complex, when compared to FRET, due to the small confocal volume (on the order of microlitres) utilized for observation [52]**.**

This seems to be further supported in a recent review by Louw, in which a meta-analysis reporting the K_d for the unliganded GR varies depending on the observation method [48]. The current results therefore suggest that the N&B technique can provide information which is comparable to previously published data concerning GR dimerization.

In future research using the N&B technique, it may be beneficial to determine the K_d using ligand binding data to directly determine mGR concentrations. Furthermore, it could be useful to employ the transfection efficiency data generated in chapter 3 to accurately determine the concentration GR contained within individual COS-1 cells. Furthermore, future studies could be performed using the mouse constructs GR dim and GR mon, to observe the effects of mutations in ligand and DNA binding domains on ligand-independent dimerization kinetics.

Aim 3 Observation of oligomerization behaviour following time course stimulation by dexamethasone.

The third aim of this research project was to make use of the N&B technique to observe dimerization over time after the introduction of the GR agonist, dexamethasone. Our results show that a higher concentration of dexamethasone (10^{-5}M), though not statistically significant, appeared to produce a stronger dimerization response at all GR concentration levels and was in fact able to produce a level of full dimerization at the 30 min time point for

Stellenbosch University https://scholar.sun.ac.za

the high [GR] condition. Interestingly, however, we observed no significant effect on the dimerization state of the GR using the concentration of 10^{-7}M dexamethasone. This finding is surprising, as previous N&B work by Presman [24], as well as saturation binding experiments by Robertson [1] indicated an ability to induce full dimerization of the GR at this concentration. As the dexamethasone used was in excess of 4 years old by the time of this study, the observed differences may be degradation of the compound over time and it may be beneficial to compare results to new stock in a future endeavour [94].

During the time course of dimerization of liganded GR, all results showed an abrupt increase in brightness state between the 15-20 minutes, following induction with dexamethasone. Remarkably, the low [GR] and medium [GR] reach their maximal increase in brightness at approximately 15 min whereas the high [GR] has a slight delay, experiencing a maximal increase at approximately 20 min. Previous work by Robertson *et al.* [1] observed a similar trend , of increasing FRET signal, and therefore GR oligomerization when observing the dimerization state of the human GR.

Much of the use of the N&B technique focuses on single time point information acquisition. For example, information such as acquired by Presman *et al.* [24] concerning the effects of different protein domains on GR dimerization, Hellriegel *et al.*[95] observing the dimerization of the uPar in the cell membrane and Clark *et al.* [85] researching the oligomerization of SHORTROOT proteins in Arabidopsis roots. To our knowledge, the use of the N&B method over a long period of time, as in our case 30 min, is the first of its kind. Based on our initial findings, it is suggested that the N&B technique could be optimized for long term observation to track oligomerization of proteins and specifically the GR over time.

These findings may yet find further use as dimerization is a character trait of multiple oligomerizing proteins; such as selecase, a caseinolytic metallopeptidase, in which protein

Stellenbosch University https://scholar.sun.ac.za

concentration modulates catalytic activity. Type 1 antifreeze protein, as found in the Barfin right eye flounder, is also known to become active at increased concentrations. Fluorescent tags applied to these proteins may provide a means to span the spectrum of physiological concentrations of these proteins and provide further insight into their kinetics and further the understanding of the role of oligomerization of proteins in physiological processes [96, 97]

We envision that future studies may include single time point analysis of cells of a known GR concentration, which are then compared to long term N&B studies to further confirm the accuracy of the N&B method over time.

4.5 Conclusion

The current research project investigated the feasibility of translating FACS related definitions for cells containing physiologically relevant levels of the GR to the confocal microscope. We demonstrated that in using FACS sorted cells, we were able to make use of the fluorescent properties of the eGFP tag attached to the mouse GRwt to produce useful RLU ranges, which match the physiologically relevant GR concentrations. Furthermore, we demonstrated that it was both possible and practical to identify cells of a desired GR concentration from an unsorted transfected population of cells with mixed GR concentrations for further experimentation. This method could possibly be extended to other fluorescent tags and other protein constructs in future and may have implications for further oligomerization studies, especially at increasing protein concentrations.

A crucial element in conducting oligomerization studies is having a stable monomeric protein against which to reference changes in oligomerization of the protein of interest. We have demonstrated that the monomeric form of the eGFP, known as the meGFP, remains stable in terms of its oligomerization state for the concentrations expected for our experiment and therefore serves as a stable baseline against which to observe dimerization. The current

Stellenbosch University https://scholar.sun.ac.za

research has highlighted the need for a stable control, but also the importance of using a stable control protein expressed at a known concentration to offer more repeatable results, especially given the propensity of some proteins to dimerize at increasing concentrations.

Our research project aimed to employ the N&B technique to observe dimerization of the GR protein. To our knowledge, this is the first time this has been attempted on the African continent.

We have shown that the N&B technique can be used to observe the effect of ligand-independent dimerization at increasing GR concentrations as previously found by Robertson [1] as well as Barry [2]. The N&B technique allowed establishing the ratio of dimers to monomeric GR , which by extension could be used to determine the dissociation constant of monomeric GR to the oligomerized protein with previously published saturation binding data.

By using the mass action formula, it was possible to effectively determine the K_d directly from the number and brightness data and the observed trends showed an increase in affinity of the GR for the oligomerized state as the cellular GR concentration increased, which is in agreement with the literature. The number and brightness assay is therefore a rapid and powerful means to acquire general trends about affinity at different concentrations and may in future be further developed to produce more accurate results in line with the literature.

Finally, the current research project attempted to observe the effects of the ligand dexamethasone on the dimerization of the mouse GRwt at increasing physiologically relevant concentrations over time. To our knowledge, this is the first time any laboratory has ever attempted to make use of the N&B assay in such a way. The technique suggested an increase in oligomerization over time which was comparable to previously published results. An abrupt increase in relative brightness appeared for each mGR concentration level. The current study

Stellenbosch University https://scholar.sun.ac.za

shares similarities with previous FRET work by Robertson [1] which observed a net increase in FRET signal as time progressed to 20min after Dex stimulation. It is possible that the observed increase is an artefact of the N&B method, which averages the brightness in a region which is observed over a period of 5 minutes. Later images taken at near complete oligomerization, will therefore produce higher values of brightness, as the average from which the brightness is calculated is based on more images with higher brightness values at total dimerization. It does however appear that future work is required to further validate the feasibility of the technique for kinetic dimerization studies.

Stellenbosch University https://scholar.sun.ac.za

Chapter 5

Conclusion

Background:

The glucocorticoid receptor is a ubiquitous protein with far reaching physiological implications for systems ranging from metabolic to immuno-regulation. In particular, two aspects of this protein's behaviour *in situ* have made for exceptionally rich fields of study and are not yet well understood. First, the function of fluctuating GR concentrations both in different tissue types, as well as in different disease states, are not well understood. Second, the effects of these concentration variations on GR dimerization and GR ligand-binding kinetics are not well understood and may hold significant implications for the pharmaceutical world if elucidated.

Development of an effective experimental model replicating the vast spectrum of GR concentrations found within the human body, as well as a method by which to observe oligomerization of the protein over time for kinetic data, is of utmost importance for future research. The current study builds on previous work by our laboratory [1,2], focusing on the effects of ligand-independent GR dimerization across the vast physiological spectrum of GR concentrations known to be found within the human body. However, as an advancement upon previous work, which was performed using human GR constructs, we sought to employ GR variants from another popular pharmacological model, the mouse. Furthermore, we sought to employ the novel N&B technique, a fluorescence correlation spectroscopy method, for the first time on the African continent to observe the oligomerization of the protein in real time and provide kinetic data over the time course of observation.

The project consisted of three distinct segments. First, it was necessary to create a spectrum of physiologically relevant GR concentrations for the mouse model. This model had to be

Stellenbosch University https://scholar.sun.ac.za

translated to a confocal microscope system, with a selection system being developed which is capable of selecting different GR containing cells from an unsorted population. Finally, the N&B technique was optimized and employed to observe the oligomerization state of the GR over a time course to acquire information about the GR under different conditions.

In Chapter 3 we examined the behaviour of various mGR variants over the course of 120 hours following transfection. Our results illustrated that the mGR variants: the mGRwt, mGRdim and mGRmon, exhibited similar behaviour following transfection over the 120-hour time course, with no discernible statistical differences being observed between the GR variants. This study also illustrated the effect of time and GR plasmid DNA concentration on the distribution of GR expression following transfection, showing that irrespective of either time or plasmid DNA concentration three distinct GR concentrations subpopulations were visualized by means of FACS over the 120-hour period following transfection. The optimum condition for maximal transfection efficiency was between 48-78 hours at a high plasmid DNA concentration (4000 ng). These results were found to corroborate previous work by Barry [2], but also work by Materna *et al.* [67] that transfection occurs as a distribution across the cell population.

A potential shortcoming of this technique pending further investigation, is the continued redistribution of sorted populations over the time period following sorting, until the time of use in the relevant technique. In addition, the process of FACS using our configuration, flow rate, nozzle and cell type, produces stresses which do not make the process practical for producing large viable populations of sorted cells, currently limiting the technique to smaller cell population studies.

Taken together however, the combination of the observed peak global transfection efficiency as well as the observed spectrum of distribution of GR concentration subpopulations, may

Stellenbosch University https://scholar.sun.ac.za

hold promise for prospective research into receptor density-based studies. Sorted cells can reasonably be expected to be used in calibration of further instrumentation, or with further optimization, to be used in conjunction with techniques such as the whole cell binding technique to produce higher resolution results at specific GR concentrations. This ability was practically demonstrated in Chapter 4 with the use of FACS to produce sorted populations of GR concentration subpopulations for the confocal microscope system.

Chapter 4, investigated and attempted to optimize the N&B assay for long term observation of receptor oligomerization in defined cell subpopulations of known GR concentrations. The results illustrated what is to our knowledge the first use of the Z stack method to translate the sorting parameters for GR containing cells from FACS to mean intensity values on the confocal microscope. Following translation of the GR concentration parameters to the confocal microscope, we used these acquired intensity ranges to illustrate that it is indeed possible to distinguish between GR concentration subpopulations in a mixed unsorted cell population and to identify GR concentration subpopulation groups which are statistically significantly distinct ($p<0.001$) and do not overlap.

In future, this technique can be modified for receptor density studies of other fluorophore tagged proteins, such as Oestrogen receptors [98], which are known to play an important role in the hormone positive development of breast cancer, another important issue, on the confocal microscope, and subsequently could be optimized for work in other confocal based techniques.

The second aim for this chapter involved evaluating the stability of a monomeric eGFP construct across the physiologically relevant GR concentrations expected for the mGR construct and observing ligand independent dimerization. The monomeric eGFP was shown to remain monomeric over our functional ranges of observation and would serve as a

Stellenbosch University https://scholar.sun.ac.za

successful reference protein for our purposes. It was shown that it was possible to observe the effects of ligand-independent GR dimerization using the N&B technique, with statistically significant increases in ligand-independent dimerization observed at increasing concentrations of GR. In addition, it was possible to illustrate the effects of ligand-independent dimerization on the K_d, showing an increase in affinity for the GR dimer conformation at increasing GR concentrations. We suggest that our K_d values (**table 4.1)** may differ from previous work in our laboratory due to the differences in the manner in which oligomerization was observed. The current study made use of N&B, a FCS based method, to determine oligomerization whereas previous work by our laboratory made use of FRET [2]. However, the K_d value of our medium[GR] population was quite similar to work by Kino *et al.* [29, 93], in which FCS was also the means by which oligomerization was determined. The medium[GR] in particular may be of interest as the transfection efficiency used to determine GR concentration from saturation binding [1], ultimately used to solve the mass action formula, most closely agrees with our work in Chapter 3.

In previous work the N&B technique is used at fixed discrete time point [6,24,85]. In these experiments, however, use of the N&B over a time course of 30 min to observe ligand-induced dimerization in a more dynamic manner to mixed results. An increase in brightness was observed which followed a similar trend as observed during FRET work previously performed by our laboratory [49] and others [24]. The sudden increase may be due to the manner in which the N&B assay accumulates information from a stack of 155 images. A stack is acquired over 5 minutes and thus averages are weighted more heavily to the monomeric state prior to the period of oligomerization, whereas the observed result will be weighted more heavily to oligomerization following oligomerization. A manner to overcome this artefact, may involve using more discreet collection times, of say 33 frames per one minute, to reduce the effect and produce a data set less distorted by frame related temporal averaging.

Stellenbosch University https://scholar.sun.ac.za

An important shortcoming of this study is the low number of iterations of experiments performed. Future studies are therefore encouraged to make use of a larger sample set. Additionally, the inclusion of the monomeric mouse construct, the GRmon and the dimerization impaired construct, the GRdim, may be considered additional improvements with which to characterize the dimerization behaviour of the mouse GR.

Future researchers in this field may also find a benefit in exploring other FCS based spectroscopy methods, such as FCCS and PCH, since the software and equipment necessary is available for use at the University without requiring major modification. Furthermore, the ability to determine K_d directly from number and brightness data may prove useful in elucidating kinetic differences not only between the mouse and human GR model. But may also prove useful in the development of novel drug compounds that capitalize on the manipulation of GR oligomerization and expression to effect intended physiological outcomes. In particular, the ability of the N&B assay to distinguish between monomers and dimers may be useful in drug development studies, particular as long term N&B studies can be used to elucidate the underlying parameters of the K_d, k_{off} and k_{on}.

Finding specific expertise in FCS techniques on the African Continent was somewhat challenging and required specialised training. In light of this training was sought abroad at the Laboratory for fluorescent dynamics in the U.S.A. Though helpful, the scope of the lectures was broad and the involvement of experts in the field in a more direct capacity, e.g. through direct cooperative efforts in post graduate studies, may prove beneficial in future studies. However, the time and budget available for an MSc project may have limited such possibilities.

In summary, the study as a whole has successfully provided a method with which to identify the spectrum of physiologically relevant GR concentrations in the human body under normal as well as diseased conditions on the confocal microscope by employing the mouse GR

Stellenbosch University https://scholar.sun.ac.za

constructs and by using the COS-1 cell line. It has additionally shown promise in using the N&B technique as a means of observing ligand-independent dimerization in the mGR construct and to observe the ligand-induced dimerization of the GR over time. Future studies may benefit from using strong collaborative efforts to bring the N&B technology to Africa as a whole.

Stellenbosch University https://scholar.sun.ac.za

Reference List

[1] S. Robertson, J. M. Rohwer, J. P. Hapgood, and A. Louw, “Impact of Glucocorticoid Receptor Density on Ligand-Independent Dimerization, Cooperative Ligand-Binding and Basal Priming of Transactivation: A Cell Culture Model,” *PLoS One*, vol. 8, no. 5, 2013.

[2] C. J. Barry, *Modelling the glucocorticoid receptor dimerisation cycle*. Stellenbosch: University Stellenbosch, 2017.

[3] M. A. Digman, R. Dalal, A. F. Horwitz, and E. Gratton, “Mapping the Number of Molecules and Brightness in the Laser Scanning Microscope,” vol. 94, no. March, pp. 2320–2332, 2008.

[4] P. S. Hench, E. C. Kendall, C. H. Slocumb, and H. F. Polley, “The effect of a hormone of the adrenal cortex (17-hydroxy-11-dehydrocorticosterone: compound E) and of pituitary adrenocortical hormone in arthritis: preliminary report.,” *Ann. Rheum. Dis.*, vol. 8, no. 2, pp. 97–104, 1949.

[5] J. A. Kadmiel, Mahita. Cidlowski, “Glucocorticoid receptor signalling in health and disease,” *Trends Pharmacol. Sci.*, vol. 34, no. 9, pp. 518–530, 2013.

[6] R. S. Chriguer, L. L. K. Elias, I. M. Da Silva, J. G. H. Vieira, A. C. Moreira, and M. De Castro, “Glucocorticoid sensitivity in young healthy individuals: In vitro and in vivo studies,” *J. Clin. Endocrinol. Metab.*, vol. 90, no. 11, pp. 5978–5984, 2005.

[7] W. X. Guo *et al.*, “Expression and cytokine regulation of glucocorticoid receptors in Kaposi’s sarcoma.,” *Am. J. Pathol.*, vol. 148, no. 6, pp. 1999–2008, 1996.

[8] E. C. Hulme and M. a. Trevethick, “Ligand binding assays at equilibrium: Validation and interpretation,” *Br. J. Pharmacol.*, vol. 161, no. 6, pp. 1219–1237, 2010.

[9] G. P. Moss, “International union of pure and applied chemistry and international union of biochemistry: Joint commission on biochemical nomenclature: Nomenclature of steroids,” *Pure Appl. Chem.*, vol. 61, no. 10, pp. 1783–1822, 1989.

[10] T. Rhen and J. a Cidlowski, “Antiinflammatory action of glucocorticoids--new

Stellenbosch University https://scholar.sun.ac.za

mechanisms for old drugs.," *N. Engl. J. Med.*, vol. 353, no. 16, pp. 1711–1723, 2005.

[11] R. Group, "Dexamethasone in Hospitalized Patients with Covid-19 — Preliminary Report," *N. Engl. J. Med.*, pp. 1–11, 2020.

[12] S. Ramamoorthy and J. A. Cidlowski, "NHI Public access," *Rheum Dis Clin North Am,* vol. 1, no. 45, pp. 15–31, 2016.

[13] S. C. Biddie, B. L. Conway-campbell, and S. L. Lightman, "Dynamic regulation of glucocorticoid signalling in health and disease," *Rheumatology*, vol. 51, no. 3, pp. 403–412, 2012.

[14] R. D. G. Malcomson and A. Nagy, "The endocrine system," *Keeling's Fetal Neonatal Pathol.*, pp. 671–702, 2015.

[15] M. Joëls, H. Karst, and R. A. Sarabdjitsingh, "The stressed brain of humans and rodents," *Acta Physiol.*, vol. 223, no. 2, pp. 1–10, 2018.

[16] F. Acconcia and M. Marino, *Steroid Hormones:Synthesis, Secretion and transport.*, vol. 7, no. 1. 2017.

[17] S. Vyas, A. J. Rodriques, M. J. Silva, F. Tronche, and O. F. X. Almeida, "Chronic Stress and Glucocorticoids: From Neuronal Plasticity to Neurodegeneration.," *Hindawi Publ. corp.*, vol. 2016, 2015.

[18] S. Nussey and S. Whitehead, *Endocrinology: An integrated Approach*. Oxford: BIOS Scientific Publishers, 2001.

[19] J. Gulfo, R. Castel, A. Ledda, M. del M. Romero, M. Esteve, and M. Grasa, "Corticosteroid-Binding Globulin is expressed in the adrenal gland and its absence impairs corticosterone synthesis and secretion in a sex-dependent manner," *Sci. Rep.*, vol. 9, no. 1, pp. 1–10, 2019.

[20] S. Vandevyver, L. Dejager, and C. Libert, "Comprehensive overview of the structure and regulation of the glucocorticoid receptor," *Endocr. Rev.*, vol. 35, no. 4, pp. 671–693, 2014.

[21] E. S. Dieken and R. L. Miesfeld, "Transcriptional transactivation functions localized to

Stellenbosch University https://scholar.sun.ac.za

the glucocorticoid receptor N terminus are necessary for steroid induction of lymphocyte apoptosis.," *Mol. Cell. Biol.*, vol. 12, no. 2, pp. 589–597, 1992.

[22] R. Kumar and E. B. Thompson, "Transactivation functions of the N-terminal domains of nuclear hormone receptors: Protein folding and coactivator interactions," *Mol. Endocrinol.*, vol. 17, no. 1, pp. 1–10, 2003.

[23] R. K. Bledsoe *et al.*, "Crystal Structure of the Glucocorticoid Receptor Ligand Binding Domain Reveals a Novel Mode of Receptor Dimerization and Coactivator Recognition," vol. 110, pp. 93–105, 2002.

[24] D. M. Presman *et al.*, "Live Cell Imaging Unveils Multiple Domain Requirements for In Vivo Dimerization of the Glucocorticoid Receptor," *PLoS Biol.*, vol. 12, no. 3, 2014.

[25] T. J. Cole *et al.*, "Targeted disruption of the glucocorticoid receptor gene blocks adrenergic chromaffin cell development and severely retards lung maturation," *Genes Dev.*, vol. 9, no. 13, pp. 1608–1621, 1995.

[26] S. Vandevyver, L. Dejager, and C. Libert, "On the Trail of the Glucocorticoid Receptor: Into the Nucleus and Back," *Traffic*, vol. 13, no. 3, pp. 364–374, 2012.

[27] E. Kirschke, D. Goswami, D. Southworth, P. R. Griffin, and D. A. Agard, "Glucocorticoid receptor function regulated by coordinated action of the Hsp90 and Hsp70 chaperone cycles," *Cell*, vol. 157, no. 7, pp. 1685–1697, 2014.

[28] W. Y. Almawi and O. K. Melemedjian, "Negative regulation of nuclear factor-κB activation and function by glucocorticoids," *J. Mol. Endocrinol.*, vol. 28, no. 2, pp. 69–78, 2002.

[29] T. Kino, M. U. De Martino, E. Charmandari, M. Mirani, and G. P. Chrousos, "Tissue glucocorticoid resistance/hypersensitivity syndromes," *J. Steroid Biochem. Mol. Biol.*, vol. 85, no. 2–5, pp. 457–467, 2003.

[30] T. E. Reddy *et al.*, "Genomic determination of the glucocorticoid response reveals unexpected mechanisms of gene regulation," *Genome Res.*, vol. 19, no. 12, pp. 2163–2171, 2009.

Stellenbosch University https://scholar.sun.ac.za

[31] J. C. Buckingham, “Glucocorticoids: Exemplars of multi-tasking,” *Br. J. Pharmacol.*, vol. 147, no. SUPPL. 1, pp. 258–268, 2006.

[32] J. M. Busillo and J. A. Cidlowski, “The five Rs of glucocorticoid action during inflammation: Ready, reinforce, repress, resolve, and restore,” *Trends Endocrinol. Metab.*, vol. 24, no. 3, pp. 109–119, 2013.

[33] R. Newton, “Molecular mechanisms of glucocorticoid action : what is important ? Molecular mechanisms of glucocorticoid action : what is important ?,” no. D, pp. 603–613, 2000.

[34] T. Kuo, A. Mcqueen, T. C. Chen, and J. C. Wang, “Regulation of Glucose Homeostasis by Glucocorticoids,” no. 872, pp. 99–126, 2015.

[35] M. Wang, “The role of glucocorticoid action in the pathophysiology of the Metabolic Syndrome,” *Nutr. Metab.*, vol. 2, pp. 1–14, 2005.

[36] S. Cohen *et al.*, “Chronic stress, glucocorticoid receptor resistance, inflammation, and disease risk,” *Proc. Natl. Acad. Sci. U. S. A.*, vol. 109, no. 16, pp. 5995–5999, 2012.

[37] E. Iob and A. Steptoe, “Cardiovascular Disease and Hair Cortisol: a Novel Biomarker of Chronic Stress,” *Curr. Cardiol. Rep.*, vol. 21, no. 10, 2019.

[38] B. C. Yao, L. B. Meng, M. L. Hao, Y. M. Zhang, T. Gong, and Z. G. Guo, “Chronic stress: a critical risk factor for atherosclerosis,” *J. Int. Med. Res.*, vol. 47, no. 4, pp. 1429–1440, 2019.

[39] M. Ancelin *et al.*, “Steroid and nonsteroidal anti-inflammatory drugs , cognitive decline , and dementia .,” vol. 33, no. 9, pp. 2082–2090, 2012.

[40] S. G. Hillier, “Diamonds are forever: The cortisone legacy,” *J. Endocrinol.*, vol. 195, no. 1, pp. 1–6, 2007.

[41] R. J. Flach Roth and A. M. Bennett, “Mitogen-Activated Protein Kinase Phosphatase-1 -A PotentialTherapeutic Target In Metabolic Disease,” *NIH public access*, vol. 14, no. 12, pp. 1323–1332, 2010.

[42] K. Ma *et al.*, “Glucocorticoid-induced skeletal muscle atrophy is associated with

Stellenbosch University https://scholar.sun.ac.za

upregulation of myostatin gene expression," *Am. J. Physiol. - Endocrinol. Metab.*, vol. 285, no. 2 48-2, pp. 363–371, 2003.

[43] J. L. Hwang and R. E. Weiss, "Steroid induced diabetes: a clinial and molecular approach to understanding and treatment," *Diabetes Metab. Res. Rev.*, vol. 30, no. 2, pp. 96–102, 2013.

[44] S. C. Manolagas and R. S. Weinstein, "Steroid-Induced Osteoporosis."

[45] N. Sundahl, J. Bridelance, C. Libert, K. De Bosscher, and I. M. Beck, "Selective glucocorticoid receptor modulation: New directions with non-steroidal scaffolds," *Pharmacol. Ther.*, vol. 152, pp. 28–41, 2015.

[46] D. Y. M. Leung and J. W. Bloom, "Update on glucocorticoid action and resistance," *J. Allergy Clin. Immunol.*, vol. 111, no. 1, pp. 3–22, 2003.

[47] E. G. Haarman, G. J. L. Kaspers, R. Pieters, M. M. A. Rottier, and A. J. P. Veerman, "Glucocorticoid receptor alpha, beta and gamma expression vs in vitro glucocorticod resistance in childhood leukemia," *Leukemia*, vol. 18, no. 3, pp. 530–537, 2004.

[48] A. Louw, "GR dimerization and the impact of gr dimerization on gr protein stability and half-life," *Front. Immunol.*, vol. 10, no. JULY, pp. 1–15, 2019.

[49] S. Robertson, J. P. Hapgood, and A. Louw, "Glucocorticoid receptor concentration and the ability to dimerize influence nuclear translocation and distribution," *Steroids*, vol. 78, no. 2, pp. 182–194, 2013.

[50] R. A. Copeland, "Conformational adaptation in drug – target interactions and residence time," pp. 1491–1501, 2011.

[51] G. Vauquelin and I. Van Liefde, "Slow antagonist dissociation and long-lasting in vivo receptor protection," *Trends Pharmacol. Sci.*, vol. 27, no. 7, pp. 355–359, 2006.

[52] D. M. Jameson, J. A. Ross, and J. P. Albanesi, "Fluorescence fluctuation spectroscopy: Ushering in a new age of enlightenment for cellular dynamics," *Biophys. Rev.*, vol. 1, no. 3, pp. 105–118, 2009.

[53] N. Teeninga *et al.*, "Genetic and in vivo determinants of glucocorticoid sensitivity in

Stellenbosch University https://scholar.sun.ac.za

relation to clinical outcome of childhood nephrotic syndrome," *Kidney Int.*, vol. 85, no. 6, pp. 1444–1453, 2014.

[54] P. M. Driver, M. D. Kilby, I. Bujalska, E. a Walker, M. Hewison, and P. M. Stewart, "Expression of 11 beta-hydroxysteroid dehydrogenase isozymes and corticosteroid hormone receptors in primary cultures of human trophoblast and placental bed biopsies.," *Mol. Hum. Reprod.*, vol. 7, no. 4, pp. 357–63, 2001.

[55] L. M. Colli, F. C. Do Amaral, N. Torres, and M. De Castro, "Interindividual glucocorticoid sensitivity in young healthy subjects: The role of glucocorticoid receptor a and β isoforms ratio," *Horm. Metab. Res.*, vol. 39, no. 6, pp. 425–429, 2007.

[56] M. Surjit *et al.*, "Widespread negative response elements mediate direct repression by agonist-liganded glucocorticoid receptor," *Cell*, vol. 145, no. 2, pp. 224–241, 2011.

[57] L. Pujols, J. Mullol, a Torrego, and C. Picado, "Glucocorticoid receptors in human airways.," *Allergy*, vol. 59, no. 10, pp. 1042–1052, 2004.

[58] J. Corzo and M. Santamaria, "Time, the forgotten dimension of ligand binding teaching," *Biochem. Mol. Biol. Educ.*, vol. 34, no. 6, pp. 413–416, 2006.

[59] G. Vauquelin and S. J. Charlton, "Long-lasting target binding and rebinding as mechanisms to prolong in vivo drug action," *Br. J. Pharmacol.*, vol. 161, no. 3, pp. 488–508, 2010.

[60] R. F. Selden, "Transfection using DEAE-dextran.," *Curr. Protoc. Immunol.*, vol. Chapter 10, p. Unit 10.14, 2001.

[61] P. J. Cranfill *et al.*, "Quantitative assessment of fluorescent proteins," *Nat. Methods*, vol. 13, p. 557, May 2016.

[62] W. C. Tseng, F. R. Haselton, and T. D. Giorgio, "Transfection by cationic liposomes using simultaneous single cell measurements of plasmid delivery and transgene expression," *J. Biol. Chem.*, vol. 272, no. 41, pp. 25641–25647, 1997.

[63] M. B. James and T. D. Giorgio, "Nuclear-Associated Plasmid, but Not Cell-Associated Plasmid, Is Correlated with Transgene Expression in Cultured Mammalian Cells," *Mol.*

Stellenbosch University https://scholar.sun.ac.za

Ther., vol. 1, no. 4, pp. 339–346, 2000.

[64] ThermoFisher Scientific, “Lipofectamine® 3000 Reagent,” no. 100022234, pp. 1–2, 2016.

[65] M. P. Calos, J. S. Lebkowski, and M. R. Botchan, “High mutation frequency in DNA transfected into mammalian cells,” *Proc. Natl. Acad. Sci. U. S. A.*, vol. 80, no. 10 I, pp. 3015–3019, 1983.

[66] P. L. Felgner *et al.*, “Lipofection : A highly efficient , lipid-mediated DNA-transfection procedure,” vol. 84, no. November, pp. 7413–7417, 1987.

[67] S. C. Materna and W. Marwan, “Estimating the number of plasmids taken up by a eukaryotic cell during transfection and evidence that antisense RNA abolishes gene expression in Physarum polycephalum,” *F[1] S. C. Matern. W. Marwan, “Estimating number plasmids Tak. up by a Eukaryot. cell Dur. transfection Evid. that antisense RNA abolishes gene Expr. Physarum polycephalum,” FEMS Microbiol. Lett., vol. 243, no. 1, pp. 29–35,* , vol. 243, no. 1, pp. 29–35, 2005.

[68] R. Kumar and E. B. Thompson, “Gene regulation by the glucocorticoid receptor: structure:function relationship.,” *J. Steroid Biochem. Mol. Biol.*, vol. 94, no. 5, pp. 383–394, 2005.

[69] H. Qian and E. L. Elson, “Distribution of molecular aggregation by analysis of fluctuation moments,” vol. 87, no. July 1990, pp. 5479–5483, 2000.

[70] P. Chen, X. Feng, R. Hu, J. Sun, W. Du, and B. F. Liu, “Hydrodynamic gating valve for microfluidic fluorescence-activated cell sorting,” *Anal. Chim. Acta*, vol. 663, no. 1, pp. 1–6, 2010.

[71] S. Maiti, U. Haupts, and W. W. Webb, “Fluorescence correlation spectroscopy: Diagnostics for sparse molecules,” *Proc. Natl. Acad. Sci.*, vol. 94, no. 22, pp. 11753–11757, 1997.

[72] L. N. Hillesheim and J. D. Mu, “The Photon Counting Histogram in Fluorescence Fluctuation Spectroscopy with Non-Ideal Photodetectors,” vol. 85, no. September, pp.

Stellenbosch University https://scholar.sun.ac.za

1948–1958, 2003.

[73] M. A. Digman, R. Dalal, A. F. Horwitz, and E. Gratton, “Mapping the number of molecules and brightness in the laser scanning microscope,” *Biophys. J.*, vol. 94, no. 6, pp. 2320–2332, 2008.

[74] R. E. Brown, “A brief account of microscopial observations made in the months of June, July and August 1827, on particles contained in the pollen of plants; and on the general existence of active molecules in organic and inorganic bodies.,” *Philos. Mag. Ann. Philos.*, vol. 4, no. 21, 1827.

[75] P. W. Wiseman, “Spatial mapping of integrin interactions and dynamics during cell migration by Image Correlation Microscopy,” *J. Cell Sci.*, vol. 117, no. 23, pp. 5521–5534, 2004.

[76] C. M. Brown and N. O. Petersen, “An image correlation analysis of the distribution of clathrin associated adaptor protein (AP-2) at the plasma membrane.,” *J. Cell Sci.*, vol. 111 (Pt 2, pp. 271–81, 1998.

[77] D. T. Chiu and R. N. Zare, “Biased Diffusion , Optical Trapping , and Manipulation of Single Molecules in Solution,” vol. 7863, no. 11, pp. 6512–6513, 1996.

[78] L. Edman, U. Mets, and R. Rigler, “Conformational transitions monitored for single molecules in solution.,” *Proc. Natl. Acad. Sci. U. S. A.*, vol. 93, no. 13, pp. 6710–6715, 1996.

[79] U. Meseth, T. Wohland, R. Rigler, and H. Vogel, “Resolution of Fluorescence Correlation Measurements,” vol. 76, no. March, pp. 1619–1631, 1999.

[80] A. G. Palmer and N. L. Thompson, “Molecular aggregation characterized by high order autocorrelation in fluorescence correlation spectroscopy,” *Biophys. J.*, vol. 52, no. 2, pp. 257–270, 1987.

[81] K. Palo, Ü. Mets, S. Jäger, P. Kask, and K. Gall, “Fluorescence intensity multiple distributions analysis: Concurrent determination of diffusion times and molecular brightness,” *Biophys. J.*, vol. 79, no. 6, pp. 2858–2866, 2000.

Stellenbosch University https://scholar.sun.ac.za

[82] Y. Chen, L.-N. Wei, and J. D. Muller, “Probing protein oligomerization in living cells with fluorescence fluctuation spectroscopy,” *Proc. Natl. Acad. Sci.*, vol. 100, no. 26, pp. 15492–15497, 2003.

[83] J. R. Unruh and E. Gratton, “Analysis of molecular concentration and brightness from fluorescence fluctuation data with an electron multiplied CCD camera,” *Biophys. J.*, vol. 95, no. 11, pp. 5385–5398, 2008.

[84] T. D. Perroud, B. Huang, and R. N. Zare, “Effect of bin time on the photon counting histogram for one-photon excitation,” *ChemPhysChem*, vol. 6, no. 5, pp. 905–912, 2005.

[85] N. M. Clark *et al.*, “Tracking transcription factor mobility and interaction in arabidopsis roots with fluorescence correlation spectroscopy,” *Elife*, vol. 5, no. JUN2016, pp. 1–25, 2016.

[86] B. M. Michalska *et al.*, “Insight into the fission mechanism by quantitative characterization of Drp1 protein distribution in the living cell,” *Sci. Rep.*, vol. 8, no. 1, pp. 1–15, 2018.

[87] K. Frudd, T. Burgoyne, and J. R. Burgoyne, “Oxidation of Atg3 and Atg7 mediates inhibition of autophagy,” *Nat. Commun.*, vol. 9, no. 1, pp. 1–15, 2018.

[88] G. D. Ruxton, “The unequal variance t-test is an underused alternative to Student’s t-test and the Mann-Whitney U test,” *Behav. Ecol.*, vol. 17, no. 4, pp. 688–690, 2006.

[89] D. Von Stetten, M. Noirclerc-Savoye, J. Goedhart, T. W. J. Gadella, and A. Royant, “Structure of a fluorescent protein from Aequorea victoria bearing the obligate-monomer mutation A206K,” *Acta Crystallogr. Sect. F Struct. Biol. Cryst. Commun.*, vol. 68, no. 8, pp. 878–882, 2012.

[90] V. Cherkas *et al.*, “Measurement of intracellular concentration of fluorescently-labeled targets in living cells,” *PLoS One*, vol. 13, no. 4, pp. 1–21, 2018.

[91] L. M. Costatini, M. Fossati, M. Francolini, and E. L. Shnapp, “Assessing the Tendency of Fluorescent Proteins to Oligomerizeunder Physiologic Conditions Conditions,” *NIH*

Stellenbosch University https://scholar.sun.ac.za

public access, vol. 13, no. 5, pp. 643–649, 2012.

[92] P. Sengupta, A. Hammond, D. Holowka, and B. Baird, “Structural Determinants for Partitioning of Lipands and Proteins Between Coexsisting Fluid Phases in Giant Plasma Membrane Vesicles,” *Biochim Biophys Acta*, vol. 23, no. 1, pp. 20–32, 2008.

[93] N. C. Nicolaides, Z. Galata, T. Kino, G. P. Chrousous, and E. Charmandari, “The human Glucocortioid receptor: Molecular Basis of Biological Function,” *Steroids*, vol. 75, no. 1, 2010.

[94] D. W. C. Lau, S. Law, S. E. Walker, and J. Lazetta, “Dexamethasone phosphate stability and contamination of solutions stored in syringes,” *PDA J. Pharm. Sci. Technol.*, vol. 50, no. 4, pp. 261–262, 1996.

[95] C. Hellriegel, V. R. Caiolfa, V. Corti, N. Sidenius, and M. Zamai, “Number and brightness image analysis reveals ATF-induced dimerization kinetics of uPAR in the cell membrane,” *FASEB J.*, vol. 25, no. 9, pp. 2883–2897, 2011.

[96] S. Mahatabuddin *et al.*, “Concentration-dependent oligomerization of an alpha-helical antifreeze polypeptide makes it hyperactive,” *Sci. Rep.*, vol. 7, no. January, pp. 1–9, 2017.

[97] M. Lõpez-Pelegrín *et al.*, “Multiple stable conformations account for reversible concentration-dependent oligomerization and autoinhibition of a metamorphic metallopeptidase,” *Angew. Chemie - Int. Ed.*, vol. 53, no. 40, pp. 10624–10630, 2014.

[98] C. Williams and C. Y. Lin, “Oestrogen receptors in breast cancer: Basic mechanisms and clinical implications,” *Ecancermedicalscience*, vol. 7, no. 1, pp. 1–12, 2013.

Stellenbosch University https://scholar.sun.ac.za

Addenda

Addendum A

The figures below serve as examples of the FACS readouts used for the determination of transfection efficiency, as well as the determination of subpopulation redistribution as described in this chapter.

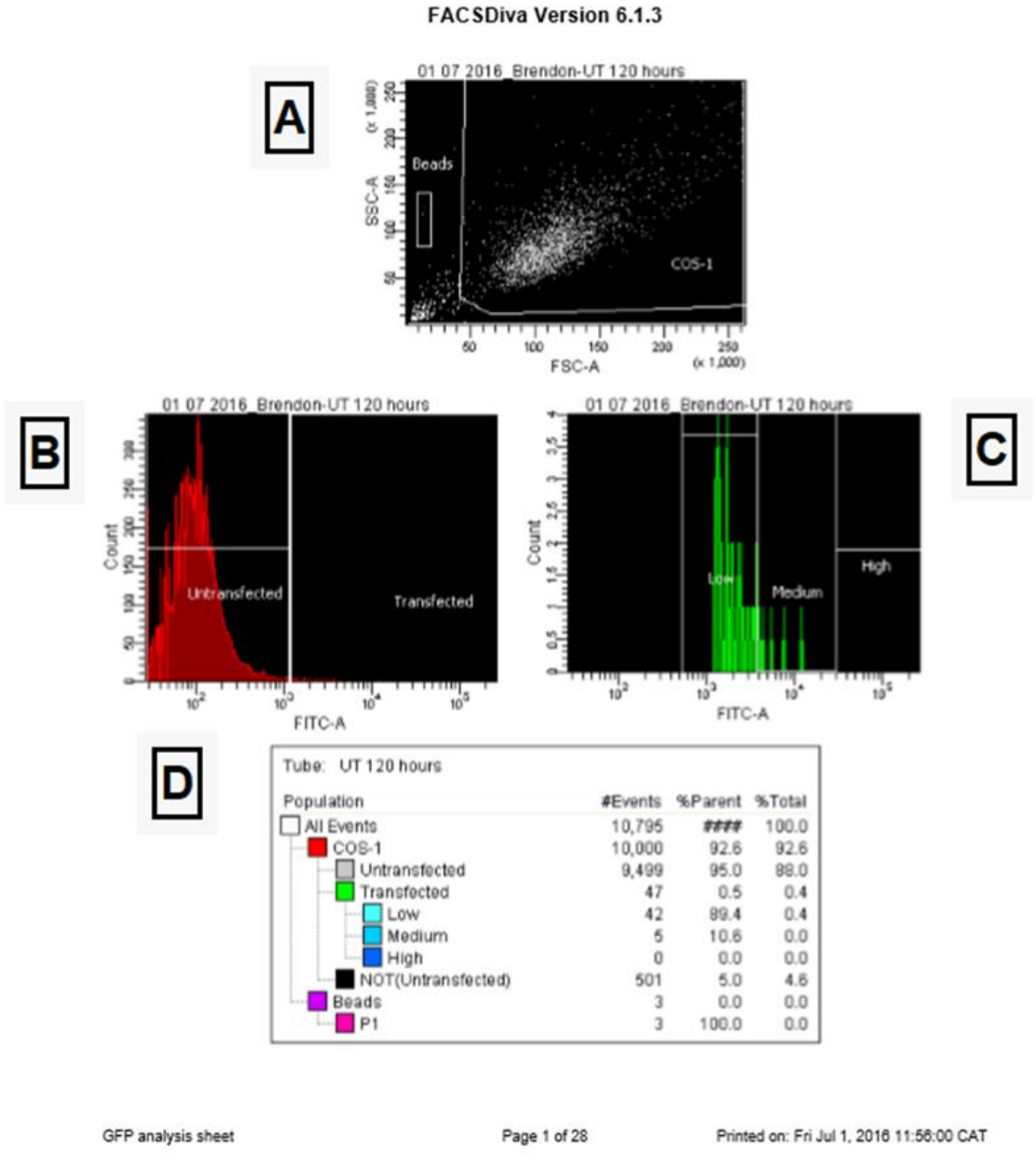

Figure A1: Determination of the effects of autofluorescent cells within the screened COS-1 cell population.

Stellenbosch University https://scholar.sun.ac.za

Figure (A) shows the observed forward scatter, and FITC-A side scatter for COS-1 cells. Data points within the enclosed polygon labelled COS-1 cells were selected as healthy cells for further scrutiny. (B) In each experiment the untransfected (pGL2 Basic) control sample was used to determine the degree of autofluorescence in the COS-1 cell line and was adjusted to produce an autofluorescence value in the transfected population under 0.5%. Figure (C) illustrates the gating parameters in accordance to previous studies and in this example illustrates the autofluoresence observed in the untransfected cell line. Table (D) provided information regarding the relationship between the net number of viable cells and cells regarded as untransfected. The percentage of untransfected cells displaying autofluorescence within previously determined sorting gates was limited to under 0.5% in all experiments.

Stellenbosch University https://scholar.sun.ac.za

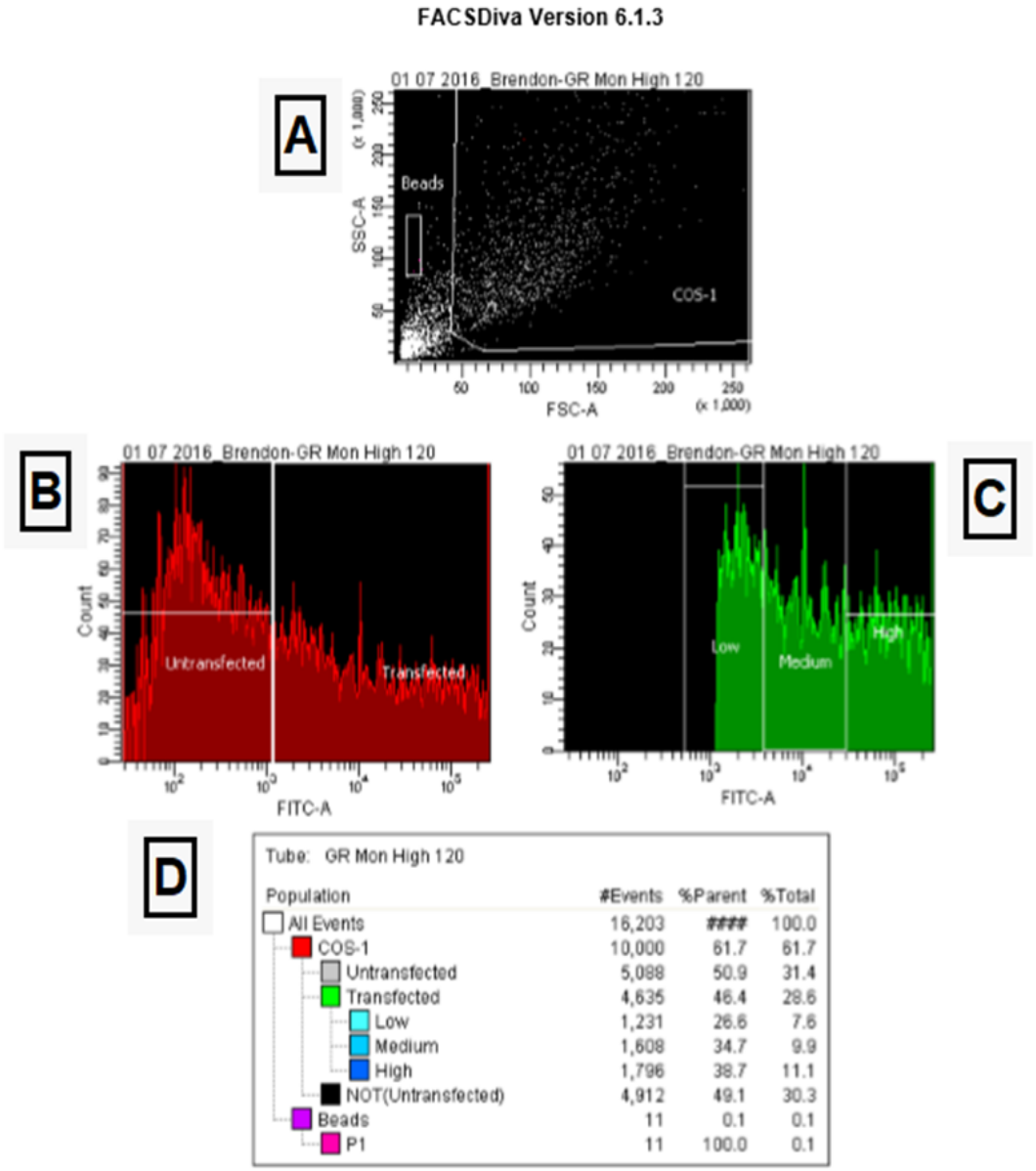

Figure A2: Raw FACS data and the means of determining the parameters of global transfection efficiency, relative transfection efficiency and absolute transfection efficiency.

Figure (A) shows the side scatter (SSCA) and forward scatter of green light (FITC-A) from the observed cell population. Data points enclosed within the polygon labelled COS-1 are indicative of whole COS-1 cells. Figure (B) shows a distinct separation between untransfected and autofluorescent cell populations (left) and transfected cell populations (right) based on the untransfected control.

Stellenbosch University https://scholar.sun.ac.za

Cells expressing a forward scatter above $10^{2.5}$ and clearly distinguishable from autofluorescing untransfected cells were selected as transfected and defined as per previous work by our laboratory into categories of low [GR], medium [GR] and high [GR].

The table (D) was interpreted in the following way to elucidate the global transfection efficiency. Global transfection efficiency was simply interpreted as the percentage transfected population of the parent population of screened cells. In this instance, 13172 cells were considered of which 44.7% were found to be expressing mGR-eGFP without the influence of cellular autofluoresence. Relative transfection efficiency was determined in the following way. The transfected population, 4472 cells in this example, were considered as a distinct parent population. The subpopulations here written as low, medium and high, represent the groups low [GR], medium [GR] and high [GR] described in text and are described as a percentage of the parent population which can be directly read from the table. Absolute distributions were determined by transforming the subpopulation percentages in terms of the ratio of the transfected population to the total observed cell population.

Stellenbosch University https://scholar.sun.ac.za

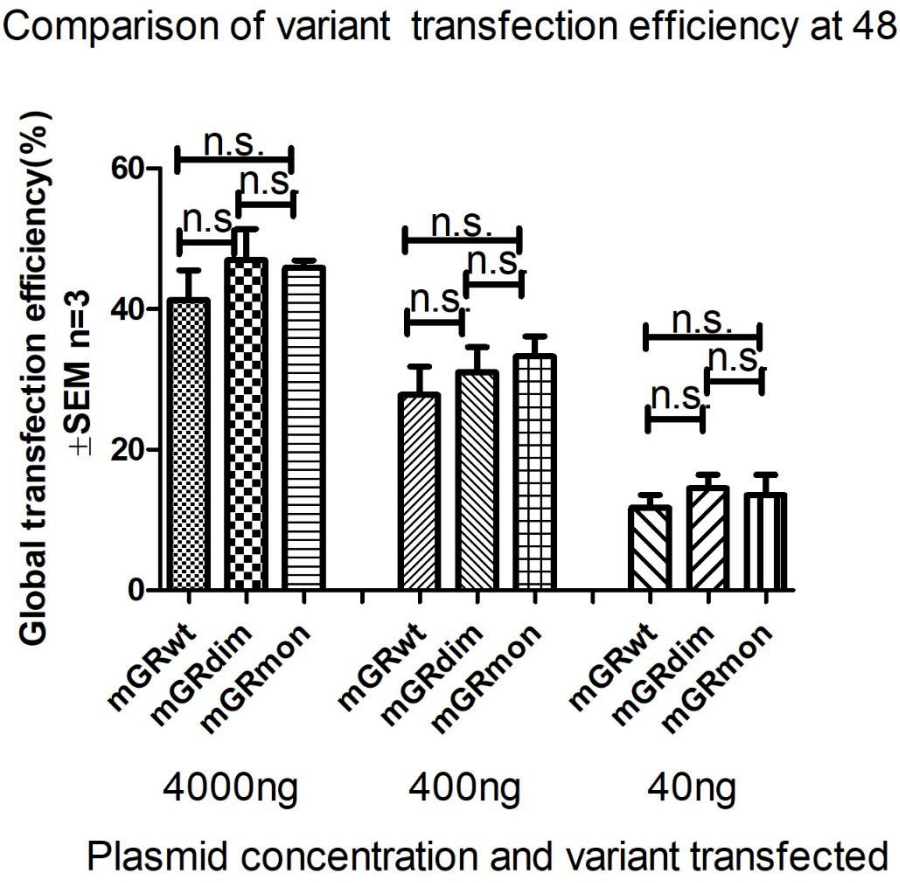

Figure A3: Comparison of global transfection efficiency for mGR variants at the 48 hour time point.

COS-1 cells were transiently transfected with increasing initial concentrations of the GR variants mGRwt, mGRdim and mGRmon. Statistical analysis was performed by one-way ANOVA followed by Tukey's multiple comparison test. "n.s." is representative of differences which were not statistically significant $p>0.05$.

Stellenbosch University https://scholar.sun.ac.za

Addendum B

Mean intensity projection of 7 overlaid images of the Z stack method with cell region of interest enclosed by the Bezier tool.